

**Investigation of Environmental and Dynamic Loading Impacts on Flexible Pavement  
Responses in Cold Climate Conditions**

by

Mohammad Hossein Shafiee

A thesis submitted in partial fulfillment of the requirements for the degree of

Doctor of Philosophy

in

Transportation Engineering

Department of Civil and Environmental Engineering

University of Alberta

©Mohammad Hossein Shafiee, 2016

# Abstract

Flexible pavement design methods have undergone a paradigm shift with particular attention to mechanistic-based approaches, which are based on the actual pavement's structural behaviour and reflect the pavement performance. The mechanistic design procedures rely on the pavement's critical responses for prediction of pavement distresses, making response measurement and prediction significantly important for pavement engineers. While a limited number of facilities around the world are capable of in-situ measurement and evaluation of pavement responses, the lack of comprehensive information on the effect of static and dynamic loads, especially on cold region pavements, concerns pavement engineers and researchers. The current study was conducted in an attempt to address the impact of vehicular and Falling Weight Deflectometer (FWD) loads on pavement responses under different environmental conditions, as well as to investigate the behaviour of pavement responses due to environmental loading. As part of this research, a series of controlled vehicle tests were conducted at the Integrated Road Research Facility (IRRF), a full-scale test road equipped with structural and environmental pavement instruments located in Edmonton, Alberta, Canada. Also, several rounds of FWD tests were implemented at instrumented sections of the IRRF to investigate the seasonal variation of recorded stresses and strains.

Promising results were obtained when applying advanced frequency domain and time-frequency domain analysis methods to evaluate the loading frequency of vehicle loads based on the field data. Analyzing the frequency at multiple speeds and at different depths from the surface using Fast Fourier Transform (FFT) led to improved dynamic modulus estimation accuracy. In addition, analyzing the asphalt longitudinal strain frequency using Continuous Wavelet

Transform (CWT) and Short-Time Fourier Transform (STFT) showed the advantage of time-frequency domain techniques in comparison to traditional time-to-frequency conversion methods.

Reasonable agreement between predicted and measured FWD-induced responses was achieved using the laboratory-determined asphalt master curves and backcalculated moduli of base and subgrade layers for dynamic simulation of pavement structure via 3D-Move software. Also, by incorporating the FWD stress time histories, an axis-symmetric Finite Element Model (FEM) was developed in ABAQUS and the prediction results were compared against the in-situ measured ones.

Monitoring the seasonal variation of strains at the bottom of Hot Mix Asphalt (HMA) and stresses within the base and subgrade layers when subjecting the pavement to FWD clearly showed the significant impact freeze/thaw cycles had on the recorded values. It was found that during the thawing period, the horizontal and vertical strains can be almost 17 and 11 times larger than their counterparts in cold months. Results from this study also indicated that the stress on top of the base layer can increase more than two times during the thaw period. In addition, the collected data over the course of sixteen months emphasized the significant effect of temperature fluctuation, in absence of traffic loading, on generating strains in three directions under the HMA layer. This analysis was fruitful and indicative of HMA thermal properties in the field.

# Preface

The dissertation in hand is the original work completed by the author and presented in the “paper-format” style. For all of the papers, I was the principal investigator and responsible for the experimental study, data analysis, and manuscript composition. My supervisor, Dr. Bayat, professionally designed and managed the research program and was the corresponding author. **Chapter 3** was published as Shafiee, M.H., Asefzadeh, A., Hashemian, L. and Bayat, A., 2015. Analysis of Loading Frequently in Flexible Pavement Using Fast Fourier Transform. *International Journal of Pavement Research and Technology*, 8(6), p.403. **Chapter 4** was accepted for publication as Shafiee, M.H., Hashemian, L., Asefzadeh, A., and Bayat, A., 2016. Time-Frequency Domain Analysis of Asphalt Longitudinal Strain. *Transportation Research Record: Journal of Transportation Research Board*, 2016. **Chapter 5** will be submitted to the *Journal of Performance of Constructed Facilities* in 2016. **Chapter 6** was published as Shafiee, M.H., Asefzadeh, A., Hashemian, L. and Bayat, A., 2015. Analysis of Loading Frequently in Flexible Pavement Using Fast Fourier Transform. *International Journal of Pavement Research and Technology*, 8(6), p.403. **Chapter 7** is under revision for publication as Shafiee, M.H., Biswas, S., Tavafzadeh, N., Hashemian, L., and Bayat, A., 2015. Field Investigation of Thermal-Induced Strains in Flexible Pavement Structures. *International Journal of Pavement Engineering*. The co-authors of the aforementioned papers actively assisted the author in data collection and production of the manuscripts.

***DEDICATED***

*To*

*My Kind Parents*

*&*

*Lovely Wife*

# Acknowledgements

I would like to express my sincere gratitude to my research supervisor, **Dr. Alireza Bayat**, for his kind support, guidance, and encouragement during my doctoral studies at the University of Alberta. I am greatly thankful for the unique research opportunities provided by Dr. Bayat and I truly appreciate his time, considerations, and financial support over the course of this journey.

I would like to acknowledge **Dr. Leila Hashemian** and **Dr. Somayeh Nassiri**, Post-Doctoral Fellows at University of Alberta, for their valuable contributions and considerable efforts. I benefited tremendously from them being part of this research. I am deeply grateful to **Dr. Mahmood Salimi** and **Dr. Nader Tabatabaee** for their valuable and kind support, as well.

I am thankful to **Dr. Ralph Haas**, **Dr. Mohamed Al-Hussein**, **Dr. Michael Hendry** and **Dr. Chong-Qing Ru**, my examining committee members for their time, suggestions, and constructive comments.

My thanks are extended to the Faculty of Graduate Studies and Research (FGSR) and Graduate Students' Association (GSA), University of Alberta, for their scholarships and travel grants.

This research could not be possible without the precious assistance of my knowledgeable friends at the University of Alberta, including but not limited to Dr. Daniel Teklu Meles, who patiently collaborated in many research activities at the IRRF test road project.

Last, but not least, thanks go to the highly respected editorial group at IRRF, including Tejay Gardiner, Lauren Wozny, Tatiana Boryshchuk, and Sheena Moore.

# Table of Contents

<b>Chapter 1 - Introduction</b> .....	<b>1</b>
Statement of the Problem .....	2
Research Objectives .....	4
Scope of Work.....	5
Structure of Dissertation.....	5
<b>Chapter 2 -Literature Review</b> .....	<b>7</b>
Pavement Response to Dynamic Loads .....	8
Vehicular Loading .....	8
FWD Loading .....	12
Environmental Impacts on Pavement Materials.....	15
Unbound Materials .....	16
Asphalt Materials.....	18
Response Prediction Models .....	24
<b>Chapter 3 -Analysis of Loading Frequency in Flexible Pavement Using Fast Fourier Transform</b> .....	<b>29</b>
Abstract .....	30
Introduction .....	31
Experimental Program.....	33
Integrated Road Research Facility.....	33
Field Study.....	35
Analysis of Loading Frequency .....	36
Fourier Representation of Pulses.....	36
Effect of Response Type, Depth and Speed .....	39
Accuracy of Dynamic Modulus Prediction.....	41
Dynamic Modulus from Laboratory.....	41
Impact of Frequency Calculation Method on Dynamic Modulus .....	43
Conclusion.....	50

Acknowledgements .....	50
<b>Chapter 4 -Time-Frequency Domain Analysis of Asphalt Longitudinal Strain .....</b>	<b>51</b>
Abstract .....	52
Introduction .....	53
Project information.....	55
IRRF Test Road Facility.....	55
Data Collection .....	57
Methodology .....	58
Continuous Wavelet Transform.....	58
Short-Time Fourier Transform .....	61
Data Analysis .....	63
Loading Frequency Determination .....	63
Response Prediction and the Influence of Frequency .....	67
Frequency Effect on Fatigue Performance .....	70
Conclusion.....	72
Acknowledgements .....	73
<b>Chapter 5 -Field Measurement and Modeling of Vertical and Longitudinal Strains from Falling Weight Deflectometer Testing.....</b>	<b>74</b>
Abstract .....	75
Introduction .....	76
Background .....	77
Description of Experiment .....	79
Measured Horizontal and Vertical Strains .....	82
Determination of Layer Moduli .....	88
Laboratory-Measured HMA Moduli .....	88
Backcalculation of Moduli .....	89
Development of Response Prediction Models .....	91
MLE Analysis with KENPAVE .....	91
FEM with ABAQUS .....	91
Modeling with 3D-Move.....	92
Prediction Results and Performance .....	92

Conclusion.....	97
Acknowledgments.....	98
<b>Chapter 6 -Seasonal Analysis of Flexible Pavement Response to Falling Weight Deflectometer .....</b>	<b>99</b>
Abstract.....	100
Introduction.....	101
Overview of IRRF Test Road Facility .....	103
Results and Discussion.....	105
FWD Testing Results in Different Seasons.....	105
Backcalculations of Layers Moduli.....	112
Analysis of Calculated Responses.....	116
Conclusion.....	119
Acknowledgements.....	120
<b>Chapter 7 -Field Investigation of Thermal-Induced Strains in Flexible Pavement Structures .....</b>	<b>121</b>
Abstract.....	122
Introduction.....	123
Objectives.....	125
IRRF Test Road Facility .....	126
Pavement Instrumentation.....	129
Data Collection and Analysis.....	130
Laboratory Investigation of Thermal Behaviour of ASG.....	130
Thermal-Induced Strain Magnitude.....	131
Irrecoverable Strains.....	139
Determination of CTC and CTE.....	141
Conclusion.....	146
Acknowledgements.....	147
<b>Chapter 8 –Conclusions and Recommendations .....</b>	<b>148</b>
Conclusions.....	149
Recommendations.....	152
<b>Bibliography.....</b>	<b>154</b>

# List of Tables

<b>Table 2-1</b> Relationships between resilient modulus and soil parameters.....	19
<b>Table 2-2</b> Relationships between HMA modulus and temperature .....	21
<b>Table 2-3</b> Relationships between HMA strain and temperature .....	23
<b>Table 2-4</b> General formulations for the multi-layer elastic system.....	26
<b>Table 3-1</b> Relationships between dominant frequency and vehicle speed.....	39
<b>Table 3-2</b> Frequency calculation scenarios considered in this study. ....	44
<b>Table 4-1</b> Comparison between $T_{HP}$ and DS.....	63
<b>Table 4-2</b> Effect of loading frequency on HMA layer's moduli.....	67
<b>Table 5-1</b> HMA physical parameters at IRRF .....	81
<b>Table 5-2</b> Haversine pulse duration at different months .....	88
<b>Table 5-3</b> Variation of backcalculated layer moduli.....	90
<b>Table 6-1</b> Summary of layers moduli from laboratory and FWD-backcalculation. ....	115
<b>Table 6-2</b> Summary of predicted responses and prediction errors.....	117
<b>Table 7-1</b> Average and standard deviation of seasonal thermal coefficients.....	145

# List of Figures

<b>Figure 2-1</b> The impact of speed on vertical stress pulse. ....	9
<b>Figure 2-2</b> Longitudinal strain pulse duration measured by ASG. ....	10
<b>Figure 2-3</b> Representation of horizontal strains in (a) time domain and (b) frequency domain..	11
<b>Figure 2-4</b> FWD equipment during field testing.....	12
<b>Figure 2-5</b> Typical FWD-induced stress pulse. ....	13
<b>Figure 2-6</b> Tensile strain pulse exclusive to the FWD load impact. ....	14
<b>Figure 2-7</b> Typical changes in the soil stiffness during the freeze and thaw periods. ....	17
<b>Figure 2-8</b> Variation of HMA modulus due to temperature. ....	20
<b>Figure 3-1</b> Gradation and physical properties of HMA mixes at IRRF.....	33
<b>Figure 3-2</b> Instrumentation layout and pavement cross-section (all dimensions are in mm). ....	35
<b>Figure 3-3</b> (a) Time domain and (b) frequency domain of measured stress pulses at 5 km/hr speed. ....	37
<b>Figure 3-4</b> (a) Time domain and (b) frequency domain of measured strain pulses at the bottom of the HMA at 5 km/hr speed.....	38
<b>Figure 3-5</b> Loading frequency determined from FFT for different response types. ....	40
<b>Figure 3-6</b> (a) Master curves at 20°C reference temperature and (b) shift factors. ....	42
<b>Figure 3-7</b> Variation of temperature at different depths within pavement. ....	43
<b>Figure 3-8</b> Comparison of stress frequency vs. speed in different methods. ....	46
<b>Figure 3-9</b> (a) Variation of $\sigma_v$ on top of GBC and, (b) $E_{est}$ and $E_{com}$ vs. speed. ....	48
<b>Figure 3-10</b> Comparison of modulus prediction errors for different approaches. ....	49
<b>Figure 4-1</b> (a) Aggregate gradation of asphalt mixes, (b) cross-section of instrumented test	

section at IRRF. ....	57
<b>Figure 4-2</b> Dilation and translation of the MHW against measured strain at 5 km/hr speed.....	59
<b>Figure 4-3</b> Typical CWT plot of longitudinal strain at 5 km/hr speed. ....	60
<b>Figure 4-4</b> Spectrogram of longitudinal strain at 5 km/hr speed. ....	62
<b>Figure 4-5</b> Variation of DF against speed using different approaches. ....	64
<b>Figure 4-6</b> Dynamic modulus master curves for (a) binder and (b) wearing layers; (c) shift factors as a function of temperature.....	66
<b>Figure 4-7</b> Measured and simulated strain pulse at 5 km/hr speed.....	68
<b>Figure 4-8</b> Comparison between predicted and measured responses. ....	69
<b>Figure 4-9</b> Comparison between $N_f$ values under considered approaches.....	72
<b>Figure 5-1</b> IRRF test sections, (a) schematic plan view and (b) instrumentation layout.....	81
<b>Figure 5-2</b> Example measured (a) vertical and (b) longitudinal strains under 570 kPa FWD stress level measured on June 5, 2015 .....	84
<b>Figure 5-3</b> Measured maximum peak (a) vertical strain, (b) longitudinal strain and (c) asphalt temperature profile.....	85
<b>Figure 5-4</b> Measured strains versus temperature. ....	86
<b>Figure 5-5</b> Haversine representation of normalized (a) vertical and (b) horizontal strains. ....	87
<b>Figure 5-6</b> Dynamic modulus master curve for binder and wearing layer at a reference temperature of 25°C.....	89
<b>Figure 5-7</b> Comparison between measurements and predictions of (a) vertical and (b) longitudinal strains.....	94
<b>Figure 5-8</b> Normalized (a) $N_f$ and (b) $RD_{HMA}$ versus different prediction models.....	97
<b>Figure 6-1</b> (a) Schematic of instrumentation, (b) Schematic cross-section and the EPC locations,	

(c) Installation of sensors at the bottom of the HMA. ....	104
<b>Figure 6-2</b> Comparison of deflection basins for different FWD tests.....	106
<b>Figure 6-3</b> Measured vertical stresses at (a) top of the GBC, (b) top of SG and (c) 1000-mm depth within SG. ....	109
<b>Figure 6-4</b> Measured (a) vertical strain and (b) horizontal strain at the bottom of HMA. ....	111
<b>Figure 6-5</b> Hysteresis curves for different FWD tests. ....	112
<b>Figure 6-6</b> (a) Master curve and (b) shift factor for the HMA, (c) Typical stress pulses at different depths for April, 2014 test.....	114
<b>Figure 6-7</b> Comparison of response prediction errors. ....	118
<b>Figure 7-1</b> (a) Pavement cross-section (b) Grain-size distribution of HMA at the IRRF.....	127
<b>Figure 7-2-</b> Plan view of the pavement monitoring test sections at the IRRF. ....	128
<b>Figure 7-3</b> Schematic of instrumentation at the bottom of the HMA. ....	129
<b>Figure 7-4</b> (a) Laboratory test setup (b) Schematic of data collection system. ....	131
<b>Figure 7-5</b> Variation of (a) $\varepsilon_l$ and (b) $\Delta\varepsilon_l$ from October 2013 to January 2015.....	133
<b>Figure 7-6</b> Variation of (a) $\varepsilon_t$ and (b) $\Delta\varepsilon_t$ from October 2013 to January 2015. ....	134
<b>Figure 7-7</b> Variation of (a) $\varepsilon_v$ and (b) $\Delta\varepsilon_v$ from October 2013 to January 2015. ....	136
<b>Figure 7-8</b> Monthly average fluctuation of thermal-induced strain.....	137
<b>Figure 7-9</b> Comparison of $\Delta\varepsilon_t$ against $\Delta\varepsilon_l$ at the bottom of the HMA.....	138
<b>Figure 7-10</b> Monthly average (a) $\varepsilon_l$ and $\varepsilon_t$ , (b) $\varepsilon_v$ from October 2013 to January 2015. ....	140
<b>Figure 7-11</b> Pavement and ambient temperature from August 2014 to January 2015. ....	142
<b>Figure 7-12</b> Thermal loading cycles and strain readings from (a) $\varepsilon_l$ (b) $\varepsilon_t$ and (c) $\varepsilon_v$ . ....	144

# Chapter 1 - Introduction

## **Statement of the Problem**

Pavement design has dramatically evolved from the empirical American Association of Highway Transportation Officials (AASHTO) 1993 Design Guide to the Mechanistic-Empirical Pavement Design Guide (MEPDG), also known as the AASHTOWare Pavement ME Design. The Pavement ME Design takes a leap forward in many aspects, including the consideration of site-specific design parameters, the damage accumulation prediction approach, as well as field calibration capabilities. Due largely to calculating fatigue and rutting damage, the Pavement ME Design procedure for Asphalt Concrete (AC) pavement incorporates response prediction models to predict the Hot Mix Asphalt (HMA) and unbound layers critical structural responses. The accumulated damage is then converted into tangible distresses, such as bottom-up fatigue cracking and rutting depth, via empirically calibrated transfer functions. Although response prediction models are commonly used for the purpose of pavement design, pavement engineers always concern themselves with accuracy and precision of such approaches.

Over the past few decades, pavement instrumentation has garnered continuous interest as a means to directly measure the pavement responses and verify the results of prediction models. As a result of this interest, several facilities, among which are the Penn State Test Track, Minnesota Road (MnRoad), Virginia Smart Road, and Ohio Test Road, have been developed and equipped with instrumentation over the years, and several experimental programs were dedicated to study and validate the predicted responses based on the in-situ measured responses. The theory of elasticity, so called the Multi-Layer Elastic Theory (MLET) in pavement engineering, is considered to be the most commonly used and state-of-the-art practice response prediction approach also adopted by MEPDG, even though different researchers have questioned its

accuracy (Ullidtz, 2000; Siddharthan et al., 2002 and Elseifi et al., 2006) One of the main simplifying assumptions of the MLET involves material behaviour. Modulus of HMA is assumed to behave linearly, while it is very well understood that HMA shows viscoelastic behaviours in response to temperature and loading frequency. Currently in the MEPDG, the viscoelastic behaviour of HMA is defined by complex modulus, and the loading frequency is defined as the inverse of loading time. Recently, concerns have been raised about the current practice for calculating loading frequency in the MEPDG. It is documented in the literature that the MEPDG approach can lead to frequency estimation errors of up to 140%, which in turn negatively affects the modulus estimation (Al-Qadi et al., 2008). Therefore, enhancing the traditional practices for calculating frequency is needed in order to improve the accuracy of response and performance prediction.

Despite the outstanding achievements made in previous full-scale test road studies in terms of pavement response measurement, there is still a viable need for monitoring and characterizing stress and strain magnitudes, especially for Canada's cold region pavements, which are prone to significant seasonal variation in material properties. To date, a limited number of facilities are capable of investigating the impact of environmental factors in the form of freeze/thaw cycles on the pavement response. In parallel, it is crucial to employ state-of-the art analysis tools such as Finite Element Method (FEM) in order to improve the response prediction accuracy compared with the prediction using conventional approaches. Also, it is essential to validate the prediction models by comparing the calculated responses with respect to the measured ones in the field.

## Research Objectives

The main goal of the study was to measure and model the response of the flexible pavement due to environmental loading and dynamic loading in the form of traffic loading and Falling Weight Deflectometer (FWD), as well as the seasonal variation of pavement responses during the year in a cold region such as Edmonton. In doing so, the pavement layers material properties in each season were defined based on laboratory and field characterization tests at corresponding environmental conditions. Also, the theoretical simulations were performed to model the in-situ measured responses in the field.

To achieve this objective, the following tasks were targeted:

- 1- Measure and evaluate the pavement responses due to controlled traffic loading and explore advanced and state-of-the art techniques to calculate the vehicular loading frequency.
- 2- Characterize the HMA moduli at different temperatures and frequencies in the laboratory; characterize the HMA and unbound layers moduli through FWD testing in the field.
- 3- Simulate the pavement responses using classical (MLET) and novel (FEM and 3D-Move) prediction models; verify the predicted ones by comparing them against the in-situ measured values.
- 4- Study the seasonal variation of pavement material moduli and structural responses during the year.
- 5- Investigate the direct impact of environmental conditions on the induced responses in the absence of traffic.

## **Scope of Work**

To achieve the objectives of this study, research was conducted at the Integrated Road Research Facility (IRRF), which is a full-scale instrumented test road located in Edmonton. The unique IRRF test track allows for the investigation of pavement dynamic responses during different seasons in a cold climate region via conducting periodic FWD tests and controlled truck loading. Also, pavement materials were characterized by conducting laboratory testing at different conditions for further use in numerical models. This way, stress, strain, and deflection measurements in the field can be used to validate the numerical models. Two pavement analysis software packages (KENLAYER and 3D-Move) and a general-purpose analysis package (ABAQUS) were employed to compute the responses within pavement. This study used pavement instrumentation and weather station data to measure the pavement environmental and ambient conditions, which helped explain the material behaviour in different seasons for the response modeling.

## **Structure of Dissertation**

This dissertation is prepared and presented in integrated-article format. Apart from the literature review and conclusions chapters, all chapters are related but separate journal papers which are published or under revision.

**Chapter 1** consists of an introduction to the conducted research and general explanation of the objectives and scope of the study.

**Chapter 2** is a quick overview of the surveyed literature on the impact dynamic loads and environmental factors have on pavement behaviour as well as the response prediction models.

**Chapter 3** discusses the measurement of traffic-induced pavement responses at IRRF through controlled vehicle testing, results of laboratory characterization of HMA, and application of Fast Fourier Transform (FFT) for determining loading frequency.

**Chapter 4** presents novel time-frequency domain analysis techniques to find the loading frequency of in-situ measured strains at the bottom of the HMA. The performance of such methods is also compared against widely used approaches via response calculation.

**Chapter 5** explains the results of field measurement when subjecting the pavement to FWD tests during the year 2015, backcalculation of layers moduli, and descriptions of three different analytical models implemented to predict pavement responses.

**Chapter 6** describes the seasonal variation of surface deflection, HMA strain, and unbound layers vertical stress based on the collected data from FWD tests carried out over the span of 2013 to 2014. In addition, this chapter elaborates on the prediction errors that resulted from modeling of the pavement system when using backcalculated sets of moduli.

**Chapter 7** provides the results of a long-term monitoring of the HMA strains induced merely by thermal loading in the field. It also contains the analysis of HMA thermal properties according to the field study.

**Chapter 8** is the summary of findings, conclusions, and recommendations for future studies.

# **Chapter 2 -Literature Review**

## **Pavement Response to Dynamic Loads**

Flexible pavement performance crucially depends on imposed traffic in the form of dynamic loading. With the aid of pavement instrumentation over the past few decades, along with continuous technological innovations, direct measurement of load-induced responses has become more accurate. Thus far, remarkable research efforts have been invested in dynamic response monitoring and measurement, and invaluable experimental data were provided at test road facilities worldwide. Still, this approach remains useful in that it allows for verification of theoretical assumptions and validation of computer models. Screening among a variety of pavement response studies revealed that load testing of the instrumented pavements is commonly undertaken by passing a truck under controlled conditions, as well as applying FWD tests, as discussed in the next section.

### **Vehicular Loading**

Extensive analytical and experimental investigations have been conducted to study pavement response due to dynamic loads, mainly through the Controlled Vehicle Loading (CVL) technique. The majority of the previous CVL studies have mainly focused on influential factors such as vehicle speed, weight, axle type, tire inflation pressure, wheel wander, etc., in order to evaluate the performance of pavement structure in different conditions (Sebaaly and Tabatabaee, 1992; Epps et al., 1998; Kennedy and Everhart, 1998; Gramsammer et al., 1999; Djakfar and Roberts, 2000; Loulizi et al., 2002; Lukanen, 2005). Among all the factors influencing stresses and strains, vehicle speed plays a significant role in the behaviour of pavement response, due in part to the viscoelastic nature of the HMA. For instance, in a study at the CPATT test road, the

impact of speed on longitudinal strain measured at the bottom of the HMA was investigated by conducting controlled vehicle tests at 5, 25, and 40 km/hr for a wheel load of 49 kN (Bayat, 2009). The CPATT study showed that measured strain increased by nearly 200  $\mu\text{m}/\text{m}$  when truck speed decreased from 40 to 5 km/hr. As illustrated in Figure 2-1, measurements of compressive vertical stress in the granular base layer at three speeds of 5, 25, and 40 km/hr resulted in larger stress pulse durations at lower speeds, which can result in different loading frequencies. Another study conducted at the Virginia Smart Road focused on investigating the impact of speed on vertical stress. Earth Pressure Cells (EPCs) installed at five different depths in the HMA, granular, and subgrade layers were used to measure the stress at truck speeds of 10, 25, 40, and 70 km/hr. It was found that stress pulse shape and therefore frequency of loading is a function of the depth below the pavement surface and vehicle speed (Loulizi et al., 2002).

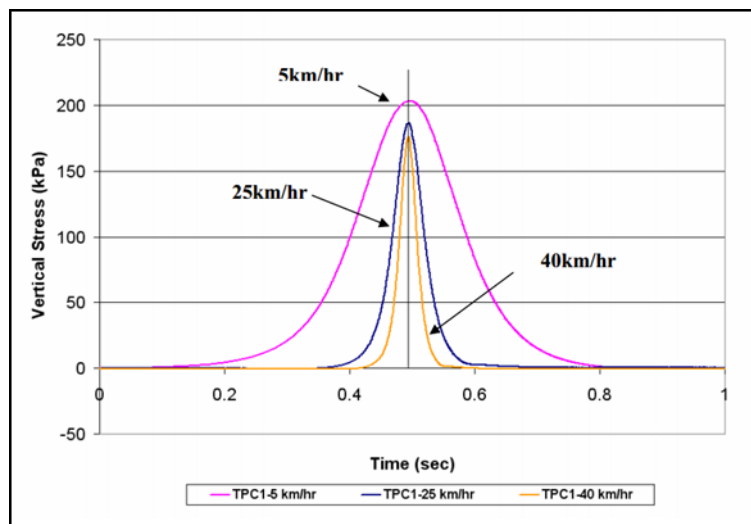


**Figure 2-1 The impact of speed on vertical stress pulse (Bayat, 2009).**

According to the reviewed literature, it is important to quantify the frequency of loading while pavement is subjected to moving vehicles at different speeds. Various researchers have investigated different approaches to accurately determine the corresponding frequency from traffic-induced stress or strain pulse duration (Al-Qadi et al., 2008; Ulloa et al., 2012; Dongre et al., 2006; Garcia and Thompson, 2008). As a matter of fact, the relations  $f=1/t$  and  $f=1/2\pi t$ , where  $f$  is the frequency in Hertz and  $t$  is time in seconds, are widely utilized for frequency calculation. The aforementioned relationships are traditionally categorized as the time-to-frequency conversion methods. Currently, MPEDG utilizes the relation  $f=1/t$  to convert the stress pulse duration to loading frequency (ARA, 2004). In the case of the longitudinal strain measured by Asphalt Strain Gauge (ASG), the pulse duration, defined for the tensile part of the strain (see Figure 2-2), can be converted to frequency using the time-to-frequency conversion methods in time domain (Garcia and Thompson, 2008).

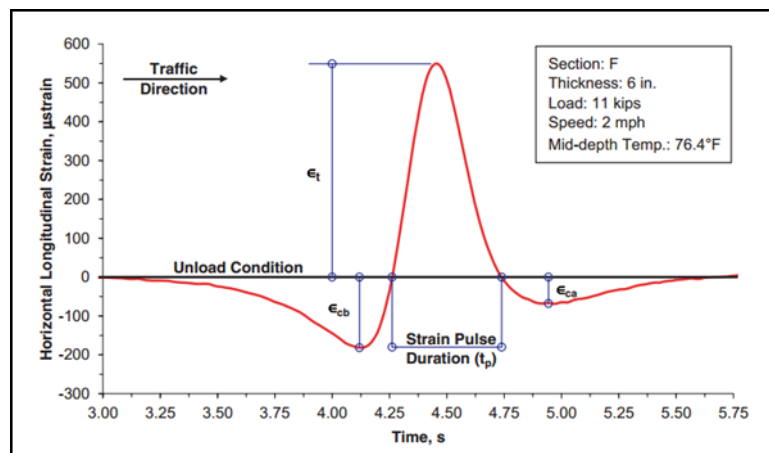
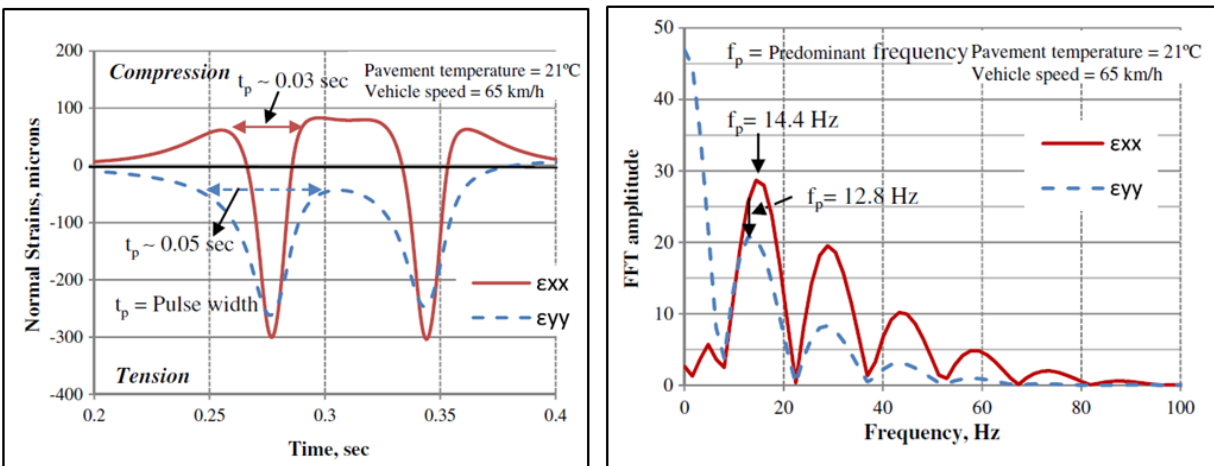


**Figure 2-2 Longitudinal strain pulse duration measured by ASG (Garcia and Thompson, 2008).**

Recently, researchers have suggested that converting the direct use of response pulse duration to frequency based on the traditional time-to-frequency conversion methods may not be reasonably accurate (Al-Qadi et al., 2008; Ulloa et al., 2012). In an effort to quantify the vehicular loading frequency based on field data, Fast Fourier Transform (FFT), as an analysis tool in frequency domain, was applied to the vertical stress pulses by Al-Qadi et al. (2008) to tackle some of the existing deficiencies of time-to-frequency conversion methods. By utilizing FFT to reveal the frequency content of the stress pulses captured at different vehicle speeds and depths from the surface, traditional analysis methods in time domain can result in 40–140% frequency calculation errors. Later, using the same technique, Ulloa et al. (2012) showed that the characteristics of different types of responses, such as strain in different directions, can be dissimilar in both time domain and frequency domain as illustrated in Figure 2-3. They also found that relying on the time domain analysis methods can ultimately lead to significant overestimation of pavement distresses, particularly bottom-up fatigue cracking.



(a)

(b)

**Figure 2-3 Representation of horizontal strains in (a) time domain and (b) frequency domain (Ulloa et al., 2012).**

However, the accuracy of frequency-domain analysis methods to obtain the loading frequency for moving loads has been a subject of controversy for the past several years. Therefore, researchers have raised the concern that more investigations are required to evaluate the subsequent impacts of FFT-determined frequencies on pavement response and performance predictions (Al-Qadi et al., 2008).

### **FWD Loading**

Non-destructive tests, including FWD testing, are widely used for structural evaluation and characterization of pavement layers moduli for flexible and rigid pavements (Shahin, 2005; Dore and Zubeck, 2008 and Haas et al., 2015). FWD exerts an impulsive load on top of the surface by dropping the specific weight from certain heights on top of the circular loading plate. Simultaneously, surface geophones record the produced deflection data at different lateral offsets from the loading plate as a result of the dynamic load, as shown in Figure 2-4. One of the main advantages of structural pavement instrumentation is to give more insight on the induced responses within the layers when subjected to external loading.



**Figure 2-4 FWD equipment during field testing.**

Several researchers have investigated flexible pavement response (i.e. stress, strain, and deflection) pulse under FWD tests in instrumented pavement sections (Akram et al., 1994; Mahoney et al., 1995; Appea et al., 2002; Loulizi et al., 2002; Ullidtz et al., 1994 and Solanki et al., 2009). Some of the most notable studies in this area are reviewed as follows. FWD tests were conducted at the Virginia Smart Road Facility in Montgomery County, Virginia, to evaluate the stress pulses captured by EPC(s) installed at different depths within the pavement. Figure 2-5 depicts a typical normalized vertical stress signal measured at a depth of 190.5 mm below the surface. Based on the measured stress pulses, it was found that different peaks are produced as a result of loading plate bouncing. Besides, it was noted that residual vertical stresses remain in the unbound material at the end of the unloading phase. This study also showed that the haversine function with a duration of 0.03 s can effectively approximate the measured stress pulses at different depths of the pavement and pavement temperatures.

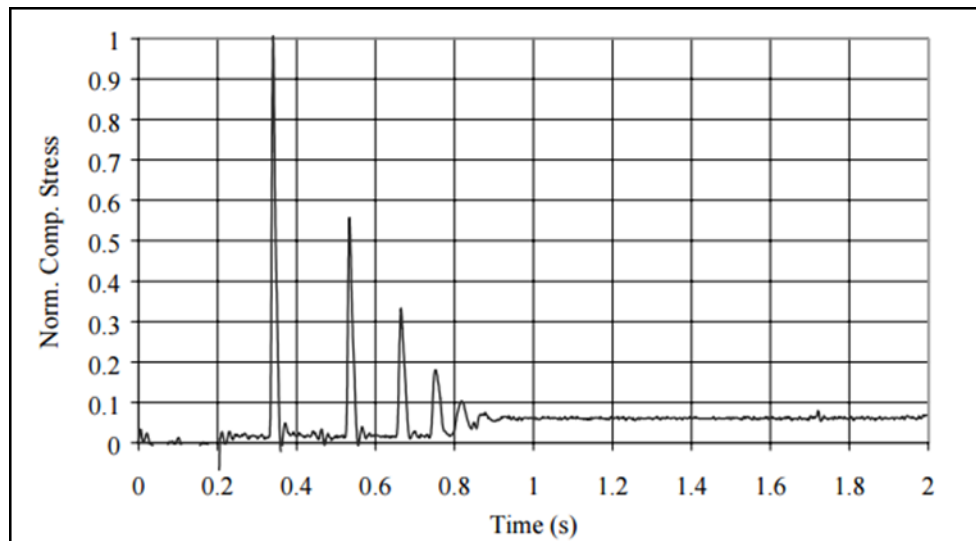


**Figure 2-5 Typical FWD-induced stress pulse (Loulizi et al., 2002).**

Akram et al. (1994) measured pavement deflection at different depths collected under FWD in two pavement sections located near Bryan, Texas. Analyzing the subgrade layer deflection recorded by Multi-Depth Deflectometers (MDDs) revealed that FWD tests' deflection pulse durations varied between 0.024 to 0.027 ms when the temperature of HMA was near 29.5°C. This study confirmed that the response duration caused by moving traffic is approximately six to seven times larger than that of the FWD. This study also showed that unlike the pulse duration for moving load, FWD pulse duration did not change with depth. At the Advance Transportation Research and Engineering Laboratory (ATREL) in Illinois, USA, FWD tests were conducted directly above ASGs in five different test sections with temperatures varying between 22.5 to 31.5°C (Garcia, 2007). Investigation of the FWD-generated tensile strain pulse indicated that the pulse shape was not symmetrical, as shown in Figure 2-6, and therefore the pulse duration was computed by doubling the rising time of the pulse.

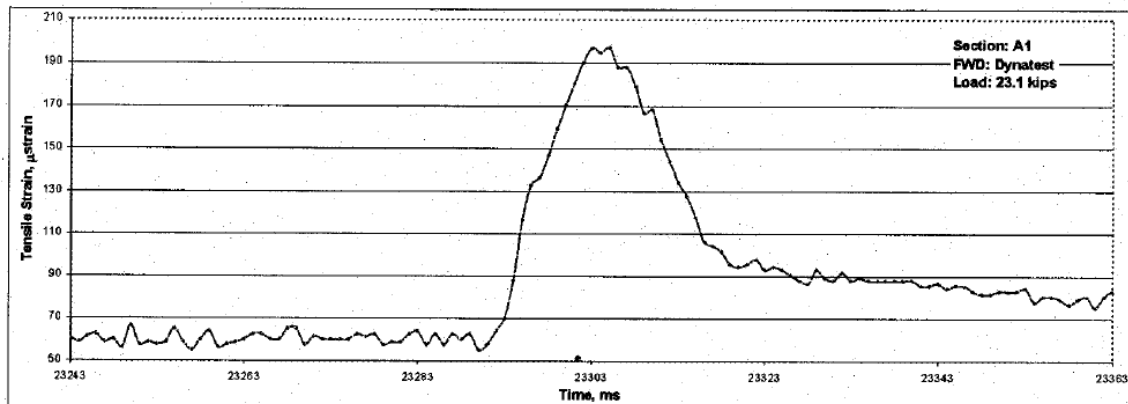


**Figure 2-6 Tensile strain pulse exclusive to the FWD load impact (Garica, 2007).**

Similarly, a study was carried out on the instrumented section of the National Center for Asphalt Technology (NCAT) test track to evaluate the asphalt strain measured at the bottom of the HMA in transverse and longitudinal directions. This study revealed that the longitudinal and transverse strains were not significantly different, possibly due to the symmetrical nature of the FWD exerted load. Results from this study indicated that the behaviour of asphalt strain is more consistent in the case of FWD loading rather than live traffic loading (Willis and Timm, 2009).

### **Environmental Impacts on Pavement Materials**

Flexible pavement performance strongly depends on its internal temperature and moisture conditions. Climatic factors, such as precipitation, temperature, freeze and thaw cycles, and depth to the water table, influence the internal temperature and moisture conditions in the pavement. Pavement material properties, such as heat capacity, surface shortwave absorptivity, thermal conductivity, susceptibility to moisture, and frost, also determine the internal temperature and moisture conditions. Generally, moisture and temperature are considered the two crucial environmental factors which affect the properties of pavement material. It is well-known that unbound materials, as in the base, subbase, and subgrade layers, are mainly affected by moisture condition. However, stiffness of bituminous materials including HMA layers is greatly affected by temperature change. The following sections discuss the importance of environmental factors as an influence on fundamental material properties in more detail.

## **Unbound Materials**

Internal moisture conditions can vary significantly in cold regions, where the pavement is exposed to seasonal freezing and thawing. During the winter, the formation of ice lenses in the subgrade and ice-bonding between the soil particles leads to stiffer unbound layers. Also, frost can penetrate into the pavement and when the frost front stretches to the frost-susceptible subgrade soil, moisture is drawn to the freezing front through capillary action and freezes in the form of ice lenses. This can increase the subgrade modulus due to the development of ice bonds between the soil particles and allow for higher strength of structure to withstand heavier loads.

The schematic in Figure 2-7 shows the annual variation in the base, subbase, and subgrade stiffness for a typical pavement. According to the figure, the critical period is when soil stiffness drops from its highest value in frozen conditions to its lowest value during thawing (Doré and Imbs, 2002). The melting ice becomes confined between the top and bottom frozen layers, and positive pore pressure is likely to occur in the soil depending on the soil drainability. Therefore, the effective stress in soil layers decreases and the bearing capacity of pavement is significantly reduced (Janoo, 2002). While the excess moisture drains out in late spring, water content decreases in the summer and the embankment surface dries out. Eventually, the amount of evaporation, which is maximized during summer, will decrease during fall, and higher precipitation induces moisture in the structure. This is followed by a recovery period, during which the pavement's stiffness recovers from its minimum level to a normal and stable level.

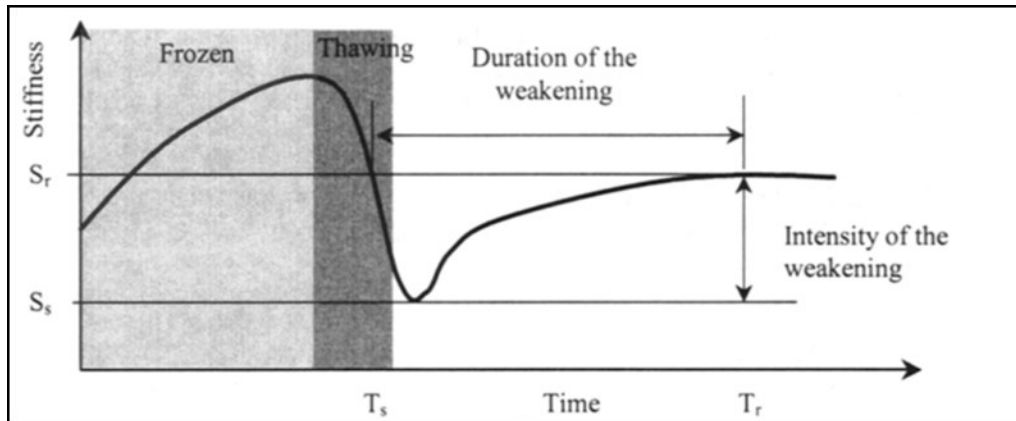


**Figure 2-7 Typical changes in the soil stiffness during the freeze and thaw periods (Doré and Imbs, 2002).**

Nondestructive testing of pavement in the form of a Falling Weight Deflectometer (FWD) test has been extensively used to measure pavement surface deflections during freeze and thaw cycles. Through backcalculating the layers moduli and studying its variation over the year, one can closely monitor the load bearing capacity of the structure as a function of climate condition. In a study conducted at the MnROAD, granular base and subgrade moduli were related to their moisture contents via laboratory tests. Using FWD backcalculation, researchers were able to characterize the variations in the base and subgrade layers stiffness against moisture content and establish seasonal trend factors (Ovik et al., 1999).

Due to seasonal changes in the unbound materials' properties, the FWD deflection basin shape and size varies depending on the layers conditions. During early thawing, when the underlying layers are still frozen, the width of the surface deflection basin is narrow and becomes wider and deeper when thawing is complete (Stubstad, 1982). The determination of frozen and unfrozen layers plays a significant role when backcalculating. Therefore, it may be necessary to consider sublayers in a single layer when both frozen and thawed portions exist in the layer in order to avoid modulus prediction errors. Hence, researchers have tried to include frost depth and frost

susceptibility characteristics of the subgrade material in modulus back analysis (Moore et al., 1969; Chamberlain, 1981).

Incorporating the moisture change effect on resilient modulus variation is a necessary step for mechanistic modeling of unbound layer properties. Thus, one can predict the changes in modulus due to change in moisture using available models, as seen in Table 2-1. Most of the soil resilient modulus prediction models capture the water content, stress, and degree of saturation as significant parameters affecting the resilient modulus. The stress level is taken into consideration mainly through bulk or octahedral stress. In addition, modulus-moisture relationships are mostly determined by performing compaction at optimum moisture content and maximum dry density.

### **Asphalt Materials**

In addition to internal moisture in the unbound layers, the internal temperature of the HMA layer influences flexible pavement performance. It is well established that the HMA is a viscoelastic material whose dynamic modulus is a function of temperature and loading rate. While other environmental factors such as moisture may have an impact on the unbound layers measured responses, temperature change is the dominant factor for bituminous material properties in the presence of suitable drainage.

In order to monitor seasonal variation of the HMA modulus, five Long-Term Pavement Performance (LTPP) program sections in Manitoba, located in dry-freeze zones, were studied by FWD testing. It was found that during the frozen period, surface deflections decreased in comparison to the equilibrium condition. Furthermore, the backcalculated HMA modulus was

**Table 2-1 Relationships between resilient modulus and soil parameters**

Equation	Parameters	Soil Type	Source
$\log M_R = c_1 + c_2(w\%) + c_3(S)$	$M_R$ =resilient modulus (psi) $w\%$ =percent water content $S$ =degree of saturation $c_i$ =regression constants	Fine-grained Subgrade	(Jones and Witczak, 1977)
$\log M_R = c_1 + c_2 S + c_3 PC + c_4 \log(\theta)$	$M_R$ =resilient modulus (psi) $PC$ =percentage compaction $c_i$ =regression constants $\theta$ =bulk stress(psi) $S$ =degree of saturation	Base/Subbase	(Rada and Witczak, 1981)
$M_R = 0.523 - 0.0225w + 0.544 \log(\theta) + 0.173SM + 0.197GR$	$M_R$ =resilient modulus (ksi) $w$ =water content $\theta$ =bulk stress(psi) $SM$ =silt factor, $GR$ =gravel factor	Coarse-grained	(Carmichael and Stuart, 1985)
$\log M_R = c_1 + c_2 \log(\theta) + c_3(w\%) + c_4(T) + c_5(\gamma_d)$	$M_R$ = resilient modulus (MPa) $\theta$ =bulk stress (kPa) $w\%$ =percent water content $T$ =temperature(°C) $\gamma_d$ =dry density(kg/ m <sup>3</sup> ) $c_i$ =regression constants	Coarse-grained subgrade	(Jin et al.,1994)
$M_R = k_1 f(w)^{k_2}$	$f(w)$ = Soil specific function for volumetric/gravimetric $k_1$ and $k_2$ = Soil specific regression coefficients	Frozen coarse-grained  Fine-grained subgrade	(Berg et al., 1996)
$M_{R(wet)} = M_{R(opt)} + \frac{dM_R}{dS} \Delta S$ $\frac{dM_R}{dS} = 1690 - 194(CLASS) - 11.2M_{R(opt)}$	$M_{R(wet)}$ =resilient modulus (MPa) $CLASS$ =AASHTO classification $\Delta S$ = change in post-compaction degree of saturation	Fine-grained Subgrade	(Drumm et al., 1997)

found to be linearly proportional to the mid-depth temperature of the HMA layer (Han et al., 1994).

The Minnesota study showed that the backcalculated modulus of the HMA increases during the winter months and decreases during the summer months. In addition, the backcalculated elastic modulus of the HMA generally increased as temperature at asphalt layer mid-depth decreased (Von Quintus and Simpson, 2002). In another study, it was found that the backcalculated HMA modulus for the LTPP sections located in freezing climate regions exceeded 30,000 MPa during the freezing season, as shown in Figure 2-8. Data showed that the HMA modulus in winter increased more than eight times with respect to its summer value (Salem et al., 2004). Similarly, different researchers have developed relationships between the HMA modulus and temperature, as shown in Table 2-2.

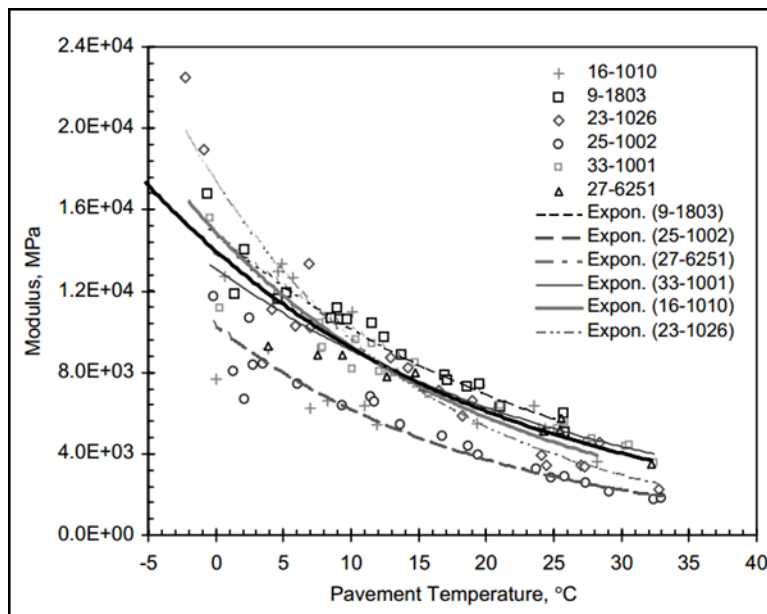


**Figure 2-8 Variation of HMA modulus due to temperature (Salem et al., 2004).**

**Table 2-2 Relationships between HMA modulus and temperature**

Equation	Parameters	Pavement Type	Source
$E_T = (3.177 - 1.673 \log T) E_{T_0}$	<p><math>E_T</math> = Asphalt modulus (MPa) at temperature T</p> <p>T = Pavement temperature (°C)</p> <p><math>E_{T_0}</math> = Asphalt modulus (MPa) at reference temperature</p>	AASHO road test data	(Ullidtz, 1987)
$E = (1 - 2.2 \log(\frac{T_{HMA}}{T_{ref}})) E_{ref}$	<p>E = HMA modulus (MPa) at <math>T_{HMA}</math></p> <p><math>T_{HMA}</math> = pavement temperature at 1/3 of depth (°C)</p> <p><math>T_{ref}</math> = pavement reference temperature (°C)</p> <p><math>E_{ref}</math> = reference modulus</p>	FWD test on Minnesota highways	(Stubstad et al., 1994)
$E = \exp(9.372 - 0.0361T)$	<p>E = HMA modulus (MPa)</p> <p>T = pavement temperature at 25 cm depth (°C)</p>	Texas LTPP sites	(Ali and Lopez, 1996)
$E = 16010 \exp(-0.0467T)$	<p>E = HMA modulus (MPa)</p> <p>T = pavement surface temperature (°C)</p>	Maine LTPP freeze/wet site	(Drumm and Meier, 2003)
$E_T = E_{25} \exp(0.031 \times (25 - T))$	<p><math>E_T</math> = HMA modulus (MPa) at temperature T</p> <p>T = HMA temperature (°C)</p> <p><math>E_{25}</math> = HMA modulus (MPa) at 25°C</p>	FWD tests at Virginia Smart Road	(Appea, 2003)
$\log(E) = 5.398 - 0.47T + 0.007H + 1.753B_{SG} - 0.420V + 0.469G_{RD}$	<p>E = HMA modulus (MPa)</p> <p>H = HMA layer thickness (mm)</p> <p><math>B_{SG}</math> = Bulk specific gravity of HMA</p> <p>V = percentage of air voids in the mix</p> <p><math>G_{RD}</math> = code for the binder grade</p> <p>T = pavement temperature (°C)</p>	LTPP freezing sites	(Salem et al., 2004)

Researchers have identified temperature as a critical factor, which significantly affects the horizontal strain response at the bottom of the HMA layer. Some of the existing relationships between temperature and HMA layers strain from the literature are listed in Table 2-3. As seen in Table 2-3, Al-Qadi et al. (2002) studied the transverse strain induced by the application of wide-base tires at the Virginia Smart Road and determined strain-temperature regression using exponential function. Later at the same test road, Loulizi et al. (2006) evaluated the effect of temperature on the horizontal tensile strain at two different speeds for a dual tire.

In another experimental program, Elseifi (2009) observed a strong agreement between the ambient temperature and the longitudinal strain at the Louisiana Accelerated Loading Facility experimental program. Elseifi also developed correction factors to shift the strain measurements at different test temperatures to a reference temperature. At the NCAT test track, Robbins and Timm (2008) characterized the tensile strain at the bottom of the HMA and reported that HMA mid-depth temperature correlated well with both the longitudinal and transverse strains. Similarly, at the Centre for Pavement and Transportation Technology (CPATT) test road located in Waterloo, Ontario, Bayat and Knight (2010) found an exponential relationship between the longitudinal strains and HMA mid-depth temperature.

Moreover, in the absence of traffic, measurements of strain caused by thermal loading at the Virginia Smart Road indicated that a very high strain range up to 350  $\mu\text{m}/\text{m}$  occurred during the spring season (Al-Qadi et al., 2005). This confirmed the importance a high stress-strain level in each cycle has in regards to thermal fatigue cracking, rather than the number of thermal loading cycles. Another study performed at the CPATT facility sought to quantify the longitudinal strains at the bottom of the HMA induced by thermal loading in a flexible pavement subjected to freeze and thaw cycles. It was found that an irrecoverable HMA longitudinal strain as high as 2,500

$\mu\text{m}/\text{m}$  existed at the bottom of the HMA layer over the course of the two-year study. This showed the severe effect of thermally-induced strains associated with thermal fatigue cracking in the HMA layer (Bayat et al., 2012).

**Table 2-3 Relationships between HMA strain and temperature**

Equation	Parameters	Pavement Type	Source
$\epsilon_{72\text{-km/hr}} = 8.567 \exp(0.1341T)$ $\epsilon_{8\text{-km/hr}} = 10.824 \exp(0.0784T)$	$\epsilon$ = Transverse strain ( $\mu\text{m}/\text{m}$ ) $T$ = Bottom of HMA layer temperature ( $^{\circ}\text{C}$ )	Strain under base asphalt mix layer under 5-kip wide base steering axle at 8 and 72 km/hr	(Al-Qadi et al., 2002)
$\epsilon_{72\text{-km/hr}} = 2.21 \exp(0.083T)$ $\epsilon_{8\text{-km/hr}} = 2.92 \exp(0.1155T)$	$\epsilon$ = Transverse strain ( $\mu\text{m}/\text{m}$ ) $T$ = Bottom of HMA layer temperature ( $^{\circ}\text{C}$ )	Stress under 39.5 kN dual tire load at different speeds Strain under 39.5 kN dual tire load at 8 and 72km/hr	(Loulizi et al., 2006)
$\epsilon = 6.584 \exp(0.0633T)$	$\epsilon$ = Longitudinal strain ( $\mu\text{m}/\text{m}$ ) $T$ = Ambient air temperature ( $^{\circ}\text{C}$ )	Strain under 105 psi dual tire at 10 mph	(Elseifi, 2009)
$\epsilon = 19.423 \exp(0.0275T)$	$\epsilon$ = Longitudinal strain ( $\mu\text{m}/\text{m}$ ) $T$ = HMA mid-depth temperature ( $^{\circ}\text{F}$ )	Strain under 20-kip single axle at 15, 25, 35, 45 mph	(Robbins and Timm, 2009)
$\epsilon = 95.452 \exp(0.048T)$	$\epsilon$ = Longitudinal strain ( $\mu\text{m}/\text{m}$ ) $T$ = HMA mid-depth temperature ( $^{\circ}\text{C}$ )	Strain under 49 kN dual wheel at 25 km/hr	(Bayat and Knight, 2010)

## Response Prediction Models

In 1880, Boussinesq developed a closed-form solution for determining two-dimensional stress, strain, and deflections at depth  $z$  and radial offset  $r$  for a concentrated load, applied on a single homogeneous, isotropic, and linear-elastic half-space. This solution method assumes stress-strain relationships based on the general Hooke's law as follows (Papagiannakis and Masad, 2008):

$$\begin{bmatrix} \sigma_z \\ \sigma_r \\ \sigma_\theta \\ \tau_{zr} \end{bmatrix} = \frac{E}{(1+\mu)(1-2\mu)} \begin{bmatrix} (1-\mu) & \mu & \mu & 0 \\ \mu & (1-\mu) & \mu & 0 \\ \mu & \mu & (1-\mu) & 0 \\ 0 & 0 & 0 & (\frac{1-2\mu}{2}) \end{bmatrix} \begin{bmatrix} \varepsilon_z \\ \varepsilon_r \\ \varepsilon_\theta \\ \gamma_{zr} \end{bmatrix} \quad (2-1)$$

$$\sigma_z = \frac{-P}{2\pi} \frac{3z^3}{(r^2+z^2)^{5/2}} \quad (2-2)$$

$$\sigma_r = \frac{-P}{2\pi} \left( \frac{3r^2z}{(r^2+z^2)^{5/2}} - \frac{1-2\mu}{r^2+z^2+z\sqrt{r^2+z^2}} \right) \quad (2-3)$$

$$\sigma_\theta = \frac{P}{2\pi} (1-2\mu) \left( \frac{z}{(r^2+z^2)^{3/2}} - \frac{1}{r^2+z^2+z\sqrt{r^2+z^2}} \right) \quad (2-4)$$

$$\tau_{zr} = \frac{P}{2\pi} \frac{3rz^2}{(r^2+z^2)^{5/2}} \quad (2-5)$$

Where:

$\sigma_z$ = Vertical normal stress,

$\sigma_r$ = Radial normal stress,

$\sigma_\theta$ = Tangential normal stress,

$\tau_{zr}$ = Horizontal shear stress in the radial direction,

$\varepsilon_z$ = Vertical normal strain,

$\varepsilon_r$ = Radial normal strain,

$\epsilon_{\theta}$  = Tangential normal strain,

$\gamma_{zr}$  = Horizontal shear strain in the radial direction,

P = Static point load magnitude,

$\mu$  = Material Poisson's ratio (defined as 0.5 to derive the equations).

Burmister developed solutions for two-layer, and later three-layer, systems by assuming linear elastic, homogeneous, isotropic, and weightless properties for the layers. The pavement structure subjected to circular uniform pressure was approximated with finite layers overlying an infinite lowest layer. Burmister defined the continuity conditions for two cases of bonded and unbonded (frictionless) interfaces (Burmister et al., 1944; Burmister, 1945). Based on the theory of elasticity developed by Love (1944), Burmister employed a stress function,  $\phi$ , for each layer to satisfy a fourth-order differential equation (equation of compatibility) using a Bessel function. Consequently, integration constants were determined from boundary conditions. Table 2-4 shows a summary of the general governing equations developed for multi-layer elastic systems.

In order to solve the differential equations for a multi-layered structure, different mathematical approaches, including inverse Hankel transforms, integral transformation techniques and transfer-matrix method, have been used in the past several decades (Huang, 2004). Multi-Layer Elastic Theory (MLET) has been extensively used for modeling flexible pavement structures and various computer programs, such as KENLAYER, BISAR, WESLEA, VESYS, CIRCLY, CHEVPC, EVERSTRESS, JULEA and ELSYM. These computer programs were developed to predict the responses for a flexible pavement structure. More information on the well-known MLET-based computer programs can be found in the literature (Haas et al., 2015).

**Table 2-4 General formulations for the multi-layer elastic system (Burmister, 1945).**

Quantity	Equation	Parameters
<b>Equilibrium</b>	$\frac{\partial \sigma_r}{\partial r} + \frac{\partial \tau_{rz}}{\partial z} + \frac{\sigma_r - \sigma_\theta}{r} = 0$	$\sigma_z$ = Vertical normal stress $\sigma_r$ = Radial normal stress $\sigma_\theta$ = Tangential normal stress
	$\frac{\partial \sigma_z}{\partial z} + \frac{\partial \tau_{rz}}{\partial r} + \frac{\tau_{rz}}{r} = 0$	$\tau_{rz}$ = Horizontal shear stress in radial direction $r$ = Radial distance $z$ = Depth
<b>Compatibility</b>	$\nabla^4 \phi = 0$ $\nabla^2 = \left[ \frac{\partial^2}{\partial r^2} + \frac{1}{r} \frac{\partial}{\partial r} + \frac{\partial^2}{\partial z^2} \right]$	$\phi$ = Stress function
<b>Stresses</b>	$\sigma_z = \frac{\partial}{\partial z} \left[ (2-\mu) \nabla^2 \phi - \frac{\partial^2 \phi}{\partial z^2} \right]$ $\sigma_r = \frac{\partial}{\partial z} \left( \mu \nabla^2 \phi - \frac{\partial^2 \phi}{\partial r^2} \right)$ $\sigma_\theta = \frac{P}{2\pi} (1-2\mu) \left( \frac{z}{(r^2+z^2)^{\frac{3}{2}}} - \frac{1}{r^2+z^2+z\sqrt{r^2+z^2}} \right)$ $\tau_{rz} = \frac{\partial}{\partial r} \left[ (1-\mu) \nabla^2 \phi - \frac{\partial^2 \phi}{\partial z^2} \right]$	$\mu$ = Poisson's ratio $P$ = Point load magnitude
<b>Displacements</b>	$w = \frac{1+\mu}{E} \left[ (1-2\mu) \nabla^2 \phi + \frac{\partial^2 \phi}{\partial r^2} + \frac{1}{r} \frac{\partial \phi}{\partial r} \right]$ $u = - \frac{1+\mu}{E} \left[ \frac{\partial^2 \phi}{\partial r^2} \right]$	$w$ = Settlement $E$ = Elastic modulus $u$ = Horizontal displacement

An extensive amount of research work has been devoted to studying the accuracy of MLET-based programs. Examining the performance of two computer programs, namely ELSYM5 and CIRCLY, at Canterbury Accelerated Pavement Testing Indoor Facility (CAPTIF) in New

Zealand revealed a sufficiently accurate prediction of vertical soil strain. Additionally, the subgrade layer strain calculated using CIRCLY was found to be more reasonable than results obtained from ELSYM5 as CIRCLY is capable of incorporating material anisotropy and can therefore better characterize subgrade plastic behavior (Saleh et al., 2003). For the Virginia Smart Road, MLET-predicted responses were validated with actual measured pavement response. This study depicted a strong agreement between the asphalt strain measured at the bottom of the HMA and its counterpart calculated by several computer programs, such as KENLAYER, ELSYM5, EVERSTRESS 5.0 and BISAR 3.0, under single and dual tire loading. However, results showed that MLET predictions underestimate and overestimate pavement responses at high temperatures and low/intermediate temperatures, respectively (Loulizi, 2006).

Considering the actual nonlinear stress-strain behaviour of unbound materials, linear elastic theory has been modified using iterative methods to account for variation of modulus with depth by finding new sublayer moduli based on the solved stress from initial moduli. Similar processes were repeated until moduli values converged to a constant value under a specified tolerance (Kasianchuk, 1968). Modeling of nonlinear materials within the KENPAVE computer program as a multi-layer system showed precise prediction of field measured deflection basin (Huang, 2004). However, due to the constraint of axisymmetric in MLET, it is difficult to introduce nonlinearity, which is the variation of modulus at different depths in layered elastic models (ARA, 2004).

Finite Element Method (FEM) is a numerical analysis technique in which the physical system is discretized into finite elements, interconnected with nodes, and assigned with specific behaviour equations. In this method, the unknown variables are expressed using appropriate algebraic governing functions, and the behaviour of each material under the applied loads is defined with

constitutive models. Finally, boundary conditions specifying the constraints of the system are applied to the problem and the unknown variables are calculated using different mathematical solution methods (Desai, 1979). FEM is broadly adopted in pavement analysis. This is mostly due to the restrictions of MLET solutions, including consideration of realistic material behaviour, modeling of actual wheel load contact pressure, and calculation of pavement response in two-dimensional axisymmetric problems (ARA, 2004).

A comparison of static 2D linear elastic FEM with a dynamic 3D viscoplastic FEM showed that the 3D model could predict the in-situ measured pavement response more accurately than the 2D model. The results also showed that maximum longitudinal and transverse stresses at the bottom of the AC layer predicted using the 3D viscoplastic model were smaller than the corresponding values provided by a 2D model, which simulates asphalt concrete as a linear elastic material (Huang et al., 2001). Using ABAQUS software at CAPTIF showed that the 3D model's results reasonably agreed with the actual strain measurements in the subgrade. This is because ABAQUS is capable of employing elastic-plastic behaviour of bituminous material in modeling (Saleh et al., 2003). In another study conducted at Virginia Smart Road, MichPave 2D and ABAQUS were utilized to simulate the pavement responses. This study showed that FEM based on viscoelastic behaviour of HMA and linear elastic properties of unbound materials could effectively predict the variation of the tensile strain at the bottom of the HMA under different temperature scenarios. However, the predicted vertical stress at the bottom of the HMA was found to be higher than the measured values by EPCs (Loulizi et al., 2006).

# **Chapter 3 -Analysis of Loading Frequency in Flexible Pavement Using Fast Fourier Transform**

A version of this chapter was published by International Journal of Pavement and Research Technology in November 2015.

## **Abstract**

Accurate calculation of traffic loading frequency plays a major role in mechanistic design of flexible pavements. Previous studies have highlighted the need for a paradigm shift in determining frequency through frequency domain analysis rather than conventional time domain-based methods. However, limited studies have experimentally investigated the impact of contributing factors including response type, depth and vehicle speed on calculated frequencies in frequency domain approach. This paper presents the results of controlled vehicle testing that focused on frequency analysis of in-situ measured pulses using Fast Fourier Transform (FFT). The tests were conducted in the Integrated Road Research Facility (IRRF) in Edmonton, Alberta, Canada. Longitudinal, transverse and vertical strains at the bottom of the Hot Mix Asphalt (HMA), as well as the vertical stresses recorded at different depths within unbound layers, were taken into account for this purpose. This study showed that dominant frequencies associated with longitudinal strain were the highest amongst those of other considered responses. Besides, the impact of speed and depths on obtained frequencies were clearly reflected. Finally, comparisons were made between the accuracy of HMA dynamic modulus prediction when using FFT-calculated frequency versus using of four well-established frequency calculation methods in time domain.

**Key words:** *Loading frequency, Fast Fourier Transform, Dynamic modulus, Pavement response.*

## Introduction

Hot Mix Asphalt (HMA) is a composite material whose viscoelastic behavior is highly dependent on temperature and loading frequency. It is well-documented in the literature that asphalt mix tends to exhibit linear behavior under lower temperatures and higher loading frequencies while its viscous behavior is more pronounced when it is subjected to higher temperatures and lower loading frequencies (Huang, 2004). According to Mechanistic- Empirical Pavement Design Guide (MEPDG) (ARA, 2004), it is crucial to experimentally characterize the viscoelastic behavior of HMA by developing a master curve for HMA dynamic modulus,  $|E^*|$ , through frequency sweep tests at different temperatures. It is also known that  $|E^*|$  master curve is determined in the lab in frequency domain, while pavement is in fact subjected to the moving vehicles in time domain. As a result, various researchers have investigated different time-to-frequency conversion methods to accurately calculate the related frequency from traffic-induced stress or strain pulse duration (Ferry, 1980; ARA, 2002; Dongre et al., 2006). Among these conversion approaches, the relations  $f=1/t$  and  $f=1/2\pi t$ , where  $f$  is the frequency in Hz and  $t$  is time in s, are widely utilized for frequency calculation. For instance, the MPEDG adopts Odemark (1940) approach to find the pulse duration and converts it to frequency using the relation  $f=1/t$ . However, recent studies have shown that the direct use of response pulse duration and converting it to frequency based on aforementioned methods in time domain can result in erroneous estimation of frequencies which can consequently affect the  $|E^*|$  (Al-Qadi et al., 2008; Ulloa et al., 2012). Al-Qadi et al. (2008) examined the accuracy of the MEPDG's frequency calculation method with respect to the frequencies obtained from Fast Fourier Transform (FFT) in frequency domain at the Virginia Smart Road. Using stress pulses recorded at two different depths under three vehicle speeds of 8, 24 and 40 km/hr, frequencies obtained based on the

MEPDG method were more than 2 times larger than those of FFT method. This study showed that using Odemark approach and conventional time-to-frequency conversion method are the possible sources of error when finding frequency in time domain.

In addition, vehicular loading induces different pulses across the asphalt layer including longitudinal, transverse and vertical strains along with vertical stress. Finding the asphalt modulus as close as possible to the modulus that produces the in-situ measured responses plays a significant role in design and performance of pavement. Due to the inherent differences between response components under traffic loading in term of pulse shape and durations, evaluation of the associated frequencies for different response types is of utmost importance. Ulloa et al. (2012) used theoretically-determined stress and strain pulses obtained from 3D-Move software (Siddharthan, 1998) to investigate the impact of response type on the calculated frequencies in frequency domain. Results from this study showed that different predominant frequencies associated with longitudinal, transverse and vertical strains at the bottom of the HMA should be considered for the pavement analysis.

Reviewing the aforementioned literature reveals that relying on existing time-to-frequency conversion methods in time domain can lead to inaccurate frequency estimation. Considering the paradigm shift of computing the frequency in frequency domain rather than time domain, this paper focuses on the impact of such influential factors as vehicle speed, response type and analysis depth on the obtained frequencies through the field study. The present study was conducted at Integrated Road Research Facility (IRRF)'s test road facility in Edmonton, Alberta, Canada and several in-situ measured response pulses were analyzed to quantify the effect of using different approaches to  $|E^*|$  prediction error.

# Experimental Program

## Integrated Road Research Facility

The IRRF's test road facility which connects the Edmonton Waste Management Centre (EWMC) to the Anthony Henday Drive (HWY 216) is located in the Northeast of the City of Edmonton, Alberta, Canada. The pavement cross section consists of 90-mm wearing layer, 160-mm binder layer on top of a 450-mm granular base course (GBC) on top of clayey sand subgrade soil (SG). Figure 3-1 shows the particle size distribution of the HMA mixes containing Reclaimed Asphalt Pavement (RAP) which were produced using PG 58-28 virgin asphalt binder. The wearing layer possessed a maximum aggregate size of 12.5 mm, while the maximum aggregate size was 25 mm for the binder layer.

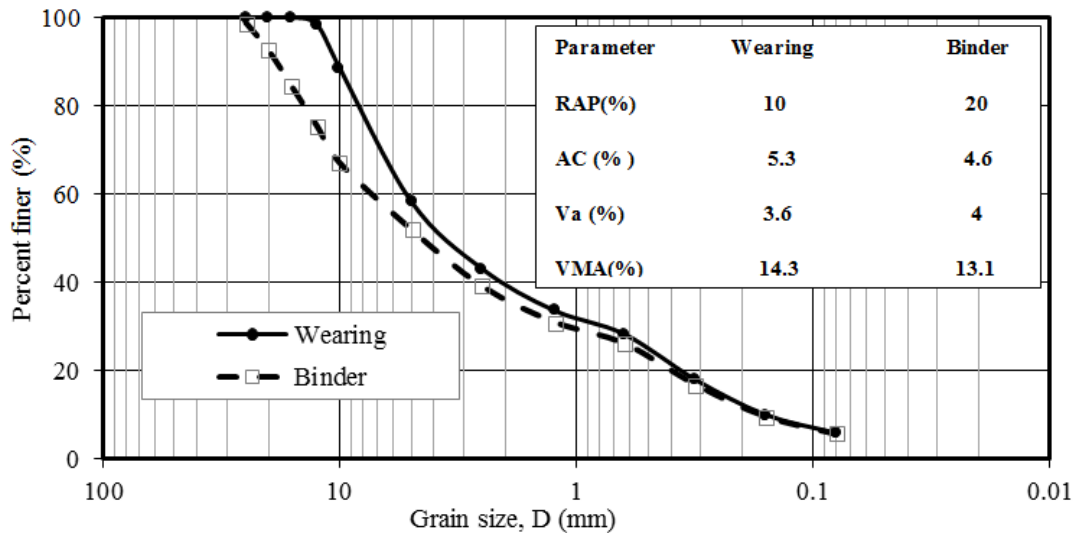
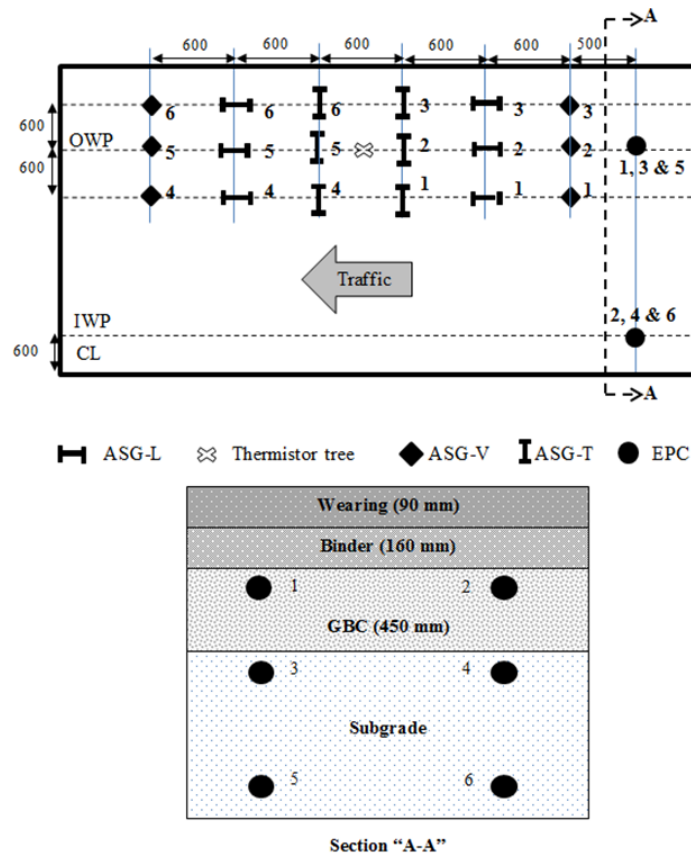


Figure 3-1 Gradation and physical properties of HMA mixes at IRRF.

There are two 20-m long monitoring sections in the test road approximately 100-m apart that are thoroughly instrumented to study the road response to traffic and environmental loading. Asphalt Strain Gauges (ASGs) and Earth Pressure Cells (EPCs) were used to collect the dynamic data at 500 Hz utilizing a high-speed CR9000X datalogger from Campbell Scientific Corp Canada<sup>®</sup>. Horizontal and vertical ASGs, supplied by Construction Technology Laboratories Inc. (CTL), were 350 ohm full-bridge sensors which were individually calibrated by the manufacturer. Also, LPTPC-S (4-20mA signal output) EPCs from RST Instruments, contained silicone strain gauge transducer and were originally calibrated by the manufacturer. Both control sections were similarly instrumented with ASGs at the bottom of the HMA layer in longitudinal, transverse and vertical direction named as ASG-L, ASG-T and ASG-V, respectively. As depicted in Figure 3-2, one array of ASGs was laid along the outer wheelpath (OWP) in parallel with two other arrays at 600-mm lateral offsets to ensure the repeatability of the measurements. EPCs were also installed on the OWP and on the inner wheel path (IWP) at three different depths within the unbound layers.



**Figure 3-2 Instrumentation layout and pavement cross-section (all dimensions are in mm).**

### Field Study

A controlled vehicle testing was carried out at the IRRF’ test road facility on August 14, 2014 using a two-axle dual tire single unit truck. The center-to-center distance between tires on the steering axle and rear axle was 2,070 mm and 1920 mm, respectively. The rear axle was loaded to 40.69 kN and the steering axle weighed 25.00 kN. Besides, the tire inflation pressure was measured equal to 870 kPa. The test runs were conducted at Section 2 of the IRRF starting from 2:30PM to 4:00PM and the HMA temperature at 20-mm depth below the surface varied between 34.1°C and 37.6°C. Seven target speeds of 5, 10, 20, 30, 40, 50 and 60 km/hr were included in the experiment along the OWP. The runs were repeated at the seven target speeds in five

replicates, resulting in a total of  $7 \times 5 = 35$  runs. Using an installed side-vehicle camera, videos were recorded during each run to check the wheelpath relative to OWP to ensure accuracy. The pressure measurement obtained from EPC (1), (3) and (5) as well as the strains recorded by ASG-V (2), ASG-L (2) and ASG-T (2) were considered for the analysis in this paper. It is noteworthy that this research focuses on the response pulses collected under the dual tire on the rear axle of the vehicle.

## **Analysis of Loading Frequency**

### **Fourier Representation of Pulses**

Fourier transform of a function  $f(t)$  in time domain can be expressed as  $F(\omega)$  described in frequency domain using complex exponentials based on Equations 3-1 and 3-2 (Wong, 2011).

$$F(\omega) = \int_{-\infty}^{+\infty} f(t)e^{-i\omega t} dt \quad (3-1)$$

$$e^{-i\omega t} = \cos(\omega t) - i \sin(\omega t) \quad (3-2)$$

For the case of discrete data or a digital signal, Discrete Fourier Transform (DFT) can be used to determine the frequency content of the given signal according to Equation 3-3.

$$F[m] = \sum_{n=0}^{N-1} f[n] e^{-i2\pi mn/N}, \quad m = 0, 1, \dots, N - 1 \quad (3-3)$$

where  $N$  is the total number of data points for a signal denoted as  $f[n]$ . On the other hand, FFT is an algorithm which facilitates the computation of the DFT especially in the computer programs.

In this paper, frequency analysis of stress and strain pulses was performed using built-in FFT routine in Microsoft Excel<sup>®</sup>. The FFT routine in Microsoft Excel<sup>®</sup> restricts the number of data in the time-domain to a power of 2 including 1024 and 2048. Therefore, all the FFT analyses in this paper were performed based on 2048 number of data points collected at 0.002 s intervals. As the FFT outputs are in the form of complex numbers, the magnitude of the FFT outputs were calculated and then normalized with respect to the initial value.

Figure 3-3 (a) shows the typical measured stress ( $\sigma_v$ ) pulses for the vehicle speed of 5 km/hr which were normalized relative to their peak values. The  $\sigma_v$  pulses clearly showed longer durations with the increase in depth. Figure 3-3 (b) depicts the corresponding normalized FFT magnitudes of the  $\sigma_v$  pulse in which frequency domain shapes were observed at different depths.

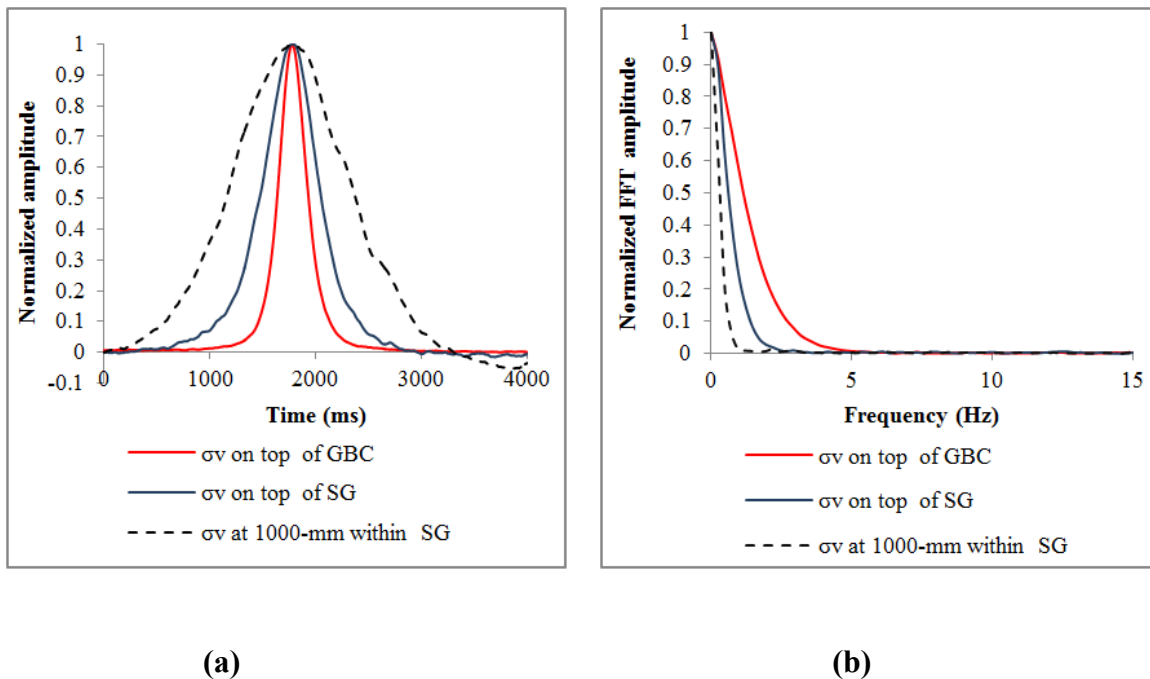


**Figure 3-3 (a) Time domain and (b) frequency domain of measured stress pulses at 5 km/hr speed.**

It was found that the area under the generated frequency spectrums tended to decrease at deeper elevations. However, contributions of the higher frequencies were more noticeable for the  $\sigma_v$  on top of GBC layer in comparison to those of subgrade layer.

Figure 3-4 (a) also shows the typical normalized strain pulses captured at the bottom of the HMA under the speed of 5 km/hr. While the strain in the longitudinal direction ( $\epsilon_l$ ) followed a compressive-tensile-compressive behavior, the transverse ( $\epsilon_t$ ) and vertical ( $\epsilon_v$ ) strains showed tensile and compressive behaviors, respectively. As presented in Figure 3-4 (b), the loading frequency spectrum associated with  $\epsilon_l$  has a local maximum at approximately 1.5Hz, while  $\epsilon_t$  and  $\epsilon_v$  exhibited decreasing trends of FFT amplitude against frequency. The observed frequency spectrums confirm that the frequency calculation under moving load heavily depends on the response type, as it will be discussed in the next section.

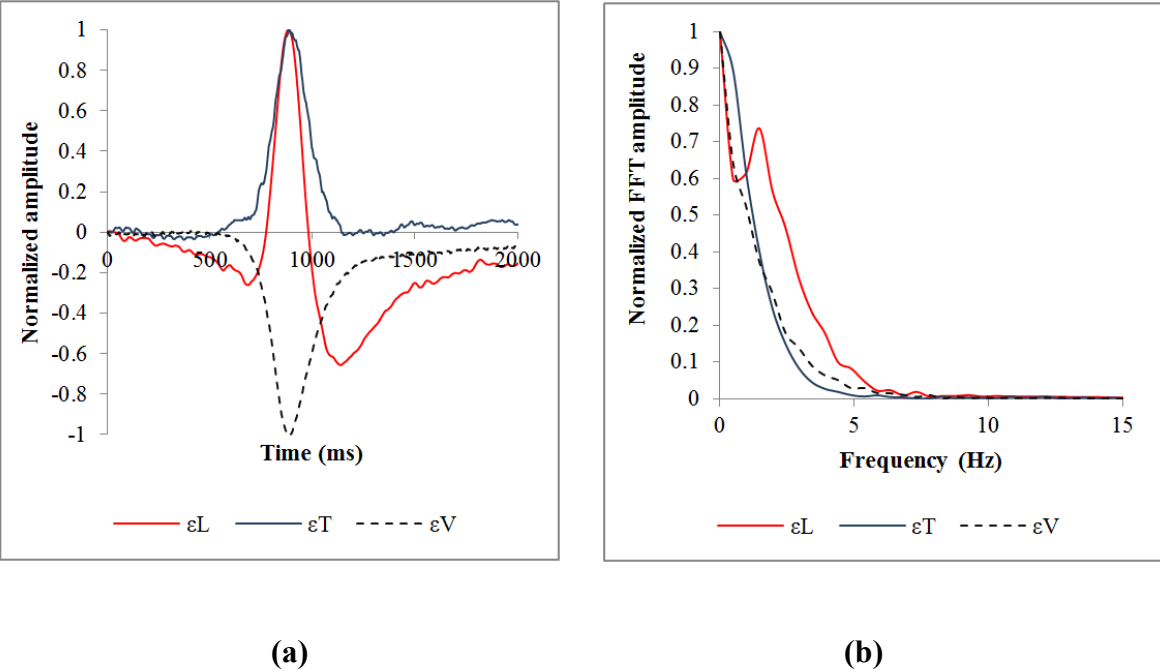


**Figure 3-4 (a) Time domain and (b) frequency domain of measured strain pulses at the bottom of the HMA at 5 km/hr speed.**

### Effect of Response Type, Depth and Speed

To investigate the effects of contributing factors on the calculated loading frequency, frequency spectrums were analyzed for the six responses at each speed. Therefore, the dominant frequencies (DF) were extracted via finding the center of mass of the frequency spectrums as recommended by Al-Qadi et al. (2008). The extracted DF values were then averaged for the five replicates and plotted against the corresponding speeds as shown in Figure 3-5. The fitted power regression models are also represented in Table 3-1 where vehicle speed ( $V$ ) in kilometer per hour is related to DF in Hertz. According to Table 3-1, the power regression models were highly accurate as the calculated  $R^2$  values varied from 0.97 to 0.99, and  $S_e/S_y$  values for all models fell below 0.3.

**Table 3-1 Relationships between dominant frequency and vehicle speed.**

Location	Regression equation	$R^2$	$S_e/S_y$
<b>Bottom of HMA</b>	$DF (\varepsilon_l) = 1.165V^{0.45}$	0.97	0.20
	$DF (\varepsilon_t) = 1.158V^{0.40}$	0.97	0.18
	$DF (\varepsilon_v) = 0.607V^{0.50}$	0.99	0.07
<b>Top of GBC</b>	$DF (\sigma_v) = 0.482V^{0.62}$	0.99	0.05
<b>Top of SG</b>	$DF (\sigma_v) = 0.415V^{0.58}$	0.99	0.11
<b>1-m within SG</b>	$DF (\sigma_v) = 0.337V^{0.57}$	0.99	0.15

Results from Figure 3-5 confirm that DF for all stresses and strains increased at higher vehicle speeds, while the impact of speed on DF was more pronounced at lower depths. A reasonable agreement between DF values of  $\epsilon_v$  at the bottom of the HMA and those of  $\sigma_v$  on top of the GBC was notable, implying the similarity between vertical stress and strain frequency at approximately the same depths. Besides, comparison between the corresponding DF values of  $\sigma_v$  at three different depths clearly illustrates that the difference between frequencies was more noticeable at higher speeds. From the analysis of DF values at the bottom of the HMA, it was found that the highest frequencies were associated with  $\epsilon_l$  in which DF value as high as 7.5 Hz was calculated at 60 km/hr vehicle speed. On the other hand, the different DF of HMA strain pulses in three directions demonstrates that the anisotropic properties of HMA needs to be taken in to account when simulating flexible pavement response to moving loads.

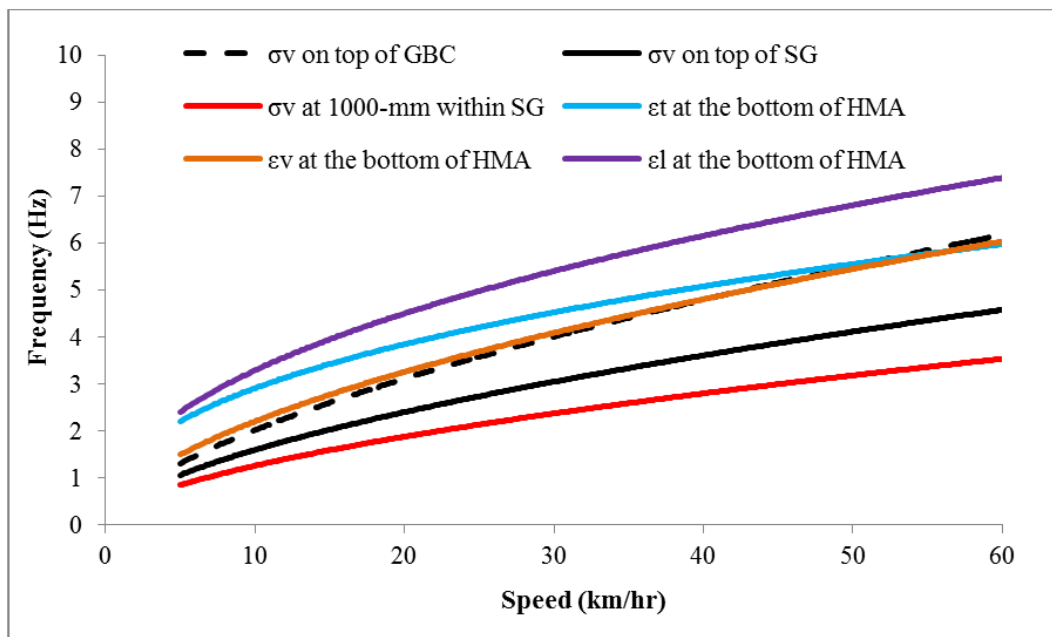


**Figure 3-5 Loading frequency determined from FFT for different response types.**

## Accuracy of Dynamic Modulus Prediction

### Dynamic Modulus from Laboratory

Due to the viscoelastic properties of HMA,  $|E^*|$  strongly depends on the loading frequency and temperature. Laboratory tests were conducted to determine the dynamic modulus for both wearing and binder layers according to AASHTO TP79 (AASHTO, 2009a). To do so, Superpave gyratory compactor was used to prepare 150-mm-diameter by 170-mm-height cylindrical specimens representing the test road mixes. These samples were later cored and cut to 100-mm-diameter by 150-mm-height specimens for dynamic modulus test. Dynamic modulus tests were carried out at temperatures of -10, 4, 20 and 35°C and frequencies of 10, 5, 2, 1, 0.5, 0.2, 0.1 and 0.01 Hz in order to develop the master curves based on AASHTO PP61 (AASHTO, 2009b). Figure 3-6 (a) depicts the constructed master curves, in which the binder course showed higher dynamic modulus compared to the wearing course considering its coarser aggregate gradation, lower bitumen content and higher RAP content. Additionally, the resulting shift factors are illustrated in Figure 3-6 (b). To later determine the  $|E^*|$  at field temperature based on experimental master curves, temperatures from asphalt thermistors embedded at different depths within wearing and binder layers were used.

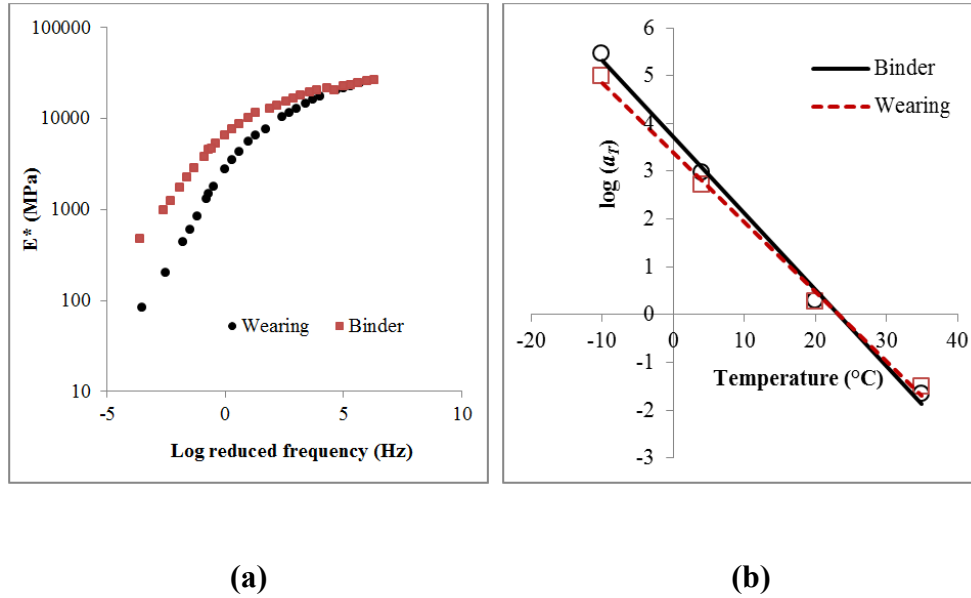


**Figure 3-6 (a) Master curves at 20°C reference temperature and (b) shift factors.**

Figure 3-7 presents the temperature profile of the HMA obtained from the field thermistors during the controlled vehicle testing. The average temperature across wearing and binder layers were determined equal to 34°C and 31°C, respectively. By applying the laboratory-established shift factors, the obtained  $|E^*|$  values at the reference temperature of 20°C were converted to the ones at the field temperatures for further analysis of  $|E^*|$  variation at different frequencies.

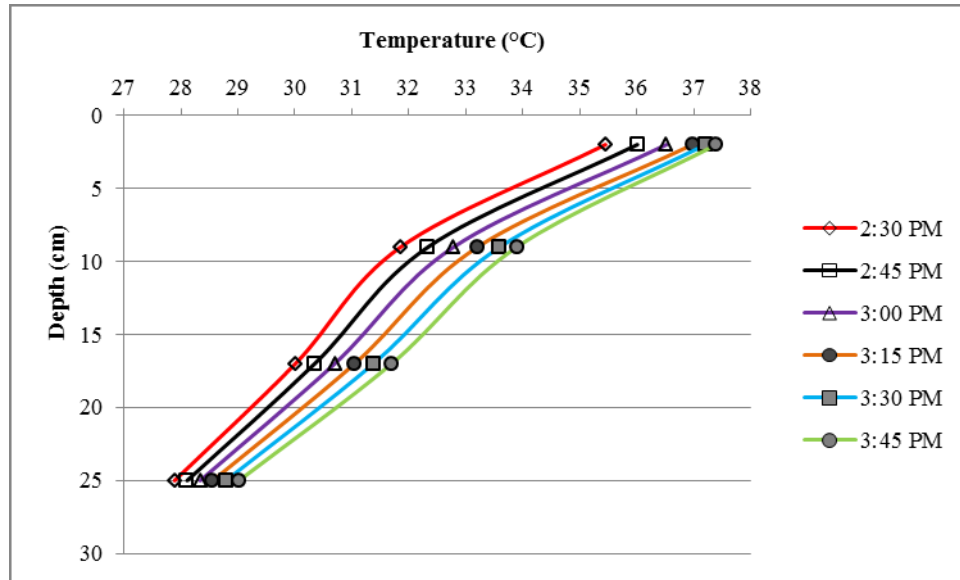


**Figure 3-7 Variation of temperature at different depths within pavement.**

### **Impact of Frequency Calculation Method on Dynamic Modulus**

To evaluate the accuracy of FFT-calculated frequencies in terms of  $|E^*|$  prediction and compare the DF values against other major frequency determination methods in time domain, different scenarios were defined as presented in Table 3-2. According to Table 3-2, four well-established frequency determination methods (cases 1 to 4) in the time-domain were selected from the literature and response pulse durations were converted to frequencies for each speed. Case 5 also demonstrates the adopted frequency calculation method in this paper which works according to the frequency spectra analysis. Among the defined cases, case 4 represents the current practice in the MEPDG for estimation of loading frequency. As presented in Table 3-2, the frameworks of frequency calculation in cases 1 to 4 consist of, firstly, finding the response pulse duration and, secondly, transforming it to frequency. Even though, the first step in cases 1 and 2 employ the actual in-situ measured pulse duration, cases 3 and 4 apply predictive equations to find the pulse duration. Moreover, pulse duration from in-situ measurements were converted to frequency

using both  $f=1/t$  in case 1 and  $f=1/2\pi t$  in case 2 in an effort to compare the resultant frequencies. However, cases 3 and 4 require that time-to-frequency conversion be conducted using  $f=1/2\pi t$  and  $f=1/t$ , respectively, as shown in Table 3-2.

**Table 3-2 Frequency calculation scenarios considered in this study.**

Methods	Loading Time	Loading Frequency	Parameters	Source
<b>Case 1</b>	t=In-situ measured pulse duration	$f=\frac{1}{t}$	t = loading time (s) f = loading frequency (Hz)	(ARA, 2004)
<b>Case 2</b>	t=In-situ measured pulse duration	$f=\frac{1}{2\pi t}$	t = loading time (s) f = loading frequency (Hz)	(Ferry, 1980)
<b>Case 3</b>	Log (t)=0.5 h-0.2-0.94 log(v)	$f=\frac{1}{2\pi t}$	t = loading time (s) h = depth (mm) v = speed (mm/s) f = loading frequency (Hz)	(Brown, 1973)
<b>Case 4</b>	$t=\frac{L_{eff}}{17.6 V}$ $L_{eff}=2(a_c+Z_{eff})$ $Z_{eff}=\sum_{i=1}^{n-1}(h_i\sqrt[3]{\frac{E_i}{E_{SG}}})+h_n\sqrt[3]{\frac{E_n}{E_{SG}}}$	$f=\frac{1}{t}$	t = loading time (s) $L_{eff}$ = Effective length (in) V= speed (mph) $a_c$ = radius of contact area (in) $E_{SG}$ = modulus of subgrade n= number of layers $h_n$ = thickness of the layer of interest (in) $E_n$ = modulus of the layer of interest (psi) f = loading frequency (Hz)	(ARA, 2004)
<b>Case 5</b>	Loading pulse in time domain	Frequency spectra using FFT	Not Applicable	-

Since the recommended procedures in cases 3 and 4 rely on the stress pulse duration, the frequency calculations were performed focusing on  $\sigma_v$  on top of GBC in order to be consistent across all methods. In this analysis, the pulse duration was defined by doubling the elapsed time between the beginning of the stress pulse to its peak. It is worth noting that backcalculated layers moduli of 210 MPa for GBC and 100 MPa for SG, obtained from Falling Weight Deflectometer (FWD) test conducted in early September 2014, were employed for calculations in case 4. Furthermore, the circular contact area was calculated by dividing the load on tire by the inflation pressure for finding the radius of contact area ( $a_c$ ). Figure 3-8 illustrates the relationships between stress frequency and speed for cases 1 to 5. It is clear that while not being very sensitive to speed increase, the frequencies obtained from case 2 were significantly lower than those of the other cases. According to the literature, the ability of loading time prediction models and time-to-frequency conversion equations in prediction of field-measured pulses depends on their specific assumptions of time pulse shape and vehicular loading (Al-Qadi et al., 2008). Therefore, this study confirmed that the underlying assumptions within case 2 lead to significant deviation from the rest of the reviewed methods. It is appropriate to note that even though the proposed approximation methods in cases 3 and 4 yielded incompatible loading time values, both methods' estimated loading frequencies were in good agreement with those of case 1 due to their particular time-to-frequency conversion approaches. In addition, case 5's frequencies were generally lower than the results from case 1 and larger than those of case 2, especially at vehicle speeds of 30 km/hr and higher. The observed overestimation and underestimation can be partially attributed to the facile approach used within cases 1 and 2 for direct time-to-frequency conversion. This is in agreement with the findings of Al-Qadi et al. (2008) for speeds of 8, 24 and 40 km/hr and stress pulses at 140 and 190-mm depths at the Virginia Smart Road.

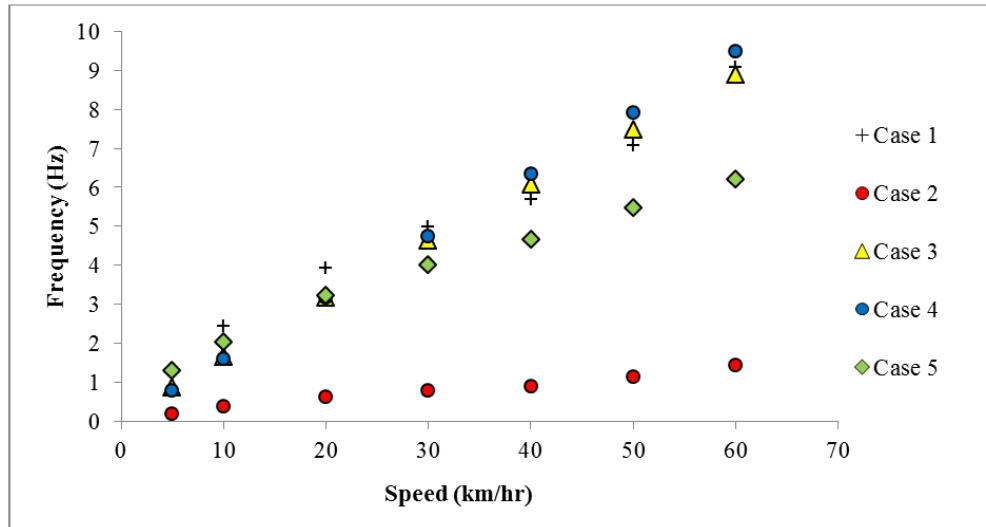
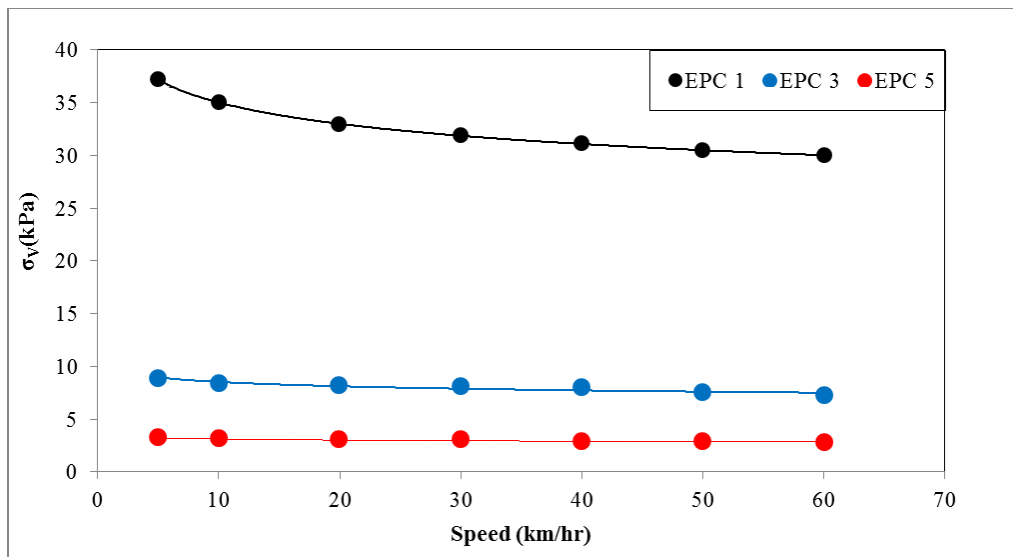


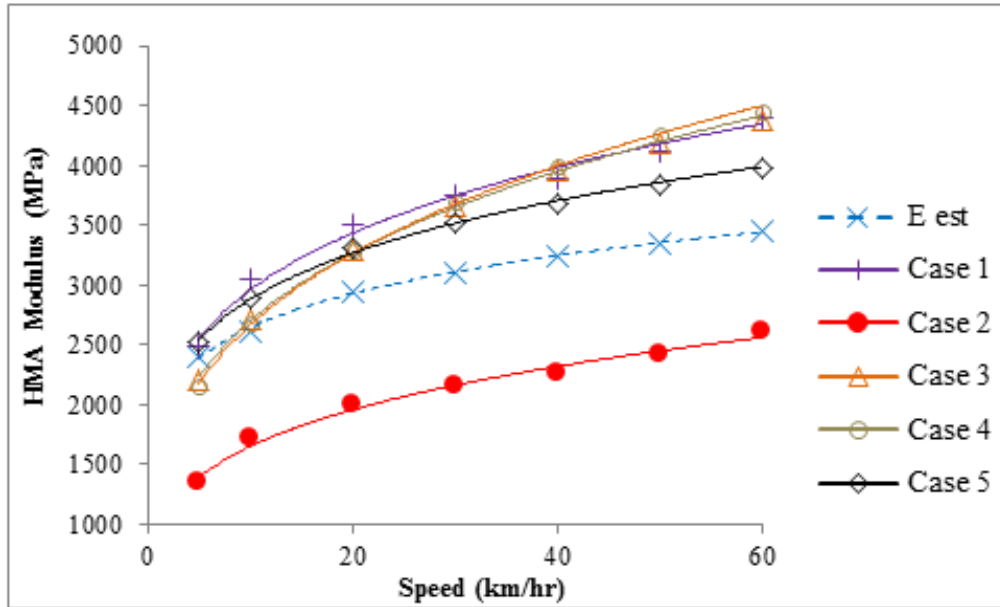
**Figure 3-8 Comparison of stress frequency vs. speed in different methods.**

In order to translate the effect of calculated frequencies on the  $|E^*|$ , it is necessary to input the calculated frequencies in the laboratory-determined HMA master curve. Therefore, for each of the cases,  $|E^*|$  values were extracted from the wearing and binder layers master curves at different obtained frequencies. Then, by calculating the weighted average of the extracted  $|E^*|$  of the two layers, a single  $|E^*|$  was generated to represent the stiffness of a combined HMA layer at any frequency. Using the weight factors of 0.36 for wearing and 0.64 for binder based on each layer thickness,  $E_{com}$  was derived at each frequency for further comparisons. On the other hand, estimation of linear elastic modulus of HMA based on the in-situ measured stresses, as depicted in Figure 3-9(a), can provide an approximate benchmark for comparing the  $|E^*|$  values. To pursue this purpose, simulation of the test section response to vehicle load was conducted using KENLAYER [1] by estimating the linear elastic moduli of HMA ( $E_{est}$ ) until the predicted  $\sigma_v$  on top of GBC converges to its in-situ measured value by  $\pm 1\%$  at each speed. During the analysis of  $E_{est}$ , the wearing and binder layers were combined and assumed as a single HMA layer, while

other parameters such as GBC modulus (210 MPa) and subgrade modulus (100 MPa) were considered constant. Figure 3-9(b) shows the variation of estimated  $E_{est}$  to match  $\sigma_v$  on top of GBC and  $E_{com}$  for the five frequency calculation cases against speed. Results showed that magnitudes of  $E_{com}$  of case 2 were noticeably lower than  $E_{est}$  and  $E_{com}$  of other cases. As expected, the  $E_{com}$  of cases 1, 3 and 4 fairly changed within the same range against speed and were larger than those of case 5 for speeds of 20km/hr and higher.



(a)



(b)

Figure 3-9 (a) Variation of  $\sigma_v$  on top of GBC and, (b)  $E_{est}$  and  $E_{com}$  vs. speed.

The effectiveness of  $E_{com}$  of the five cases with respect to  $E_{est}$  was evaluated in terms of percentage of prediction error, PPE:

$$PPE = \frac{E_{com} - E_{est}}{E_{est}} \times 100 \quad (3-4)$$

Figure 3-10 depicts the PPE of the  $E_{com}$  for different cases in which positive values contribute to over-estimated  $E_{com}$ , whereas negative values contribute to under-estimated  $E_{com}$ . The distribution of the PPEs for the five cases suggests that case 5 had the lowest median and possessed less variation in comparison to other cases. Almost similar patterns were observed for cases 3 and 4 and both methods resulted in a wide range of PPE including over-estimated and

under-estimated values. Although, the median of PPEs in case 1 was fairly closed to those of cases 3 and 4, the PPEs of case 1 varied within a more limited range. This is supported by the fact that the standard error of PPEs in case 1 (2.8 %) was less than that of PPEs in case 3 (4.8%) and case 4 (5.4%). In overall, case 2 exhibited the highest PPEs with values as high as 44. Therefore, the use of FFT to calculate DF may generally result in more efficient prediction of the HMA dynamic modulus over the tested range of speeds. Moreover, the lowest standard error of PPEs in case 5 (1.3%) amongst all considered cases confirms that case 5 is less sensitive to speed variation compared to four other methods.

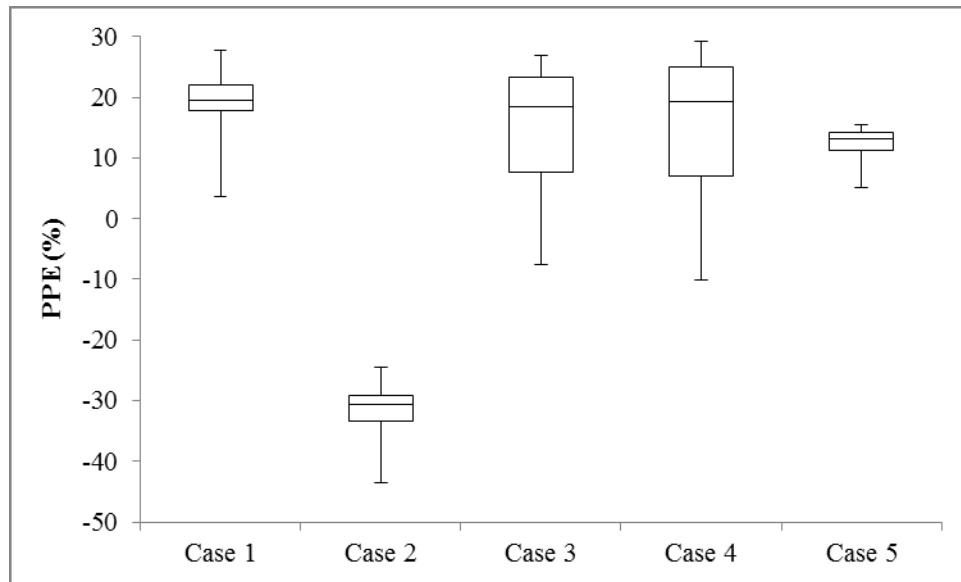


**Figure 3-10 Comparison of modulus prediction errors for different approaches.**

## **Conclusion**

This paper investigated the use of FFT for calculation of frequency associated with longitudinal, transverse and vertical strains at the bottom of the HMA as well as the vertical stress at different depths within unbound materials. In this study which was conducted at the IRRF's test road facility, responses from several controlled vehicle testing performed at different speeds were utilized and relationships were developed to approximate dominant frequencies as a function of vehicle speed. The observed differences between obtained dominant frequencies revealed that longitudinal strain possessed the highest frequencies in comparison to transverse and vertical strains. Besides, the calculated frequencies noticeably decreased at deeper elevations, while a reasonable agreement between frequencies of vertical strain at the bottom of the HMA and vertical stress on top of the GBC was observed. Focusing on the vertical stress response on top of GBC, results from FFT method were compared to those of four other widely-used time-domain frequency calculation methods. Finally, comparisons between the  $|E^*|$  determined from five different cases with respect to the estimated modulus matching in-situ measured vertical stresses showed that FFT yields more accurate and reliable moduli.

## **Acknowledgements**

The authors gratefully appreciate the assistance of Alberta Transportation, Alberta recycling, and The City of Edmonton who provided financial and in-kind support for the construction and instrumentation of the IRRF's test road. Alberta Transportation is also acknowledged for conducting the FWD tests for this study. The close cooperation of Tetra Tech EBA FWD test crews during testing is also greatly appreciated.

# **Chapter 4 -Time-Frequency Domain Analysis of Asphalt Longitudinal Strain**

A version of this chapter was published by the Transportation Research Record journal in February 2016.

## **Abstract**

This paper evaluates the application of time-frequency domain analysis methods, such as Continuous Wavelet Transform (CWT) and Short-Time Fourier Transform (STFT), in the extraction of Dominant Frequency (DF) from asphalt longitudinal strain signals. This study used the pavement response data collected at the fully-instrumented Integrated Road Research Facility (IRRF) in Edmonton, Alberta, Canada. Promising results were achieved when using CWT and STFT to determine the DF of the measured longitudinal strain at the bottom of the asphalt layer at different vehicular speeds. The obtained DFs were also compared with the corresponding values according to conventional time-to-frequency conversion methods. Results showed that a frequency calculation using the inverse of tensile pulse duration leads to noticeably larger frequencies in comparison to the ones associated with CWT and STFT methods. In order to evaluate the accuracy of the determined frequencies and the corresponding HMA's moduli, strains were predicted utilizing the KENPAVE program. This analysis showed the advantage of using time-frequency domain methods, as they led to more reasonable agreements between the measured and predicted responses. Finally, the impact of frequency calculation methods on the potential fatigue cracking life was assessed by taking the estimated HMA's moduli and strains into account. It was found that the fatigue cracking life can be overestimated nearly 45 percent when considering the frequency as a reciprocal of pulse duration compared to prediction based on time-frequency domain methods.

**Key words:** *Asphalt Longitudinal Strain, Time-Frequency Domain, Continuous Wavelet Transform, Short-Time Fourier Transform and fatigue Life.*

## Introduction

Hot Mix Asphalt (HMA) is widely recognized as a viscoelastic material whose stiffness is a function of temperature and loading frequency (ARA, 2004). Through field study, several researchers to date have focused on the calculation of traffic-induced loading frequency as a key parameter required for determining HMA's dynamic modulus (Al-Qadi et al., 2008; Garcia and Thompson, 2008; Hu et al., 2009; Ulloa et al., 2012; Fakhri et al., 2013). However, the majority of the performed studies are based on conventional time-to-frequency conversion methods. It is also known that under the newly developed Mechanistic Empirical Pavement Design Guide (MEPDG), loading frequency, which plays a significant role in the processes of response and performance prediction, is calculated using the  $f = 1/t$  relationship, where  $f$  is the frequency (Hz) and  $t$  is the pulse duration (s) (ARA, 2004). Another widely used approach in the field of polymer rheology describes the conversion between cyclic frequency ( $f$ ) in hertz and loading time ( $t$ ) in seconds as  $f=1/2\pi t$  (Dongre et al., 2006). Al-Qadi et al. (2008) investigated the inadequacies and deficiencies of the conventional time-to-frequency conversion methods by processing the in-situ measured pressure time histories in frequency domain rather than time domain. This study showed that utilizing Fast Fourier Transform (FFT) to obtain the frequency content of the pressure signals can reveal the Dominant Frequency (DF), which can alternatively be used in estimating HMA dynamic modulus rather than the conventional methods. In another study conducted by Ulloa et al. (2012), DF prediction models were developed as a function of vehicle speeds using frequency domain analysis of several theoretically-calculated response time histories. This study found that the fatigue and rutting performances predicted via the use of DF in conjunction with multi-linear elastic analysis are very similar (within  $\pm 10\%$ ) to the ones based on dynamic viscoelastic analysis of responses.

Even though Fourier analysis is frequently used for transforming a given signal from time domain to frequency domain, it still suffers from inherent limitations. For instance, Fourier analysis can only provide information on the frequency domain of the signal without offering time resolution. In other words, while the frequency content of the signal can be determined by Fourier analysis, the time of each frequency cannot be established. Another disadvantage of Fourier analysis is that it cannot be effectively applied to time-variant, non-stationary signals which have different frequency components at different times. Therefore, in order to examine the signals in time and frequency domains simultaneously, more advanced and sophisticated methods, including Continuous Wavelet Transform (CWT) and Short-Time Fourier Transform (STFT), are applied. Reviewing the literature indicates the application of time-frequency domain analysis in a wide range of pertinent engineering data, for example, characterization of pavement surface roughness data (Wei and Fwa, 2004; Papagiannakis et al., 2007; Ayenu-Prah and Attoh-Okine, 2009). However, employing the time-frequency analysis methods to evaluate the pavement response signals measured under a moving load has not yet been studied.

Considering that the longitudinal strain at the bottom of the HMA is regarded as the primary factor for the development of bottom-up fatigue cracking, the objective of this research is to investigate the application of CWT and STFT approaches to extract the DFs of such pavement response. This research will focus on (1) variation of longitudinal strain DFs when subjecting the pavement to different vehicular speeds, (2) quantifying the accuracy of the obtained DFs with respect to prediction of in-situ measured strains, and (3) assessing the impact of the frequency calculation approach on bottom-up fatigue cracking potential. To pursue the above objectives, data collected from controlled vehicle testing at the Integrated Road Research Facility (IRRF) was processed for frequency calculations.

## **Project information**

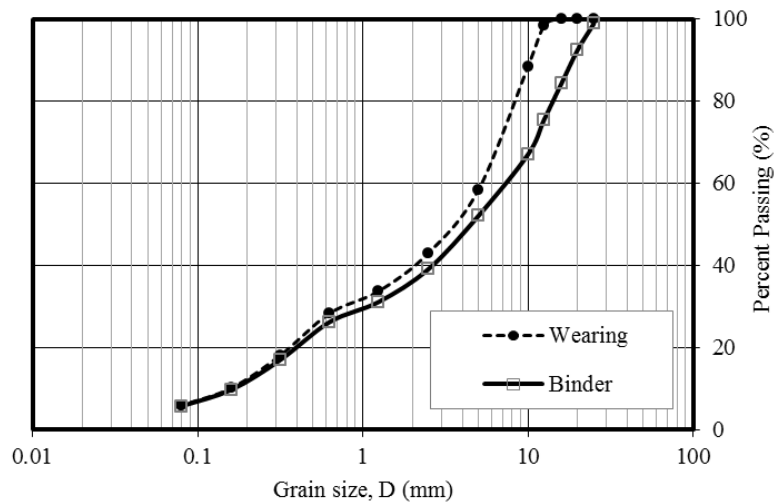
### **IRRF Test Road Facility**

The IRRF is a state-of-the-art research facility located in Edmonton, Alberta, Canada. The construction of the IRRF was finished in 2013, and it includes two fully instrumented pavement performance monitoring sections approximately 500 m long and placed 100 m from each other. This two-way test road will function as an access road to the Edmonton Waste Management Center (EWMC) when opened to traffic in late 2015. The flexible pavement structure of the IRRF consists of a 90 mm wearing layer on top of a 160 mm binder layer, as well as a 450 mm granular base course and prepared subgrade soil.

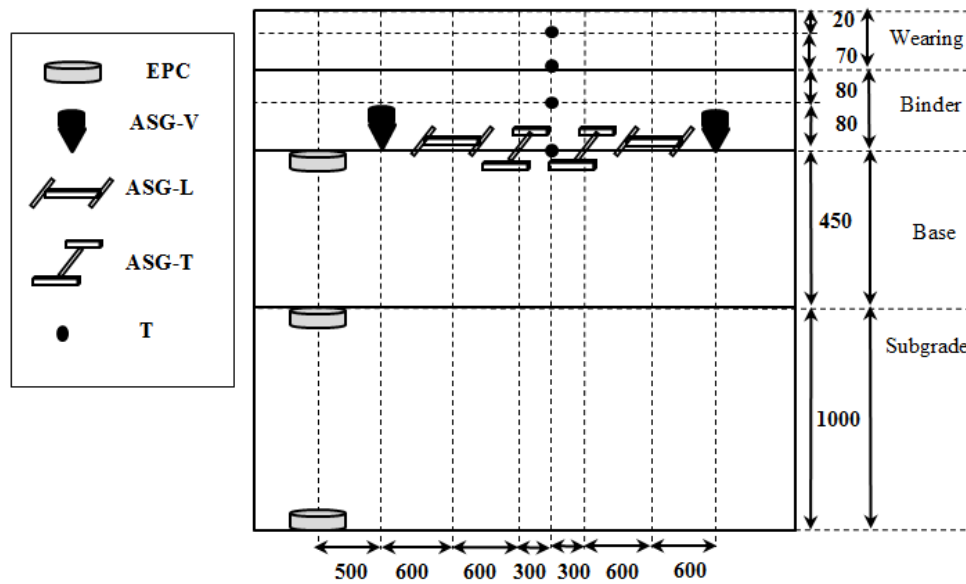
Construction of the IRRF's test road took place in two stages. During the first stage in August 2012, the binder layer (with asphalt content of 4.58 percent by mass of total mix, air void of 4.0 percent and Voids in the Mineral Aggregate [VMA] of 13.1 percent) was built over base and subgrade layers. Throughout the second stage in August 2013, the wearing layer (with asphalt content of 5.30 percent based on mass of total mix, air void of 3.6 percent and VMA of 14.3 percent) was added on top of the binder layer. Figure 4-1(a) depicts the aggregate gradation of the two mixes. It is worth mentioning that the Reclaimed Asphalt Pavement (RAP) content was 20 percent in the binder and 10 percent in the wearing layer. The virgin binder and the binder extracted from the RAP materials were graded as PG 58-28 and PG 70-28, respectively. Besides, the binder in the mix resulting from blending RAP material met the PG 58-28 grade. The base material with maximum particle size of 19 mm was classified as Well-Graded Gravel (GW) in accordance with the Unified Soil Classification System (USCS). Similarly, the subgrade soil with maximum particle size of 0.5 mm was classified as Clayey Sand (SC). Based on the results

from Falling Weight Deflectometer (FWD) testing conducted in early September 2014, the back-calculated moduli of base and subgrade layers were determined as 210 and 100 MPa, respectively.

Figure 4-1(b) shows the typical instrumentation layout of pavement performance monitoring sections at the IRRF. To measure the strains at the bottom of the binder layer, Asphalt Strain Gauges (ASGs) were placed in longitudinal (ASG-L), transverse (ASG-T) and vertical (ASG-V) directions. Furthermore, Earth Pressure Cells (EPCs) were installed to collect the vertical stress within unbound layers. The dynamic data is recorded at 500 Hz utilizing a high-speed CR9000X datalogger from Campbell Scientific Corp. Canada. Monitoring HMA layers temperature at different depths is also conducted via asphalt thermistors (T) at 5-minute intervals.



(a)



(b)

**Figure 4-1 (a) Aggregate gradation of asphalt mixes, (b) cross-section of instrumented test section at IRRF (all units in mm).**

### Data Collection

During a controlled vehicle testing on August 14, 2014, a two-axle dual tire single unit truck was used to capture responses at 5, 10, 20, 30, 40, 50 and 60 km/hr speeds. The steering and rear axle loads were 2,550 and 4,150 kg, respectively, with the tires' inflation pressure 870 kPa. The testing process was planned to align the center of the dual tires of the rear axle along the outer wheel path. For accuracy purposes, videos were recorded by a camera mounted at the side of the vehicle during each run to later check the wheelpath relative to gauge location with the aid of pavement markings. As a result, induced responses under dual-tire configuration were recorded without lateral offset relative to the gauges. This study focuses on longitudinal strain measured at the bottom of the binder layer, as well as temperature data within two HMA layers.

## Methodology

### Continuous Wavelet Transform

In the Continuous Wavelet Transform (CWT), a signal is converted from time domain to time-frequency domain using a waveform function called a *wavelet*. In this method, the time domain signal is represented by dilated and translated forms of a basic wavelet, which satisfies admissibility condition and finite energy functions. More detailed information on the mathematical basics of wavelet functions can be found in the literature (Addison, 2002). It is well known that HMA longitudinal strain follows a compression-tension-compression behavior, and its shape is very similar to the Mexican Hat Wavelet (MHW) among several existing wavelet functions. Therefore, the MHW, as illustrated in Equation 4-1, was selected in this study to analyze the longitudinal strain signals:

$$\psi\left(\frac{t-b}{a}\right) = \left[1 - \left(\frac{t-b}{a}\right)^2\right] \times e^{-\frac{1}{2}\left(\frac{t-b}{a}\right)^2} \quad (4-1)$$

where  $\psi\left(\frac{t-b}{a}\right)$  depicts the MHW,  $a$  is the scale parameter and  $b$  is the position parameter. According to Equation 4-1, the MHW can be stretched/squeezed and moved along the t-axis by varying parameters  $a$  and  $b$ , respectively. Figure 4-2 shows the MHW constructed with different values of  $a$  and  $b$ , along with the normalized longitudinal strain measured at the bottom of the HMA at 5 km/hr vehicle speed. Comparing the MHWs associated with  $a = 96$  and  $a = 200$  clearly shows the impact of a larger scale on stretching of the resultant MHW. Figure 4-2 also suggests that with change in position parameter, one can obtain the shifted version of the MHW.

Therefore, it is of utmost importance to identify the appropriate scale and position parameters so that the produced wavelet is reasonably coincidental with the HMA strain, as it will be discussed later.

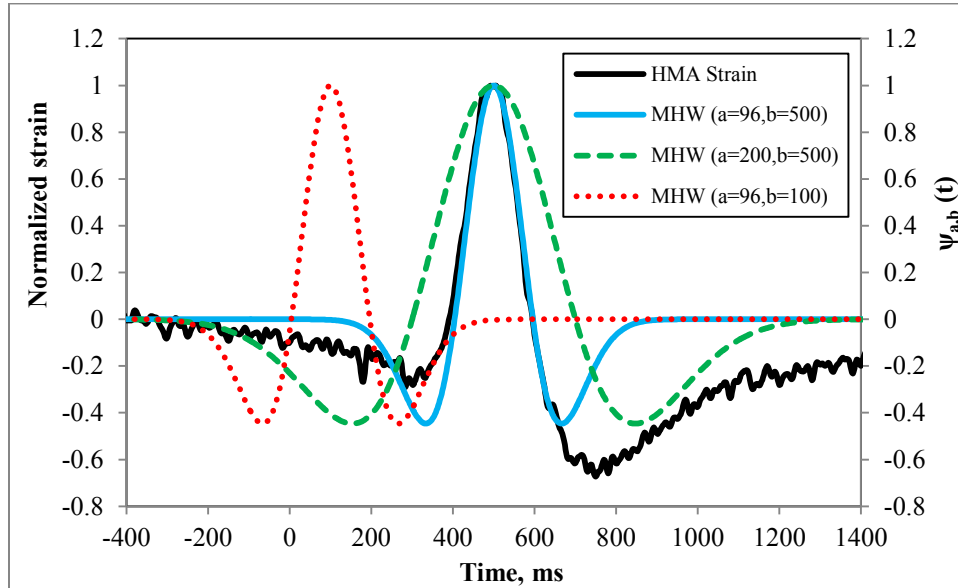


**Figure 4-2 Dilation and translation of the MHW against measured strain at 5 km/hr speed.**

Mathematically, the CWT of a signal in time domain,  $x(t)$ , is expressed as:

$$T(a, b) = \frac{1}{\sqrt{a}} \int_{-\infty}^{+\infty} x(t) \psi^* \left( \frac{t-b}{a} \right) dt \quad (4-2)$$

where  $T(a, b)$  is the CWT of  $x(t)$  based on the dilated and translated wavelet  $\psi \left( \frac{t-b}{a} \right)$ . The asterisk in Equation 4-2 indicates the complex conjugate of the wavelet function, and  $\frac{1}{\sqrt{a}}$  denotes a weighting factor, which is considered for the sake of energy conservation. Based on the mechanics of the wavelet transform, the positive contribution to the integral in Equation 4-2 occurs when the wavelet and the signal possess the same signs, while opposite signs lead to

negative contribution to the integral (Addison, 2002). Thus, the CWT of  $x(t)$  highlights the positive and negative contributions of the wavelet to the aforementioned integral over ranges of scales and positions. Accordingly, CWT of the HMA strain based on the MHW can be found using MATLAB Wavelet Toolbox, as shown in Figure 4-3. Figure 4-3 also demonstrates that larger positive values of  $T(a, b)$  are associated with reasonable local matching of the MHW and HMA strain. This implies that structures within strain pulse were identified by the MHW; hence, the local minimums of  $T(a, b)$  corresponded to peak compressive segments of the HMA strain, while the local maximum of  $T(a, b)$  was noted where peak tensile strain existed.

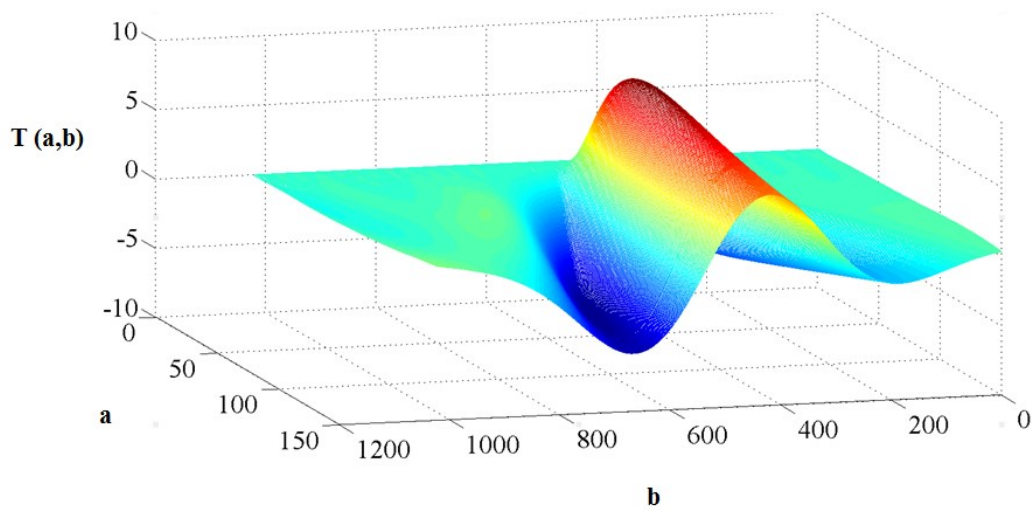


**Figure 4-3 Typical CWT plot of longitudinal strain at 5 km/hr speed.**

By definition, wavelet variance,  $\sigma^2(a)$ , reflects the average energy associated with scale  $a$  in the signal of length  $\tau$  as below:

$$\sigma^2(a) = \frac{1}{\tau} \int_0^\tau |T(a, b)|^2 db \quad (4-3)$$

Practically, peaks in the  $\sigma^2(a)$  plot indicate the scale of dominant energy features in the signal, e.g. the HMA longitudinal strain, which are defined as Dominant Scales (DS). To approximate the frequency from scale  $a$ , the following equation is normally used:

$$F_a = \frac{F_c}{a \Delta} \quad (4-4)$$

where  $F_a$  depicts the pseudo-frequency corresponding to the scale  $a$  in Hz,  $F_c$  is the central frequency of wavelet, which is equal to 0.250 Hz for the MHW, and  $\Delta$  is the sampling period (Misiti et al., 1997).

### Short-Time Fourier Transform

In the Short-Time Fourier Transform (STFT), a given signal in time domain is divided into definitive time intervals by sliding a window function along a time axis (Gröchenig, 2013). Therefore, the Fourier transform of the pre-windowed signal is calculated to find the local spectrum of the signal around time instants. The STFT of a signal in time domain,  $x(t)$ , is expressed as:

$$X_{STFT}(\tau, f) = \int_{-\infty}^{+\infty} x(t) w(t - \tau) e^{-i2\pi ft} dt \quad (4-5)$$

where  $w(t - \tau)$  is the sliding window function (which was a Hamming window) with a length of 400 sample points in this study. In this approach, the magnitude squared of STFT,  $|X_{STFT}(\tau, f)|^2$ , returns the spectrogram of the considered  $x(t)$ , signifying the energy density surface of the STFT. A typical spectrogram calculated by STFT for the HMA strain obtained at 5 km/hr vehicle speed is illustrated in Figure 4-4. The time instants in Figure 4-4 depict the midpoint of each window having 300 overlapped sample points with adjacent windows. The plotted spectrogram obtained from MATLAB shows that a strong power band appeared at approximately 0 to 5 Hz. Interestingly, the observed power band was more pronounced during the tensile segment, from approximately 0.8 to 1.2 seconds, and unloading phase of the strain pulse starting from 1.2 to 1.6 seconds. Based on this method, the frequency carrying the maximum energy among all frequencies is the DF, which needs to be extracted for further analysis.

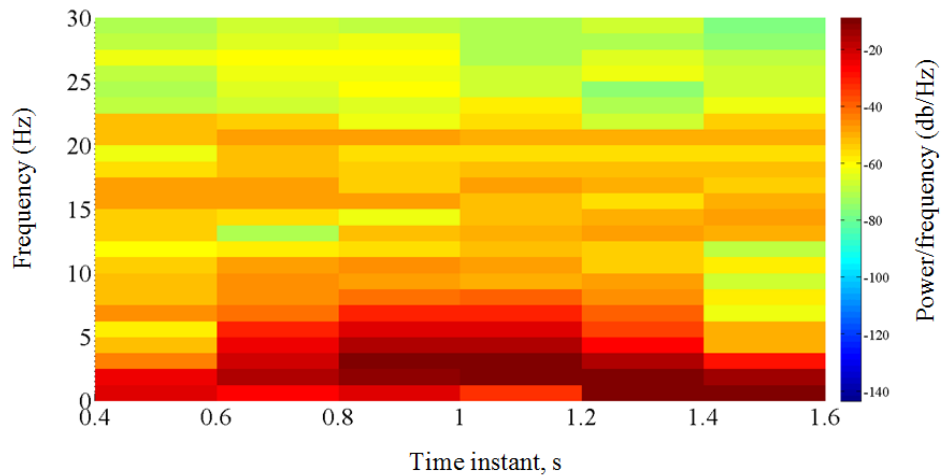


**Figure 4-4 Spectrogram of longitudinal strain at 5 km/hr speed.**

## Data Analysis

### Loading Frequency Determination

In order to evaluate the applicability of the proposed work in terms of frequency determination, CWT and STFT were applied to the HMA strains collected under seven vehicle speeds. As a result, wavelet variances were found for each strain signal according to the CWT approach in an attempt to extract the DS magnitudes. Table 4-1 provides a summary of the extracted DS magnitudes, as well as half-pulse durations ( $T_{HP}$ ), measured as the time interval between the start and maximum of tensile strain. The corresponding DS and  $T_{HP}$  values indicate a reasonable agreement between the two parameters. The average of percentage error, showing the difference between measured  $T_{HP}$  and estimated DS, was equal to 9.3 for all tested speeds. On the other hand, both DS and  $T_{HP}$  tended to decrease at higher speeds expectedly due to the viscoelastic behavior of HMA.

**Table 4-1 Comparison between  $T_{HP}$  and DS.**

Speed (km/hr)	5	10	20	30	40	50	60
$T_{HP}$ (ms)	102	62	44	40	32	28	24
DS	96	53	41	37	30	26	22
Difference (%)	6.3	16.9	7.3	8.1	6.6	7.7	9.1

Consequently, for the DS values shown in Table 4-1, pseudo-frequency was found using Equation 4-4, as illustrated in Figure 4-5. For the sake of comparison, Figure 4-5 also depicts the acquired DF(s) related to the highest energy determined using the STFT approach, in addition to the frequencies calculated based on the two conventional approaches, namely  $f = 1/t$  and  $f = 1/2\pi t$ , when  $t$  is the pulse duration. As can be seen from Figure 4-5, significantly higher frequencies were observed when using the  $f = 1/t$  approach rather than those of the three other approaches. Moreover, the attained frequencies using the CWT approach were in approximately the same range as the ones calculated by the  $f = 1/2\pi t$  method, and results from the STFT approach led to fairly higher frequencies, especially at speeds greater than 40 km/hr. As shown in Figure 4-5, power functions were fitted to the data using least square regression in order to relate the calculated frequencies with the vehicular speed. The developed equations evidently showed a reasonable correlation between HMA strain frequency and speed, with the coefficient of determinations 0.98, 0.99, 0.98 and 0.97 in the cases of  $f = 1/t$ , STFT,  $f = 1/2\pi t$  and CWT approaches, respectively.

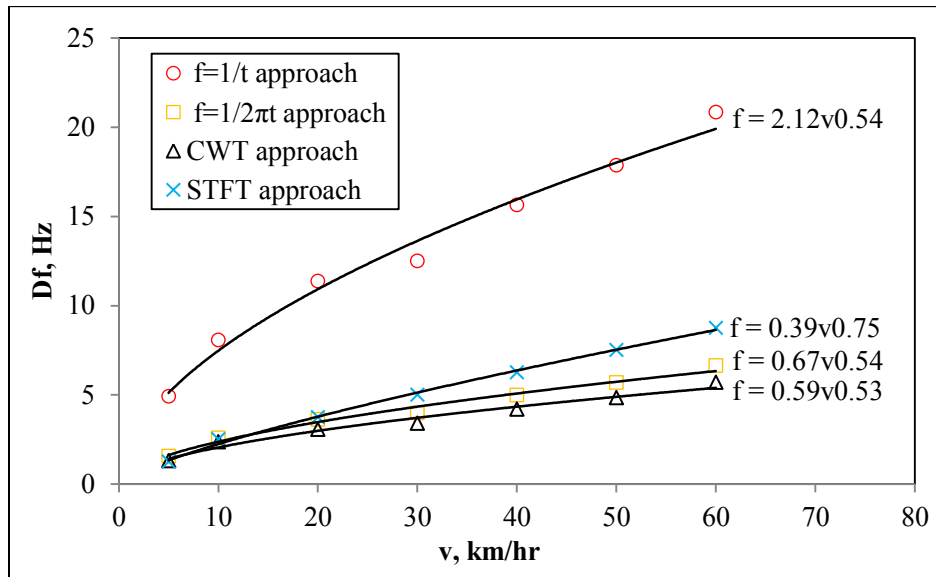
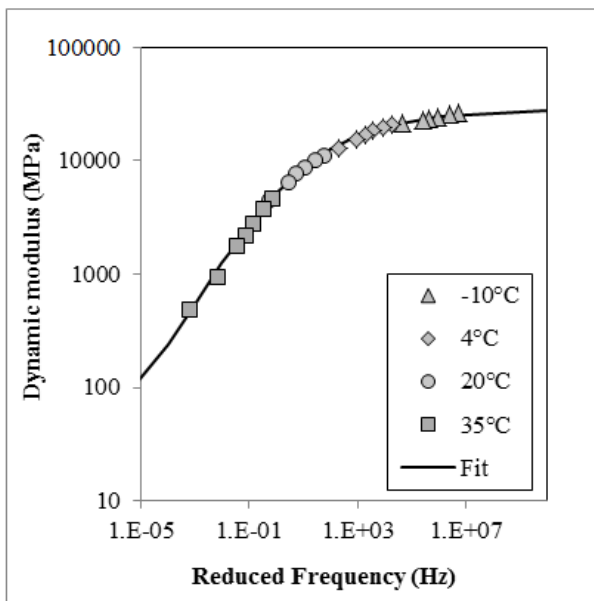
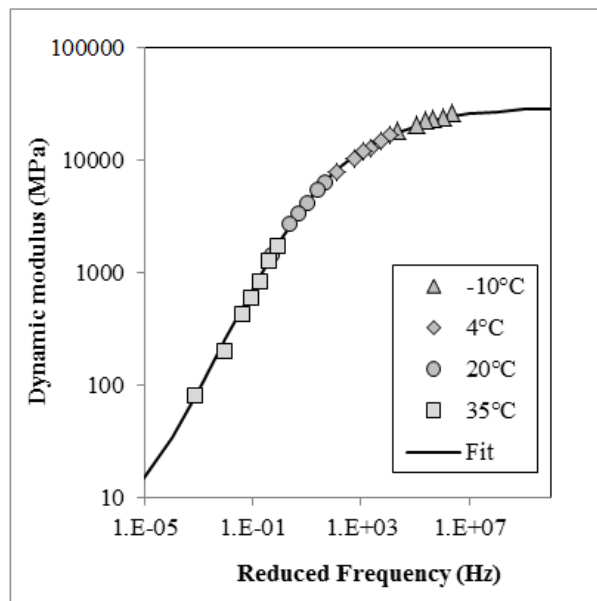


**Figure 4-5 Variation of DF against speed using different approaches.**

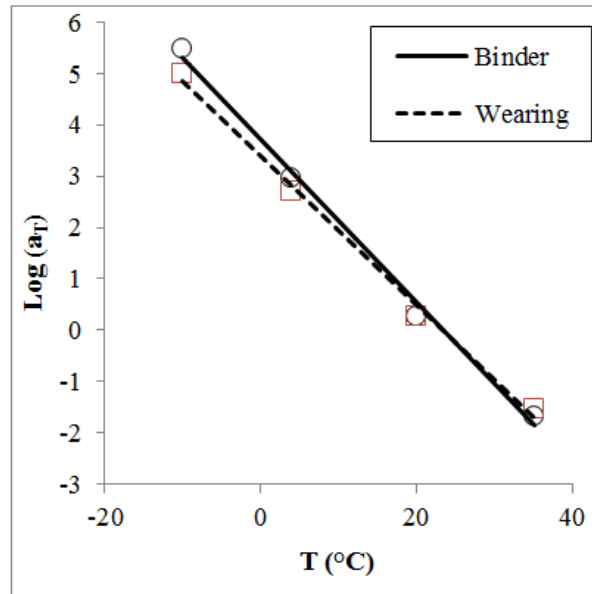
To account for the impact of frequency on the HMA behavior, this research applied results from dynamic modulus tests (AASHTO TP79) carried out on 100 mm diameter by 150 mm height cylindrical specimens. Using a UTM 100 machine from IPC, tests were conducted at frequencies of 10, 5, 2, 1, 0.5, 0.2, 0.1 and 0.01 Hz and temperatures of -10, 4, 20 and 35°C. Figures 4-6(a) and (b) show the laboratory-determined master curves at 25°C reference temperature constructed using frequency-temperature super positioning for binder and wearing layers, respectively, as well as the fitted sigmoid functions. Figure 4-6(c) also shows the variation of obtained shift factors ( $a_T$ ), which are needed for describing the dependency of dynamic modulus against temperature ( $T$ ).



(a)



(b)



(c)

**Figure 4-6 Dynamic modulus master curves for (a) binder and (b) wearing layers; (c) shift factors as a function of temperature.**

Depending on the determined frequencies in each method and asphalt temperature, the values of  $E_{HMA}^*$  were estimated with the developed master curve. It should be noted that the temperature data captured at the mid-depth of each layer by asphalt thermistors was used to conduct the analysis. The average mid-depth temperature of the wearing layer was 34°C and 31°C in the binder layer. Once the temperatures and frequencies were known from field data, a dynamic modulus of each layer was estimated based on HMA master curves. Table 4-2 summarizes the moduli of wearing ( $E_w$ ) and binder ( $E_b$ ) layers, which were adjusted for in-situ measured temperatures under different frequency calculation scenarios. Overall, both  $E_w$  and  $E_b$  based on the conventional  $f = 1/t$  approach tended to be the highest among four considered approaches. As well, notable change in the magnitude of calculated moduli at varying speeds was reflected in Table 4-2. Given the set of moduli for different speeds, the induced responses within pavement

structure can be predicted and compared against the measured ones to evaluate the examined approaches from response prediction view point, as explained in the next section.

**Table 4-2 Effect of loading frequency on HMA layer's moduli.**

Speed (km/hr)	Assigned Representative Modulus of HMA (GPa)							
	$f = 1/t$		$f = 1/2\pi t$		CWT		STFT	
	$E_w$	$E_b$	$E_w$	$E_b$	$E_w$	$E_b$	$E_w$	$E_b$
<b>5</b>	1.42	5.03	0.88	3.68	0.81	3.49	0.80	3.45
<b>10</b>	1.74	5.70	1.09	4.23	1.05	4.14	1.08	4.20
<b>20</b>	1.98	6.18	1.26	4.64	1.17	4.44	1.28	4.69
<b>30</b>	2.05	6.32	1.31	4.76	1.22	4.56	1.44	5.05
<b>40</b>	2.23	6.66	1.43	5.05	1.33	4.82	1.57	5.35
<b>50</b>	2.35	6.86	1.51	5.22	1.41	5.01	1.69	5.60
<b>60</b>	2.48	7.10	1.61	5.43	1.51	5.23	1.79	5.81

### Response Prediction and the Influence of Frequency

To simulate the pavement structure's responses under a different set of HMA layers moduli, this study used KENPAVE (Huang, 2004), which is a widely used multi-linear elastic program. During development of the KENPAVE model, the FWD back-calculated layers moduli of 210 MPa for base and 100 MPa for subgrade were employed. A simplified method recommended by Loulizi et al. (2002) was adopted to simulate the moving circular load in a layered elastic system. To do so, responses were initially found at certain radial distances relative to the load and, subsequently, time histories were developed through dividing those distances by the known vehicle speed. Figure 4-7 shows an example of simulated and measured longitudinal strain time histories. Focusing on the tensile portion of the longitudinal strain, the peak tensile strains

predicted based on CWT, STFT and conventional  $f = 1/2\pi t$  approaches were closer to the in-situ measured value as opposed to the case of  $f = 1/t$ . This comparison convincingly demonstrates the advantage of the former approaches over the latter in prediction of tensile strain. Nonetheless, there were two major shortcomings of layered elastic modeling. First, a significant difference between predicted and in-situ measured peak compressive strains was noticed under all scenarios over the course of both loading and unloading phases. Second, residual strain observed at the end of the unloading phase cannot be properly modeled in a layered elastic system. Knowing that the inherent limitations within the Multi-Layer Elastic Theory (MLET) can potentially influence the accuracy of response predictions, use of advanced analysis methods such as the Finite Element Method (FEM) can be also considered for future research.

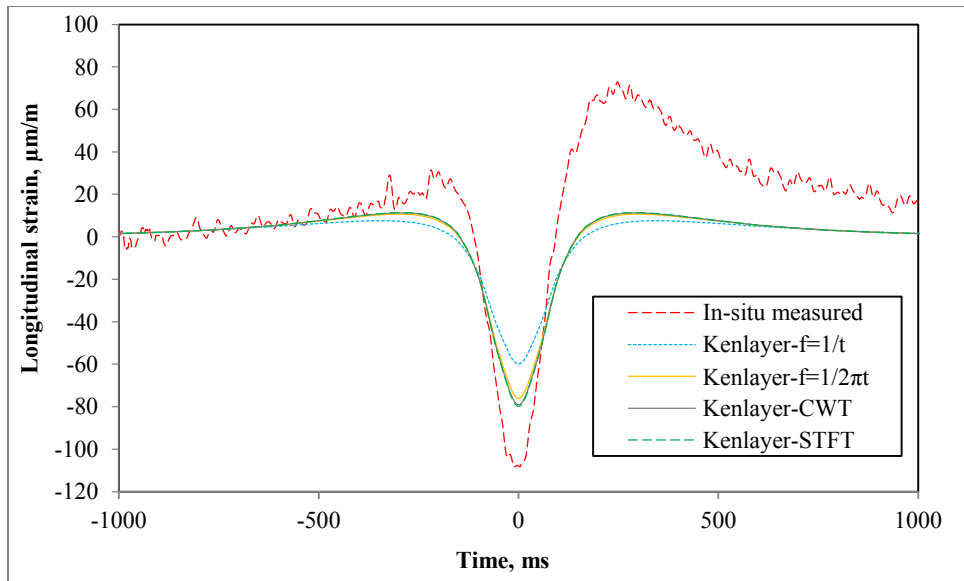


**Figure 4-7 Measured and simulated strain pulse at 5 km/hr speed.**

Peak predicted strains were plotted against the measured ones in Figure 4-8 to assess the influence of frequency calculation methods on the level of agreement between two sets of data. It

was concluded from both measured and predicted data that an increase in vehicle speed results in lower peak strains. As shown in Figure 4-8, the longitudinal strains were under-predicted, especially at lower speeds, while less deviation between predicted and measured strain was observed when using the CWT approach. In general, using the  $f = 1/t$  approach led to maximum deviation from field measurements in comparison to other approaches. Ulloa et al. (2012) also reported underestimation in longitudinal strain prediction when using the  $f = 1/t$  approach. Hence, on the basis of the adopted methodology for calculating frequency, the magnitude of response prediction error can vary, which in turn affects the predicted performance of the HMA. Since evolution of tensile longitudinal strain at the bottom of the HMA substantially controls the bottom-up fatigue cracking distress, the next section will discuss assessment of the proposed methodologies in regards to distress prediction.

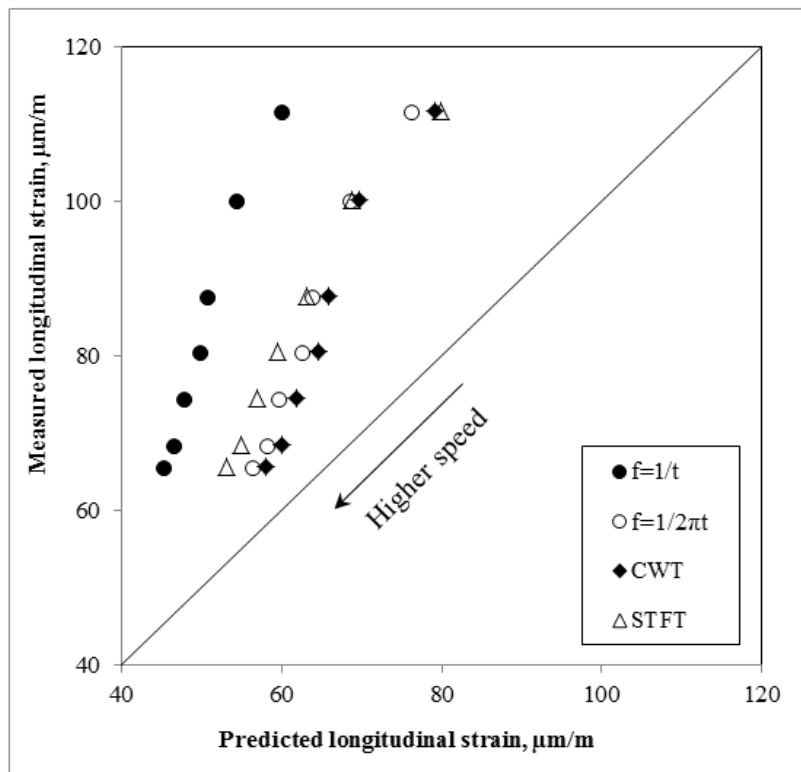


**Figure 4-8 Comparison between predicted and measured responses.**

## Frequency Effect on Fatigue Performance

To translate the effect of frequency calculation approaches into more tangible indices, fatigue life of the test section was computed with commonly used prediction models. To do so, the predicted responses from the four approaches were used in the Asphalt Institute (AI) model in order to investigate the range of variation in predicted fatigue life. Equations 4-6 to 4-8 show the fatigue life prediction model used in the AI model, which uses tensile strain at the bottom of the HMA layer, as well as the modulus of the HMA layer to predict the bottom-up fatigue cracking life of the pavement (Asphalt Institute, 1982).

$$N_f = 0.00432 \times C \left( \frac{1}{\varepsilon_t} \right)^{3.291} \left( \frac{1}{E_{HMA}} \right)^{0.854} \quad (4-6)$$

$$C = 10^M \quad (4-7)$$

$$M = 4.84 \left( \frac{V_b}{V_b + V_a} - 0.69 \right) \quad (4-8)$$

where,  $N_f$  = number of repetitions to fatigue cracking,  $C$  = laboratory to field adjustment factor,  $\varepsilon_t$  is the tensile strain at the bottom of the HMA,  $E_{HMA}$  is the elastic modulus of HMA (psi),  $V_b$  = percent of effective binder and  $V_a$  = percent of air voids. Equations 4-6 to 4-8 were used to establish  $N_f$  for the tested speeds using the KENPAVE-predicted  $\varepsilon_t$ . Operating under the hypothesis that wearing and binder layers can be combined as one layer for fatigue analysis, their weighted average volumetric and stiffness properties were calculated to represent the characteristics of an equivalent layer. As shown in Figure 4-9, a relative performance analysis was conducted by following the AI model. According to Figure 4-9, CWT and STFT methods produced almost similar  $N_f$  values to those resulting from the  $f = 1/2\pi t$  method. Conversely, the use of  $f = 1/t$  method yielded the highest  $N_f$  among the four methods in question. For

instance, in the case of 5 km/hr speed, the established  $N_f$  using  $f = 1/t$  method was nearly 40, 44 and 45 percent overestimated in comparison to  $f = 1/2\pi t$ , CWT and STFT methods, respectively. Also, a lower level of disagreement was observed between  $N_f$  values obtained based on the  $f = 1/t$  method and those of the three other methods at higher speeds. This investigation underlines the importance of CWT and STFT methods as powerful alternative analysis tools which can be suitably used for frequency determination of longitudinal strain signals. When applied to actual field data, CWT and STFT approaches demonstrated more favorable features than conventional time-to-frequency conversion methods, such as a higher level of detail in time-frequency domain and more efficient response prediction.

Results of this study showed that the proposed methods can be practically considered in the mechanistic design of flexible pavements as a means for enhanced interpretation of traffic-induced strain signal. Therefore, such techniques can be incorporated within pavement response models to better approximate the critical strains in the structure. Finally, time-frequency domain analysis of strain pulses provides more realistic frequencies of the traffic loading, which can potentially be used to improve the level of accuracy in the mechanistic design of the pavement with respect to the fatigue behavior of HMA.

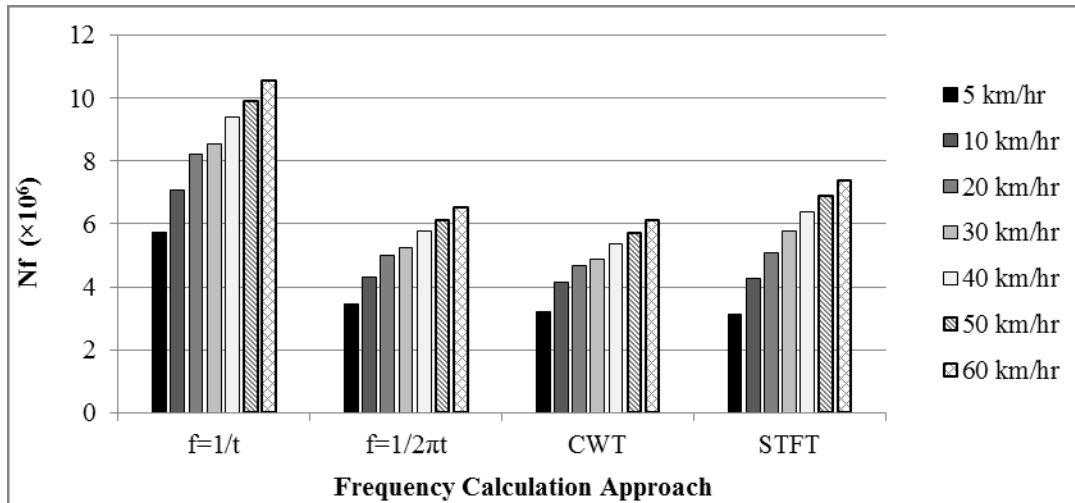


**Figure 4-9 Comparison between  $N_f$  values under considered approaches.**

## Conclusion

The following findings can be obtained from the present study:

1. The CWT was successfully applied to asphalt longitudinal strain signals and the proposed method effectively showed the variation of the DFs at different vehicle speeds.
2. The STFT spectrogram of the longitudinal strain signal can be used to extract the DF of the traffic loading. Relatively close frequencies were found when using STFT and CWT methods.
3. Comparison between time-frequency domain analysis methods such as CWT and STFT with the conventional time-to-frequency conversion methods of  $f = 1/t$  and  $f = 1/2\pi t$  clearly showed larger frequencies and consequently larger HMA layers moduli in the case of the  $f = 1/t$  approach.

4. By utilizing the associated HMA layers moduli from the four examined methods to predict the in-situ measured responses, the accuracy of each method was investigated. HMA strains obtained using CWT and STFT approaches matched fairly closely with those of the  $f = 1/2\pi t$  approach.
5. It was found that using the  $f = 1/t$  approach can result in more underestimated asphalt strain than CWT and STFT approaches.
6. By comparing the two conventional time-to-frequency conversion methods, this study indicated the advantage of the  $f = 1/2\pi t$  approach relative to the  $f = 1/t$  approach based on the field-measured pavement responses.
7. Considering the effect of frequency calculation methods on the fatigue life performance of the tested road section, it was concluded that the predicted fatigue life based on the  $f = 1/t$  approach is within 40 to 45 percent longer than those of the other three methods.

## **Acknowledgements**

The authors greatly appreciate the financial and in-kind support of Alberta Transportation, Alberta Recycling, and the City of Edmonton for the construction and instrumentation of the IRRF's test road. The authors also thank Alberta Transportation for conducting the Falling Weight Deflectometer (FWD) tests for this study.

# **Chapter 5 -Field Measurement and Modeling of Vertical and Longitudinal Strains from Falling Weight Deflectometer Testing**

A version of this chapter will be submitted to the Transportation Research Record Journal in August 2016.

## **Abstract**

This study investigates longitudinal tensile and vertical compressive strains at the bottom of the Hot Mix Asphalt (HMA) layer subjected to Falling Weight Deflectometer (FWD) during different seasons at the fully instrumented Integrated Road Research Facility (IRRF) located in Edmonton, Alberta, Canada. First, dynamic strain pulses were measured and characterized with respect to their shapes and durations. Also, the impact of HMA layer temperature in different seasons on the in-situ measured strains was evaluated, and strong relationships between peak strain values and temperature were found. Second, some well-established analysis packages, KENLAYER, 3D-Move and ABAQUS, were used to predict the measured responses based on the backcalculated and laboratory-determined moduli. Finally, by utilizing the bottom-up fatigue cracking and rut depth prediction models recommended in the Mechanistic-Empirical Pavement Design Guide (MEPDG), the impact of strain prediction error on the estimated performance was also evaluated. It was found that the potential fatigue life can be overestimated up to 5.7 times relying on the KENLAYER-predicted longitudinal strain, while the potential rut depth of HMA is less affected, up to 2.1 times, based on the corresponding vertical strains.

**Keywords:** *Hot Mix Asphalt, Longitudinal Strain, Vertical Strain, Falling Weight Deflectometer, Performance.*

## **Introduction**

It is well established that the longitudinal and vertical strains at the bottom of the Hot Mix Asphalt (HMA) layer are responsible for bottom-up fatigue cracking and rutting distresses according to the Mechanistic-Empirical Pavement Design Guide (MEPDG) (ARA, 2004). Although the field-measured strains have been previously studied in several Accelerated Pavement Testing (APT) facilities (Ullidtz et al., 1994; Mahoney et al., 1995; Appea et al., 2002; and Wu et al., 2002), a limited number of facilities have the capability to measure the pavement response under dynamic loading for both vertical and horizontal asphalt strains. Therefore, characterization and evaluation of such critical responses in the field are of utmost importance for calibration of the MEPDG. In addition, most of the previous studies have attempted to predict and validate the HMA layer responses through the commonly used Multi-Layer Elastic (MLE) programs such as CHEVPC (Warren and Dieckman, 1963), KENLAYER (Huang, 2004), ELSYM5 (Ahlborn, 1972), WES5 (Van Cauwelaert et al., 1989), etc.; however, it is well understood that the underlying and simplifying assumptions within MLE programs require more investigation. As a result, prediction of the vertical compressive and horizontal tensile strains using more advanced approaches, including Finite Element Method (FEM) and continuum-based finite layer approach, is advantageous in many aspects when dealing with dynamic loading behavior and complex material properties.

The current study focuses on the field measurement, evaluation and prediction of vertical and horizontal strains within the HMA layer induced by Falling Weight Deflectometer (FWD) testing in different months at the Integrated Road Research Facility (IRRF) in Edmonton, Alberta, Canada. In this paper, the effect of temperature variation on the magnitude and shape of the

captured strain pulses was examined and models were developed to approximate the pulse duration of the responses. To further investigate the behavior of pavement structure under FWD tests, three response prediction programs were used to calculate the pavement responses. The study also addressed the impact of response prediction errors on the potential performance of the pavement test section using MEPDG performance prediction models.

## **Background**

Different researchers have focused on field measurement of FWD-induced pavement responses and prediction of such responses when using the backcalculated pavements' layers moduli from FWD testing. This section reviews some of the most notable studies in this area.

FWD tests were performed at the Pacific Car and Foundry Company (PACCAR) Technical Center in Mt. Vernon, Washington (Mahoney et al., 1995) to measure the induced horizontal strain at the surface and bottom of the HMA layer using asphalt strain gauges (ASGs). Initially, the layers moduli were backcalculated using the EVERCALC program (Mahoney et al., 1989); subsequently, the layers moduli were used in the CHEVPC program to predict the strains. The study showed that the ratio of the measured to predicted strains was almost one for the HMA layer temperatures in the range of 6°C to 8°C. The findings by Mahoney et al. (1989) were confirmed by a similar study at the Virginia Smart Road Facility in Montgomery County, Virginia (Appea et al., 2002). The EVERCALC-backcalculated layers moduli were used in KENLAYER to predict pavement responses. They found that the predicted horizontal strains at the bottom of the HMA layer agreed very well with the measured values for when the temperature of the HMA layer was recorded at 35°C during the test. Finally, they concluded that

a good consistency existed between measured and predicted responses from MLE programs when testing HMA at medium and high temperatures (Appea et al., 2002).

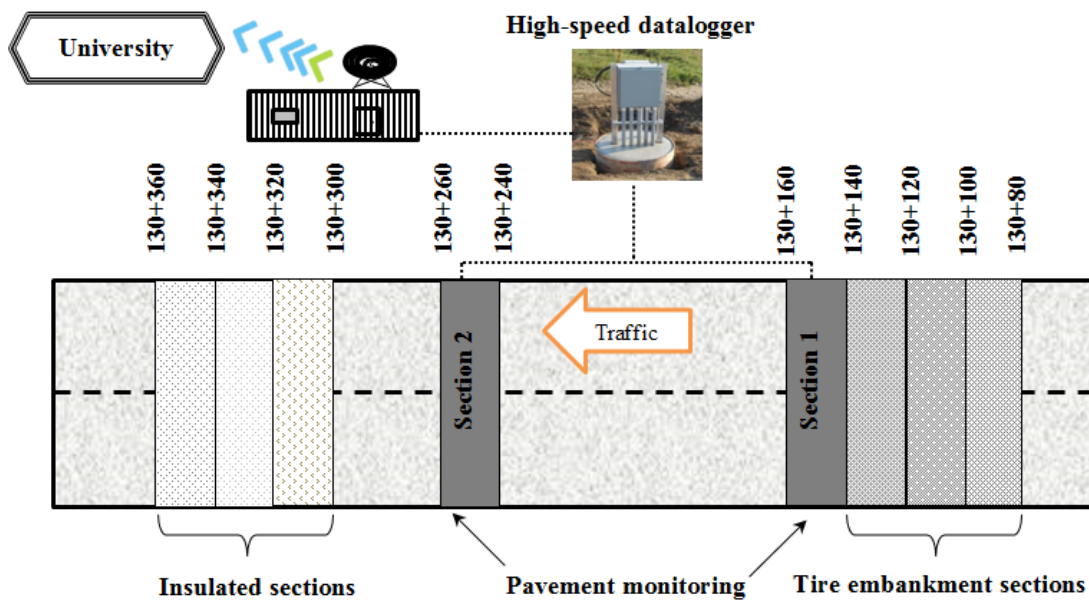
Contradictory to the above evidence showing that good agreements between the measured and predicted responses had been observed, an experimental study by Solanki et al. (2009) showed a wide range of error (1 to 24 percent) between the predicted and measured horizontal strain in the asphalt layer. The study was conducted on the instrumented section of interstate I-35 in central Oklahoma, and KENLAYER, which is an MLE program, was used for the pavement response prediction. The observed discrepancy was attributed to two invalid assumptions made about the static nature of FWD load and infinity of layers in the MLE approach. Comparison between WES5-predicted asphalt horizontal strains and those of the FEM showed the advantage of using FEM to achieve better agreement with field results. Unsatisfactory agreement between measured and WES5-predicted responses was attributed to the non-linear elastic behavior of subgrade soil, which was not taken in to account during the modeling according to Ullidtz et al. (1994). While employing the advanced analysis tools such as FEM to simulate the response from instrumentation under FWD load is a leap forward in mechanistic design, large asphalt strain prediction errors as high as 50 percent were also noted in the literature (Yin, 2012). FWD loadings at the National Center for Asphalt Technology (NCAT) were simulated using 3D-Move (Siddharthan et al., 2000), which is a continuum-based finite-layer analytical model, in an attempt to minimize the prediction errors by finding an equivalent vehicular speed for the FWD tests (Leiva-Villacorta and Timm, 2013). Promising results were obtained in predicting the asphalt strain using this approach, but the obtained equivalent speed was found to be as high as 190 km/h (Leiva-Villacorta and Timm, 2013).

Different researchers have focused on field measurement of FWD-induced pavement responses and prediction of such responses when using the backcalculated pavements' layers moduli from FWD testing. This section reviews some of the most notable studies in this area.

## **Description of Experiment**

The experimental program was conducted at the IRRF test road which is part of a new access road to the Edmonton Waste Management Center (EWMC) located in northeast section of the city of Edmonton, Alberta, Canada. The test road is subjected to the traffic of more than 1000 garbage trucks per day, transporting municipal waste materials to EWMC. As shown in Figure 5-1 (a), two 20-m long sections at the IRRF (Sections 1 and 2) are instrumented for pavement response and performance monitoring. Sections 1 and 2 are stretched from Station 130+140 to 130+160 and 130+240 to 130+260, respectively. During their construction in summer 2012, the test sections were instrumented with various structural and environmental monitoring gauges at different depths in the pavement system. A CR9000X high-speed data logger from Campbell Scientific Corp of Canada is used to collect the dynamic structural responses from both Sections 1 and 2 at 500 Hz. Figure 5-1 (b) shows the instrumentation layout at the bottom of the HMA layer with a total of 36 ASG's installed: six in the longitudinal (ASG-L), six in the transverse (ASG-T) and six in the vertical (ASG-V) direction. This study used the data obtained from ASG-V and ASG-L as indicated by the shaded circles in Figure 5-1 (b). HMA temperature data was recorded using the embedded asphalt thermistors (AT) at four different depths. Earth pressure cells, not shown, were also installed within the pavement system to collect the vertical stresses in unbound layers.

A 90-mm thick wearing course and a 160-mm thick binder course were used in Sections 1 and 2. Table 5-1 shows the physical properties of the two HMA layers. A 450-mm thick well-graded granular base course with a maximum particle size of 19 mm was placed on top of a clayey sand subgrade soil. The subgrade soil possessed a maximum particle size of 0.5 mm, and had Liquid Limit (LL) of 25 and Plasticity Index (PI) of 9 percent.



(a)

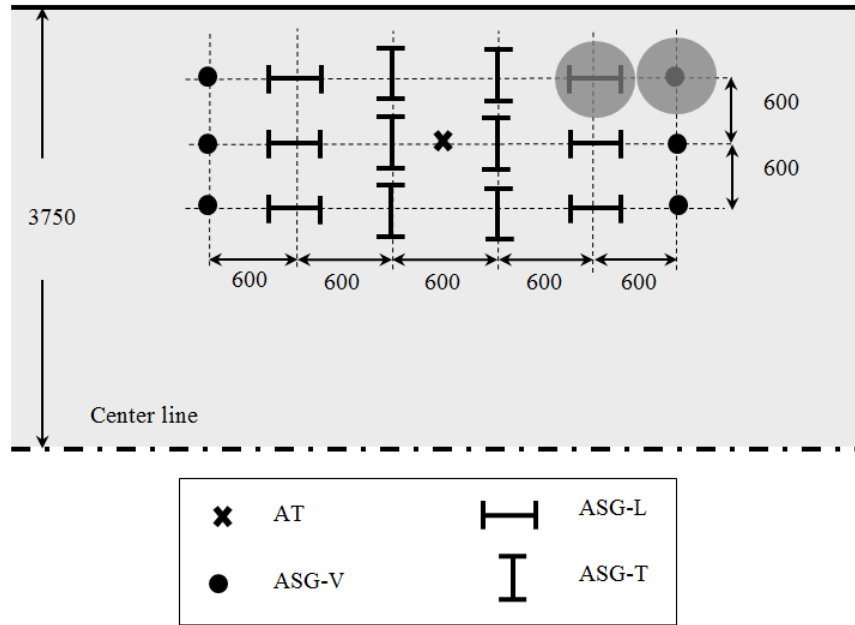


**Figure 5-1 IRRF test sections, (a) schematic plan view and (b) instrumentation layout (all units in mm)**

**Table 5-1 HMA physical parameters at IRRF**

Physical Property	Values	
	Binder Course	Wearing Course
Max. Aggregate size (mm)	25	12.5
Reclaimed Asphalt Pavement (RAP) content (%)	20	10
Binder Content by Weight of Mix (%)	4.58	5.30
Virgin Binder Grade	PG 58-28	PG 58-28
RAP Binder Grade	PG 70-28	PG 70-28
Void in Mineral Aggregate (VMA) (%)	13.1	14.3
Void Filled with Asphalt (VFA) (%)	69.4	74.9
Air Voids (%)	4	3.6
Density (kg/m <sup>3</sup> )	2355	2344
Marshal Stability (KN)	17.7	16.9
Flow (mm)	2.25	2.50

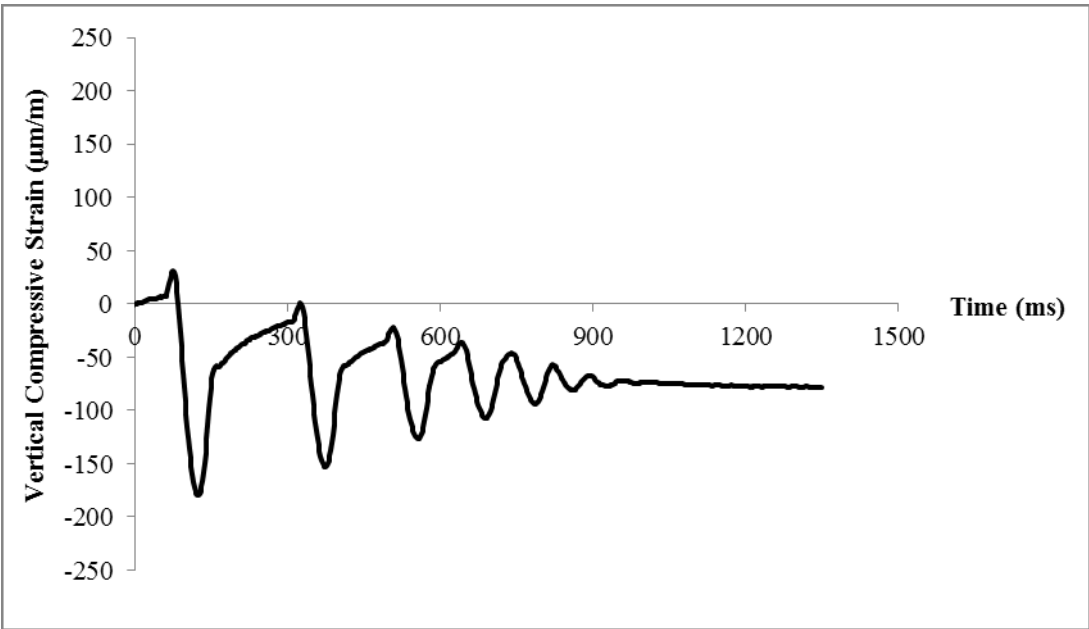
FWD tests were conducted on March 12, April 8, April 21, May 5, May 25, June 5, July 9, August 18 and October 14, 2015 along Sections 1 and 2 at the specified sensor locations. During the testing, the HMA layer temperature was recorded at depths of 20, 90, 170 and 250 mm from the surface every five minutes. At each test location, three drops were made at three stress levels of approximately 370, 570, and 730 kPa. Dynatest 8000 FWD was used for testing with nine-sensor configuration at 0, 200, 300, 450, 600, 900, 1200, 1500, 1800 mm from the center of the load plate.

## **Measured Horizontal and Vertical Strains**

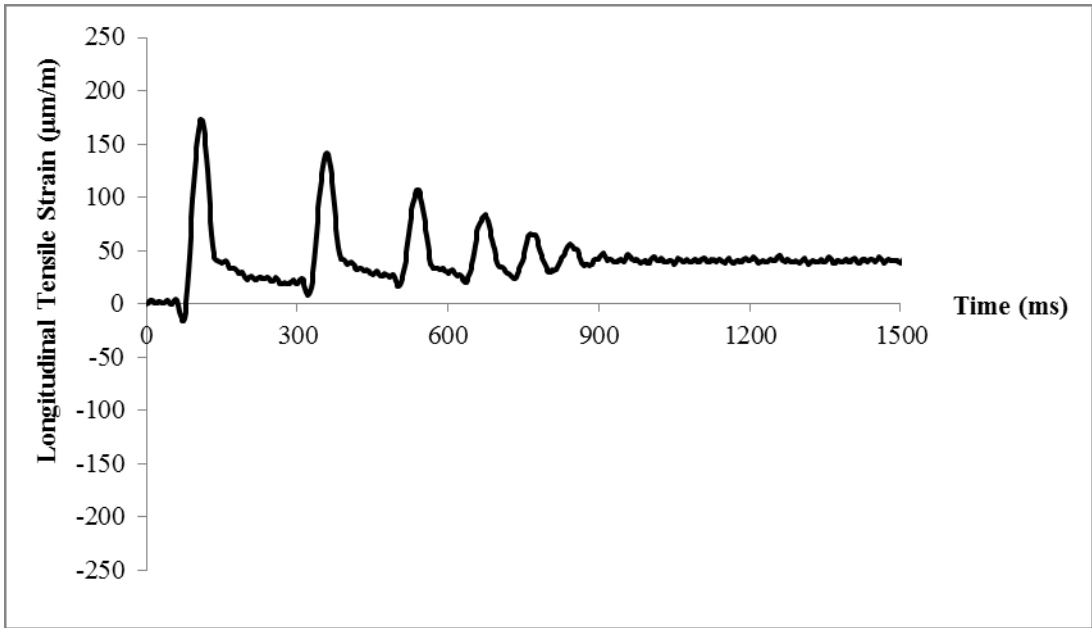
Nine FWD tests (each including three drops) were conducted on top of the ASG-V to capture the vertical compressive strain and on top of the ASG-L to capture the longitudinal tensile strain at the bottom of the HMA in Section 2 (see Figure 5-1). Note that out of the three drops, the pulses induced under the medium stress level of almost 570 kPa were used for analysis. It should be noted that FWD tests conducted at any given gauge location resulted in negligible responses at the adjacent gage locations, and thereby this study focuses only on the pulses under the load plate.

As an example, strain pulse measurements for the FWD tests conducted on June 5, 2015 are provided in Figure 5-2(a) and (b). The tensile strains are indicated as positive values while the compressive strains as negative. It is evident from Figure 5-2(a) and (b) that both gauges experienced multiple (about 7) peaks lasting approximately 900 ms due to the bouncing effect of the FWD impact loading. Figure 5-2(a) and (b) show that some residual strains remained at the end of each unloading phase which was about the same magnitude as the ultimate residual strain

after 900 ms. This appears to be the effect of the static weight of the falling loads as also reported by Loulizi et al. (2002). Focusing on the first pulse with the maximum peak, the in-situ measured strains at different months were compared as shown in Figure 5-3(a) and (b). Results show that the shape of the recorded pulses was not quite symmetrical, especially in the case of vertical strain. For all measured strains, the temperature profile of the HMA at the time of testing is depicted in Figure 5-3(c). It is worth mentioning that the temperature data at the closest five minute interval to the FWD test time was considered for each test. A wide range of HMA temperature is noted when comparing the temperature profiles during the performed tests. Data showed that the surface temperature recorded at a depth of 20 mm from the surface varied from 9.8°C to 43.3°C, while the temperature at a depth of 250 mm changes in the range of 1.8°C to 31.4°C. The recorded temperature profiles indicated that on average, the HMA temperature decreased at the rate of about 0.3°C per 1 cm depth of HMA layer.

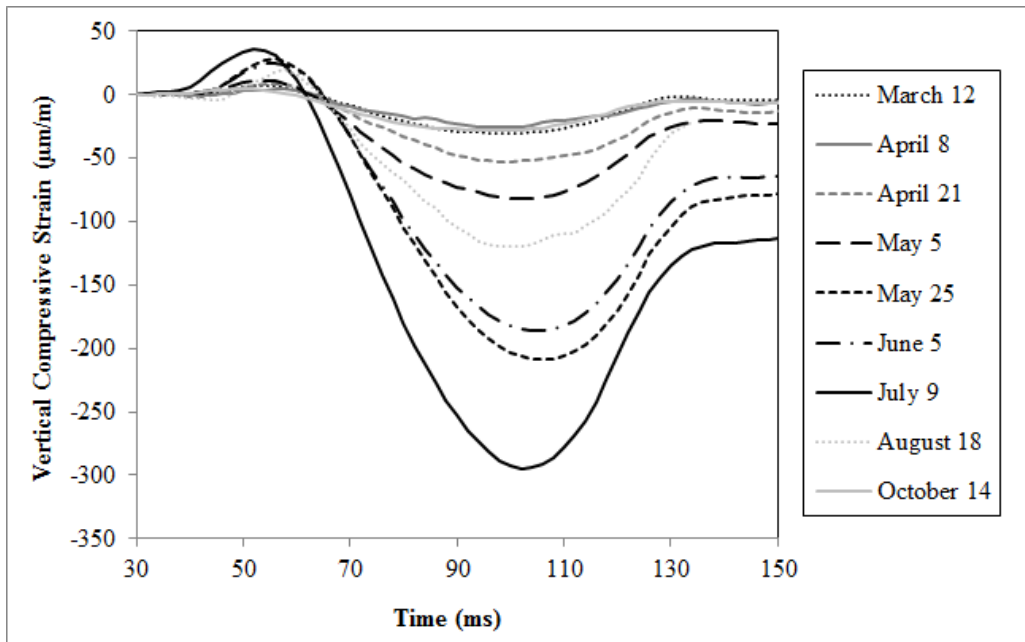


(a)

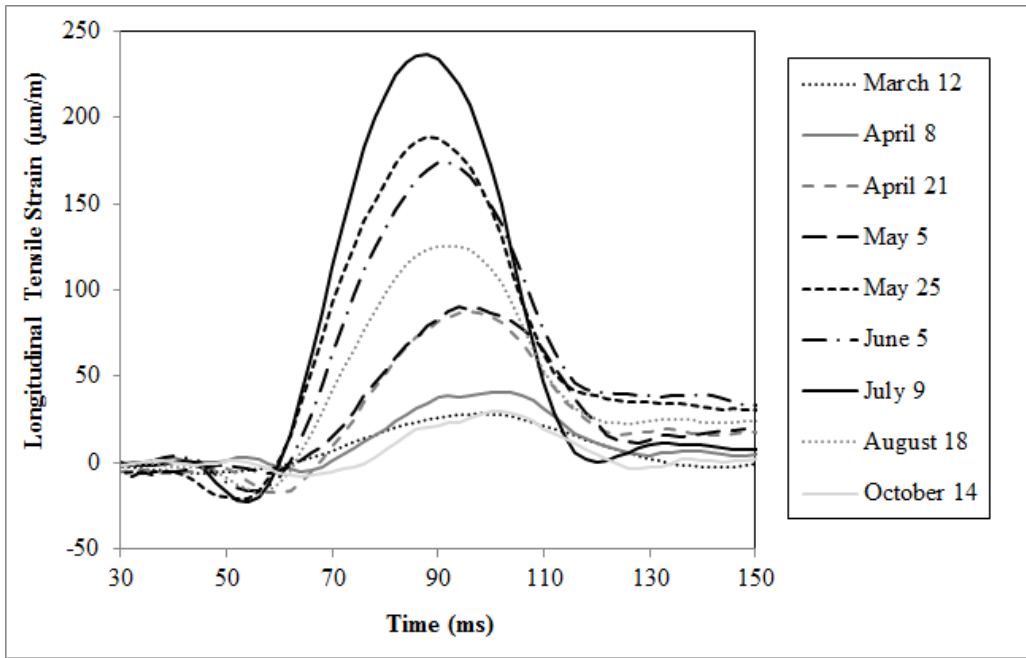


(b)

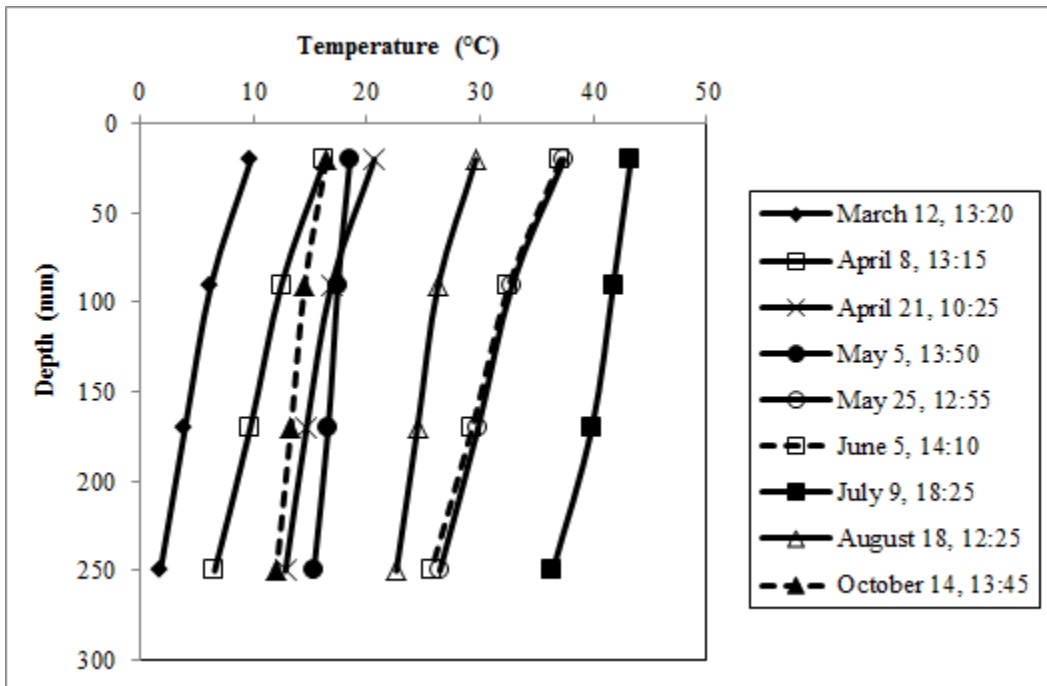
Figure 5-2 Example measured (a) vertical and (b) longitudinal strains under 570 kPa FWD stress level measured on June 5, 2015



(a)



(b)



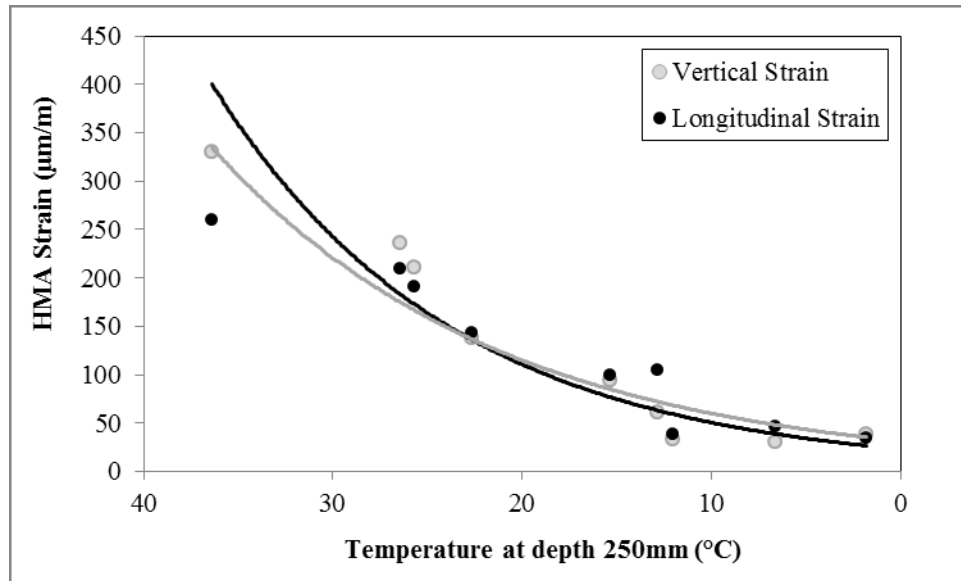
(c)

Figure 5-3 Measured maximum peak (a) vertical strain, (b) longitudinal strain and (c) asphalt temperature profile.

The recorded pulses show the effect of temperature on the measured HMA strains, owing to the viscoelastic behavior of HMA. To understand the strain-temperature behavior of the HMA layer, the measured peak strains were plotted against the corresponding HMA temperature (T) at a depth of 250 mm from the surface in Figure 5-4. It appears that exponential regression models represented by Eq. (5-1) for vertical strain and Eq. (5-2) for longitudinal strain can be used to relate the peak strain and temperature.

$$\varepsilon = 31.198 e^{0.0652 T}, R^2 = 0.87 \quad (5-1)$$

$$\varepsilon = 23.018 e^{0.0785 T}, R^2 = 0.89 \quad (5-2)$$



**Figure 5-4 Measured strains versus temperature.**

To quantify the duration of the strain pulses based on the experimental field data, the normalized strain pulses were closely fitted by a haversine function, which is considered to represent the actual waveform in pavement (Loulizi et al. 2002), using Eq. (5-3).

$$y = \sin^2\left(\frac{\pi}{d}t + \frac{\pi}{2}\right) \quad (5-3)$$

where, t is the time and d is the pulse duration. Figure 5-5 shows the typical measured and fitted response pulses for a FWD test conducted in the month of June. Table 5-2 shows the variation of the calculated (fitted) pulse durations for the two strain types. According to Table 5-2, the strain pulse durations in the vertical direction ranged between 95 to 110 ms, however the corresponding values in the longitudinal direction were in the range of 73 to 88 ms. Therefore, the vertical strain pulses were generally more elongated than the corresponding longitudinal strain pulses indicating the anisotropic properties of the HMA. Testing showed that the strain pulse durations were relatively consistent in each direction and the HMA temperature did not noticeably affect the FWD pulse duration.

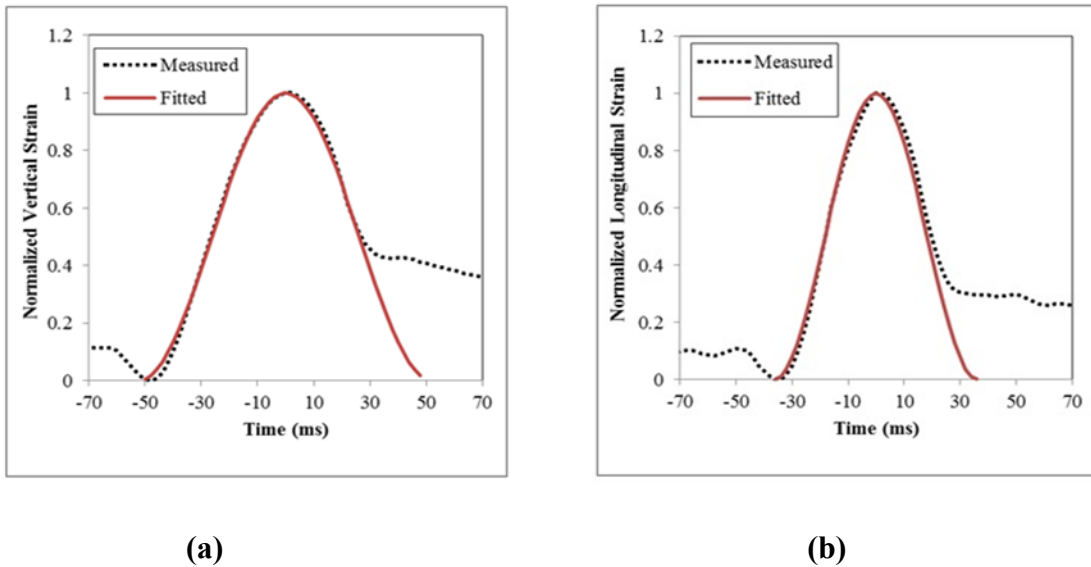


**Figure 5-5 Haversine representation of normalized (a) vertical and (b) horizontal strains.**

**Table 5-2 Haversine pulse duration at different months**

FWD Test Date in 2015	Temperature at 250 mm depth (°C)	Calculated Pulse Duration (ms)	
		Vertical	Longitudinal
March 12	1.8	99	88
April 8	6.6	97	82
April 21	12.8	95	80
May 5	15.3	104	81
May 25	26.45	110	80
June 5	25.7	105	73
July 9	36.4	106	75
August 18	22.6	95	77
October 14	12.0	98	85

## **Determination of Layer Moduli**

### **Laboratory-Measured HMA Moduli**

To account for the viscoelastic behavior of the HMA and thereafter modeling this behavior in 3D-Move software as will be discussed later, dynamic modulus tests were carried out following AASHTO TP79 (2009). Superpave gyratory compacted specimens were prepared and later cored and cut into a diameter of 100 mm and a height of 150 mm. Four test temperatures of -10, 4, 20 and 35°C, and eight frequencies of 10, 5, 2, 1, 0.5, 0.2, 0.1 and 0.01 Hz were used to construct the master curves for both wearing and binder courses. Figure 5-6 shows the laboratory-determined master curves at the reference temperature of 25°C following the procedure

described in MEPDG. Thus, at any temperature, such as the in-situ measured field temperature, the master curves can be “shifted” in order to find the HMA dynamic modulus.

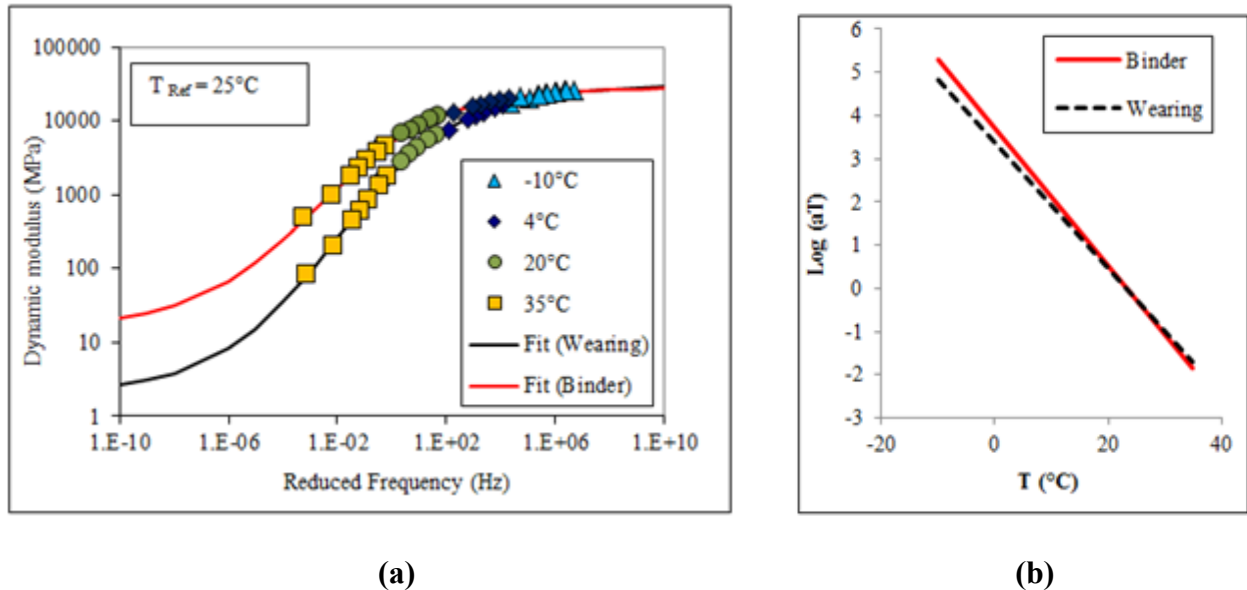


**Figure 5-6 Dynamic modulus master curve for binder and wearing layer at a reference temperature of 25°C.**

### Backcalculation of Moduli

To investigate the elastic modulus of HMA, base and subgrade layers, deflection data from the FWD tests were used to backcalculate the pavement layers moduli. The deflection basins recorded at the two test locations were similar. Therefore, the deflection basins obtained from the FWD tests conducted on top of the ASG-V were used for backcalculation. Before backcalculation, FWD deflections were normalized relative to their corresponding target loads according to ASTM D5858 (2008). A stiff layer was considered in EVERCALC, and the depth to stiff layer was set to be calculated internally by the software. Typical values of 3500, 200 and 50 MPa recommended in ASTM D5858 were used to define the seed values for HMA and base

and subgrade, respectively. Further, the Poisson's ratio of 0.35 for HMA and 0.4 for base and subgrade were selected as outlined in ASTM D5858.

Table 5-3 exhibits the seasonal variation of backcalculated moduli as a result of different environmental conditions. During the backcalculation, the two asphalt layers were combined to form one layer with the thickness of 250 mm. According to Table 5-3, the backcalculated moduli of the unbound layers were influenced by freeze and thaw cycles during the analysis period. As reported elsewhere (Tavafzadeh et al., 2016), the moisture content of the soil increased during the thaw period starting in April, while it gradually decreased from April to July during the recovery period. The magnitude of the HMA modulus was the lowest in July, whereas the lowest base and subgrade moduli occurred late May and July, respectively.

**Table 5-3 Variation of backcalculated layer moduli.**

FWD Test Date in 2015	Backcalculated Moduli (MPa)			RMSE* (%)
	HMA	Base	Subgrade	
March 12	12050	400	350	0.90
April 8	9400	230	120	0.13
April 21	7440	270	130	0.45
May 5	6100	290	125	0.09
May 25	1200	150	120	1.7
June 5	1800	200	120	0.20
July 9	660	215	115	0.25
August 18	3300	240	145	1.55
October 14	9550	255	150	0.85

\*  
Root Mean Square Error

## **Development of Response Prediction Models**

To evaluate the validity of the set of backcalculated and laboratory-determined moduli, pavement responses were calculated based on the MLE theory, and compared against two other methods, namely FEM and continuum-based finite-layer. In doing so, KENLAYER (Huang, 2004), a widely used MLE-based pavement design and analysis software, ABAQUS (Dassault Systèmes, 2013), a powerful and general-purpose finite element program, and 3D-Move (Siddharthan et al., 2000), an efficient analytical model based on continuum-based finite-layer approach, were used.

### **MLE Analysis with KENPAVE**

To evaluate the validity of the backcalculated moduli, pavement responses were calculated based on the MLE using KENLAYER. First, the EVERCALC-backcalculated moduli were used to define layers properties for all performed FWD tests. The wearing and binder courses were assumed to have identical backcalculated moduli as previously explained. Consequently, the loading was defined as static load uniformly applied over a circular area, resulting in FWD stress levels.

### **FEM with ABAQUS**

A two-dimensional axisymmetric plane strain model, with the same structure as in the case of KENLAYER, was developed in ABAQUS to quantify the vertical and longitudinal strains at the bottom of the HMA layer. The roller supports were considered for the vertical edges of the

pavement and the hinge supports were considered at the foundation to restrain the vertical and lateral displacements. Also, the interfaces of the adjacent layers were considered fully bonded, where separation and slip were not allowed. An implicit dynamic scheme assuming linear elastic analysis was executed considering four Gaussian nodes on each discretized domain (CAX8). Backcalculated moduli were assigned to each layer and the dynamic condition of the applied FWD load was taken into account using the stress time histories collected from FWD tests.

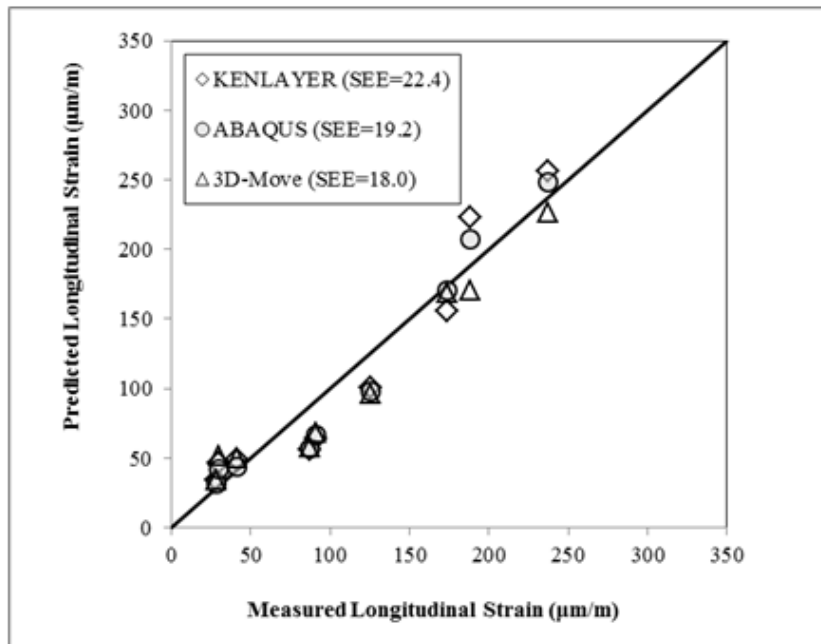
### **Modeling with 3D-Move**

In order to incorporate the viscoelastic properties of HMA, the pavement structure was modeled using 3D-Move analysis software developed at the University of Nevada, Reno. Accordingly, the laboratory-determined HMA master curves for wearing and binder courses along with the backcalculated base and subgrade moduli were separately assigned to each layer. To simulate the dynamic loading of FWD, a circular moving load with uniform contact stress was defined in the software. According to the literature (Ullidtz, 1987), the equivalent speed attributed to the FWD-exerted load ranges from 60 to 80 km/h. As a result, the speed of the moving load was set to 70 km/h for 3D-Move analysis.

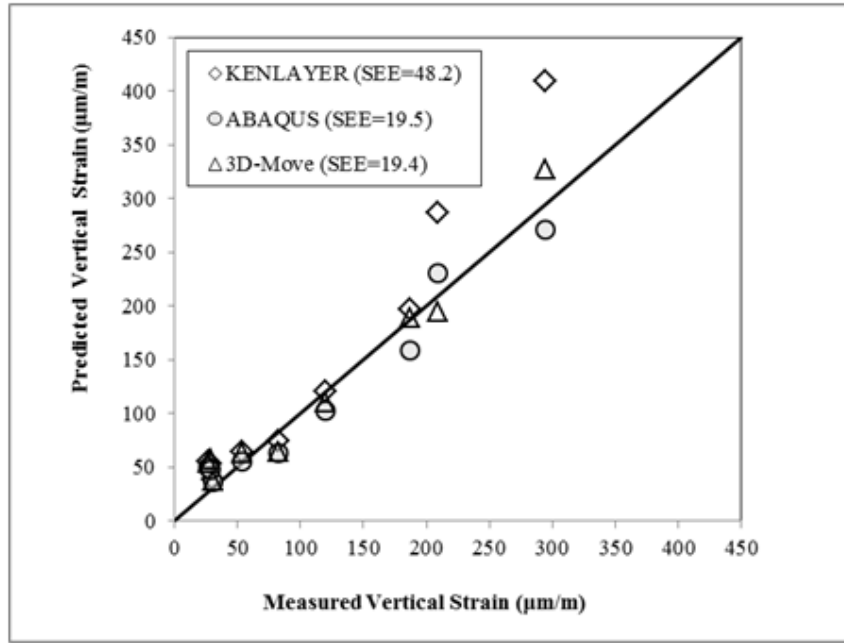
### **Prediction Results and Performance**

To investigate the agreement between computed and measured pavement responses, the computed strains were plotted against the measured ones as shown in Figure 5-7 (a) and (b). It can be seen that the agreement was better at low strain levels (which happened in colder months when the HMA behaves more elastically). At higher strain levels (during warmer months where

HMA behavior is viscoelastic), the MLE program KENLAYER over-predicted the vertical and longitudinal strains. The calculated Standard Error of Estimate (SEE) values for the ABAQUS and 3D-Move analyses were found to be more consistent compared to KENLAYER. The computed responses using 3D-Move software were mostly in agreement with the measured ones.



(a)



(b)

**Figure 5-7 Comparison between measurements and predictions of (a) vertical and (b) longitudinal strains.**

To translate the effect of errors in computed pavement responses into more tangible indices, fatigue and rutting performance of the test section were calculated. Subsequently, the computed responses from the three methods were used in the MEPDG performance models in order to investigate the corresponding errors in predicting fatigue and rutting performance. Eq. (5-4) shows the fatigue life prediction equation used in MEPDG. This equation uses the tensile strain at the bottom of the HMA layer ( $\epsilon_t$ ) as well as HMA modulus ( $E_{HMA}$ ) to predict the bottom-up fatigue cracking life of the pavement ( $N_f$ ) (ARA, 2004).

$$N_f = 0.00432 \times k'_1 \times C \left( \frac{1}{\epsilon_t} \right)^{3.9492} \left( \frac{1}{E_{HMA}} \right)^{1.281} \quad (5-4)$$

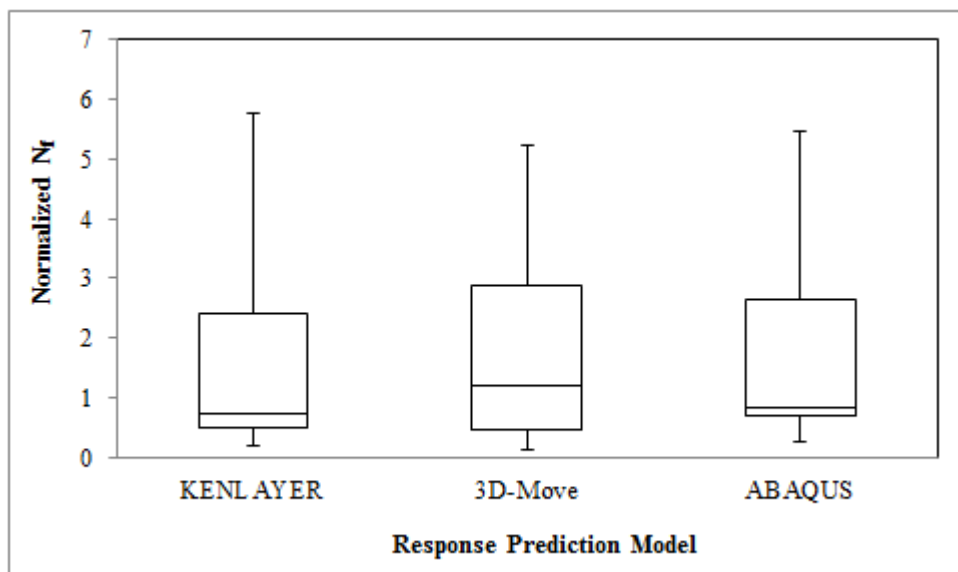
In which,  $k'_1$  is the correction parameter for different HMA layer thicknesses and C is the laboratory to field adjustment factor. Eq. (5-5) is also used in the MEPDG to find the Rut Depth in the HMA ( $RD_{HMA}$ ) as a function of the resilient strain of HMA ( $\epsilon_r$ ), temperature (T), number of load repetitions (N) and HMA layer thickness ( $h_{HMA}$ ) (ARA, 2004).

$$RD_{HMA} = k_1 \times 10^{-3.15552} \times T^{1.734} \times N^{0.39937} \times h_{HMA} \times \epsilon_r \quad (5-5)$$

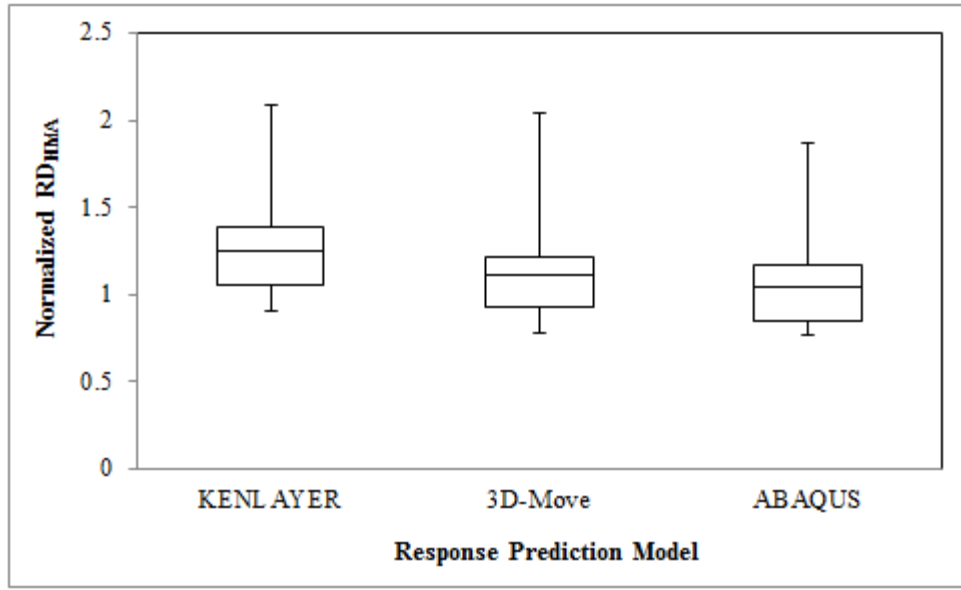
in which  $k_1$  is the depth confining factor determined based on  $h_{HMA}$  and the depth of point of interest. By calculating the  $N_f$  and  $RD_{HMA}$  for each FWD test, once with respect to the measured strains, and then with respect to the computed strains, one can assess the amount of performance prediction errors caused by the three previously described methods.

The longitudinal strain captured by ASG-L was used as the tensile strain of the HMA ( $\epsilon_t$ ), and the vertical strain from ASG-V was used as the resilient strain of the HMA ( $\epsilon_r$ ). The calculated  $N_f$  and  $RD_{HMA}$  based on the computed strains were normalized relative to the measured strains as shown in Figure 5-8 (a) and (b), respectively. It is interesting to note from Eq. (5-4) and Eq. (5-5) that, the normalized  $RD_{HMA}$  solely depends on the ratio of the computed vertical strain to the measured vertical strain, while the normalized  $N_f$  depends on the ratio of the measured longitudinal strain to the computed longitudinal strain to the power of 3.9492. Figure 5-8 (a) demonstrates the negative effect of strain prediction error on the predicted  $N_f$  for each response prediction model. The analysis showed that the range of variation in  $N_f$  was not significantly different among different methods. However, the under-prediction of the longitudinal strain resulted in over-prediction of  $N_f$ , up to 5.7 times when using KENLAYER, 5.2 times when using 3D-Move and 5.4 times when using ABAQUS. More promising results were obtained regarding the normalized predicted  $RD_{HMA}$  as shown in Figure 5-8(b). The normalized  $RD_{HMA}$  varied in a

more limited range than the normalized  $N_f$ , suggesting that the vertical strain computation errors did not cause as much performance prediction error in terms of rutting. Figure 5-8(b) also confirms that the estimated  $RD_{HMA}$  based on KENLAYER computed responses were reasonably comparable to those of the other methods. Results showed that the maximum values of normalized  $RD_{HMA}$  were equal to 2.1, 2.0 and 1.8 based on the KENLAYER, 3D-Move and ABAQUS modeling, respectively.



(a)



(b)

Figure 5-8 Normalized (a)  $N_f$  and (b)  $RD_{HMA}$  versus different prediction models.

## Conclusion

Field measurements for FWD-induced longitudinal tensile and vertical compressive strains were conducted at the full-scale instrumented section of the IRRF. Evaluating the in-situ measured strains showed that the haversine function can closely approximate the pulse shape and the pulse durations in the vertical directions were somewhat larger than those of the longitudinal direction. Consequently, the impact of HMA temperature on the measured peak strains was estimated by developing regression equations with acceptable precisions. Using the backcalculated and laboratory-determined moduli, comparisons were made between measured in-situ response and those computed from KENLAYER, 3D-Move and ABAQUS software. Results showed that the advantage of using the ABAQUS and 3D-Move particularly for computed vertical strain.

However, KENLAYER computed longitudinal strains as well as the vertical strain at lower temperatures were also reasonably accurate. Utilizing the MEPDG performance prediction equations, it was concluded that the discrepancy between computed and measured strain can adversely impact the accuracy of predicted fatigue life more than that of the predicted rut depth in HMA.

## **Acknowledgments**

The financial and in-kind support of Alberta Transportation, Alberta Recycling, and the City of Edmonton for the construction and instrumentation of the IRRF test road is greatly appreciated. The authors also thank Alberta Transportation for conducting the Falling Weight Deflectometer (FWD) tests for this study.

# **Chapter 6 -Seasonal Analysis of Flexible Pavement Response to Falling Weight Deflectometer**

A version of this chapter was published by International Journal of Pavement and Research Technology in September 2015.

## **Abstract**

Seasonal variation in pavement material properties can affect the in-situ measured pavement responses including deflections, stresses and strains. While previous field studies have mostly focused on the seasonal changes in Falling Weight Deflectometer (FWD)'s deflection basin, the simultaneous variations of stresses and strains were not usually monitored. The present study assesses seasonal impact on horizontal and vertical strains at the bottom of Hot Mix Asphalt (HMA) as well as unbound layers stress at different depths. Several FWD tests were conducted from October, 2013 to December, 2014 in instrumented test road facility in Edmonton, Alberta, Canada. The obtained results showed that the pressure on top of base layer in the thaw season can exceed the one in the freeze season twice as much. Similarly, significant seasonal variations of horizontal and vertical strains at the bottom of the HMA were noticed. The present study concludes that using backcalculated layers moduli may result in overestimation of the vertical stress within unbound layers and HMA horizontal strain, while underestimating HMA vertical strain.

**Key words:** *Seasonal variation, Pavement response, Falling weight deflectometer, Backcalculation*

## **Introduction**

Seasonal variation in material properties of flexible pavement may cause significant changes in pavement responses such as stress, strain and deflection within the structure. On the other hand, according to the Mechanistic Empirical Pavement Design Guide (MEPDG) (ARA, 2004), long-term pavement performance prediction models are considerably influenced by the critical pavement responses under loading. Therefore, it is crucial to evaluate the seasonal variation of pavement layers characteristics via nondestructive testing equipment such as Falling Weight Deflectometer (FWD) (Shahin, 2005). Several researchers have attempted to theoretically investigate the seasonal changes in pavement responses based on the measured surface deflection basins under FWD and backcalculation of different pavement layers moduli (van Gurp, 1995; Simonsen et al., 1997; Drumm and Meier, 2003). However, few field experiments have been conducted to investigate direct measurement of strain changes at the bottom of the Hot Mix Asphalt (HMA) and stress changes within unbound layers due to seasonal variations. Under the Seasonal Monitoring Program (SMP) of the Federal Highway Administration Long Term Pavement Performance (LTPP), seasonal change in the horizontal strain at the bottom of the HMA and vertical strain on top of the subgrade were modeled through layered elastic approach (Drumm and Meier, 2003). This research showed that thaw weakening of the structure can pose a concern in terms of greater vertical strain on top of the subgrade, whereas the summer's horizontal strain was critically high. In a study conducted by Simonsen et al. (1997), approximation of asphalt and subgrade strains using finite element modeling (FEM) revealed noticeably higher subgrade strains during the thaw period, while maximum asphalt strain occurred when surface temperature was the highest.

Based on several studies conducted at instrumented pavement sections to measure pavement response under FWD, a wide range of error exists between the measured and theoretically predicted values. Ullitz et al. (1994) conducted FWD tests in southern Sweden and the Danish Road Testing Machine (RTM) to measure tensile strain at the bottom of the HMA and stress on top of the subgrade. Utilizing MODULUS 4.0 (Scullion and Michalak, 1991) to backcalculate the layer's moduli and using WES5 (Van Cauwelaert et al., 1989) computer program to predict responses, the study revealed discrepancy between the measured and the predicted values. This research indicated that non-linear elastic behavior of subgrade soil is probably attributed to disagreement between the measured and the predicted responses. Performing FWD tests along an instrumented pavement section in Oklahoma, Solanki et al. (2009) also reported 104 to 164 and 4 to 22 percent prediction errors between measured and predicted stresses on top of the natural subgrade and the granular base, respectively. They concluded that invalid underlying assumptions in the linear elastic theory such as consideration of homogeneous, isotropic, and linear elastic materials and also static modeling of the FWD load rather than a dynamic impulse load are responsible for the observed discrepancies. In an attempt to predict horizontal strain in HMA and stress within unbound layers, simulation of FWD was performed using three-dimensional Finite Element Model (FEM) while considering subgrade as a nonlinear elastic layer (Yin, 2012). This research showed that measured values were over-predicted from 20 to 49 percent on average irrespective of FWD loading magnitude. It was concluded that due to the temperature gradient across the thick HMA layer, consideration of one single backcalculated modulus for the whole layer can lead to erroneous predictions.

The scope of the aforementioned studies has not generally included a year-round series of FWD tests to validate the accuracy of using backcalculated layers moduli for response prediction.

However, the seasonal monitoring of stresses and strains can provide more insight in terms of both seasonal variation of pavement material, as well as effectiveness of backcalculated layers moduli for response prediction. The present study was conducted at Integrated Road Research Facility (IRRF)'s test road facility in Edmonton, Alberta, Canada to address the seasonal variation in pavement responses from October, 2013 to December, 2014. Horizontal and vertical strain at the bottom of the HMA, as well as vertical stress within unbound layers were monitored through several applications of FWD test on top of Asphalt Strain Gauges (ASG) and Earth Pressure Cells (EPC). In addition to seasonal monitoring of the induced responses, the accuracy of using backcalculated layers moduli for prediction of the in-situ measured responses in different seasons was also evaluated.

## **Overview of IRRF Test Road Facility**

The IRRF's test road facility is the new access road to Edmonton Waste Management Center (EWMC) located in the Northeast of the City of Edmonton, Alberta, Canada. Once opened to traffic, the test road is subjected to more than 500 garbage trucks per day, transporting waste materials to EWMC. The test road comprises two approximately 100-m apart pavement monitoring sections with 250-mm HMA layer, placed on top of a 450-mm granular base course (GBC) on top of clayey sand subgrade (SG) soil.

During construction in the summer of 2012, the test sections were instrumented with ASGs (Model CEA-06-125UT-350 from the CTL Group) and EPCs (Model LPTPC12-S from rst instruments) at different depths in the unbound layers. High-speed CR9000X datalogger from Campbell Scientific Corp Canada is used to collect the dynamic responses of both sections at

500 Hz under current FWD tests as well as future traffic. Both sections are similarly instrumented at the bottom of the HMA layer with six ASGs laid in the longitudinal direction (ASG-L), six ASGs laid in the transverse direction (ASG-T) and six vertical ASGs (ASG-V). Figures 6-1 (a) and (b) show the instrumentation layout, which is replicated in the two sections at the IRRF's test road. One array of ASG was laid along the outer wheelpath (OWP). To ensure repeatability and reliability of measurements under live traffic, the arrangement of the ASGs along the OWP was replicated in two additional lines, 600 mm to the right and 600 mm to the left of the OWP. EPCs were installed at two locations, on the OWP and on the inner wheelpath (IWP). As seen in Figure 6-1 (c), each location includes three EPCs installed at three different depths. EPC 1 and 2 were installed on the top of the GBC; EPC 3 and 4 were installed at the top of SG, and EPC 5 and 6 were installed at 1000-mm from the top of SG layer to monitor the distribution of load in the pavement underlayers.

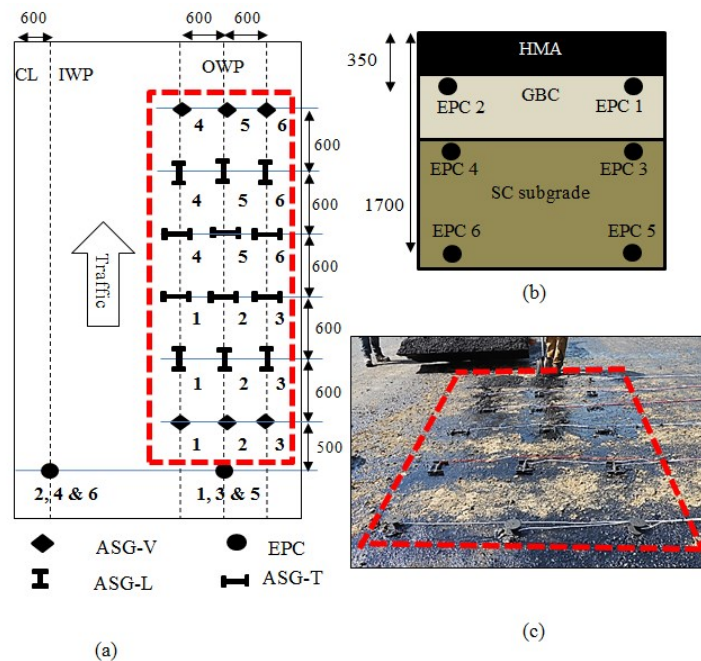


**Figure 6-1 (a) Schematic of instrumentation, (b) Schematic cross-section and the EPC locations, (c) Installation of sensors at the bottom of the HMA (all dimensions are in mm).**

## Results and Discussion

### FWD Testing Results in Different Seasons

FWD tests were conducted in October 2013 and April, July, September, October, November, December 2014 at specific sensor locations. During the testing, the HMA layer temperature was measured at 20 mm from the surface. At each test location, three drops were embarked at three stress levels using a Dynatest 8000 with sensor offsets at 0, 200, 300, 450, 600, 900, 1200 mm from the center of the load plate.

Three FWD drops were conducted at three locations along the OWP: on top of ASG-T 2, ASG-V 2 and EPC 1, 3 and 5. In each FWD test, a total of three pulses from each one of the sensors representing horizontal tensile strain ( $\varepsilon_t$ ), vertical compressive strain ( $\varepsilon_v$ ) both at the bottom of the HMA, stress ( $\sigma_v$ ) at top of the GBC and  $\sigma_v$  on top of SG and  $\sigma_v$  at 1000-mm within SG were available for analysis. It should be noted that the FWD tests conducted at one gage location resulted in negligible responses at adjacent gage locations, and thereby this study focuses only on the pulses under the load plate.

To compare deflection variations in different seasons, deflection basins obtained on top of EPC 1 were plotted for the seven FWD tests in Figure 6-2. Comparison of deflection bowls evidently indicated lower deflections in colder months of the monitoring period and higher deflections during the thaw period. Results showed that the maximum central deflection under the load plate recorded in April, 2014 was 10 times larger than the minimum corresponding value in December, 2014. FWD tests performed in freeze period (i.e. November, 2014 and December, 2014) resulted in almost similar deflection basins. Also, consistent deflection basins were

observed in October, 2013 and October, 2014 as the pavement was not subjected to traffic load over this time period.

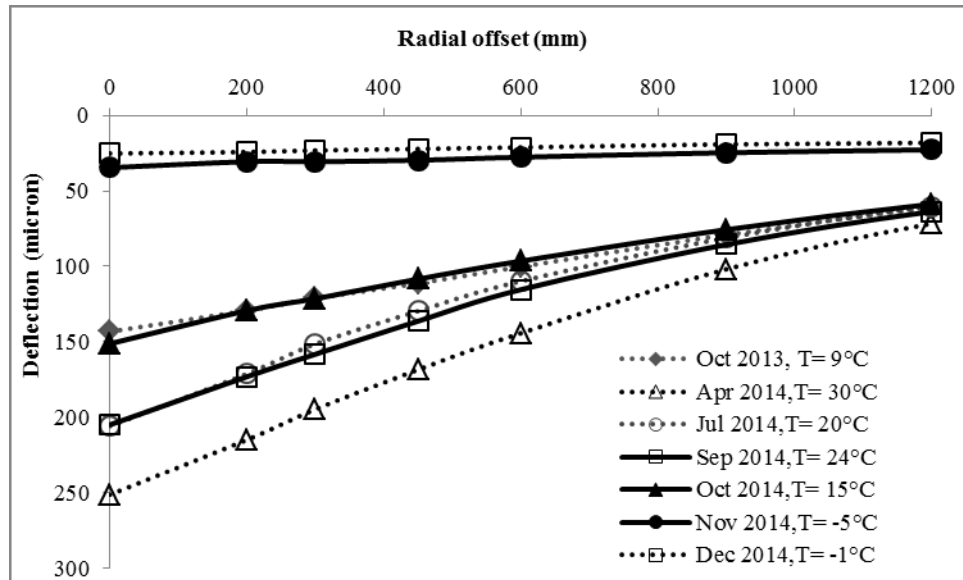
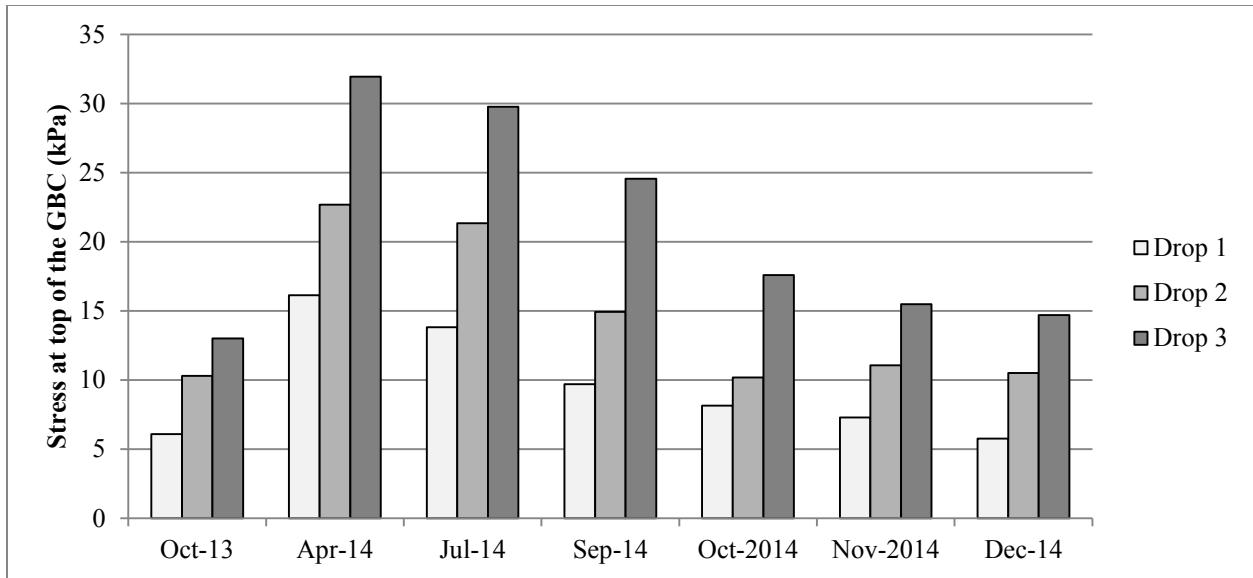


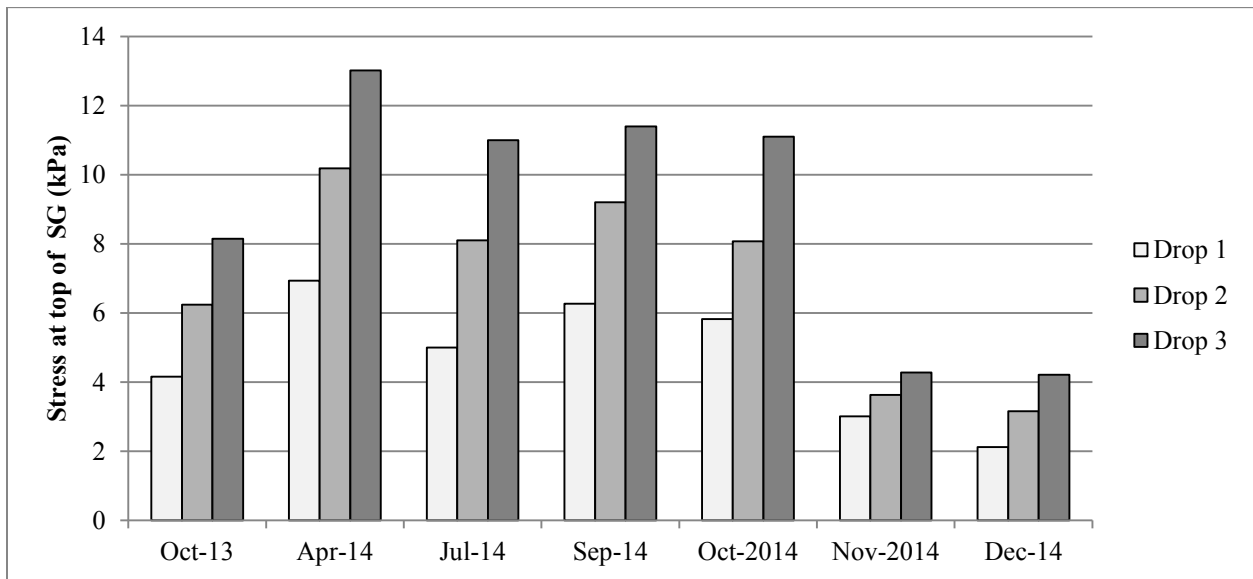
**Figure 6-2 Comparison of deflection basins for different FWD tests.**

Analysis of pavement instrumentation responses was conducted to monitor the seasonal variation of  $\sigma_v$  within unbound layers as well as the  $\epsilon_r$  and  $\epsilon_v$  at the bottom of the HMA. The distribution of  $\sigma_v$  within the base and subgrade can be investigated when the FWD loading was conducted over EPC 1 which is located on top of EPC 3 and EPC 5. The analyses of the  $\sigma_v$  measured by EPC 1, EPC 3 and EPC 5 were performed to investigate the impacts of depth and FWD stress levels on the  $\sigma_v$ . Figure 6-3(a) shows the variation of  $\sigma_v$  measured on top of the GBC when subjecting the pavement to three FWD stress levels. The collected data suggests a consistent increase in the  $\sigma_v$  as the stress levels increased. Testing at the highest FWD stress, maximum recorded  $\sigma_v$  of 32.0 kPa occurred in April, 2014 and minimum value was determined to be 14.5 kPa in December, 2014 implying a noticeable decrease through evolution of recovery followed by freeze periods.

Furthermore, the average increase in the  $\sigma_v$  at GBC was 54 and 123 percent when the average FWD stress increased from 386 to 566 and 762 kPa, respectively. Figure 6-3(b) also depicts the changes in  $\sigma_v$  measured on top of SG showing that the recorded pressure ranged between 13.0 kPa (April, 2014) and 4.2 kPa (December, 2014) under the highest FWD stress level. The increasing trend of the measured  $\sigma_v$  versus higher FWD stress levels was observed, indicating on average 45 and 88 percent larger values when subjecting the pavement to drop 2 and 3, respectively. In an attempt to evaluate the decrease of  $\sigma_v$  in depth, it was found that  $\sigma_v$  on top of SG was 68 percent less than the associated value on top of GBC in December 2014, while the difference decreased to 28 percent in October 2014. Looking at variation of the  $\sigma_v$  at 1000-mm depth within SG as illustrated in Figure 6-3(c), the proportion of the pressure resulting from uniformly distributed circular load of FWD load in SG was not significant. The range of variability of  $\sigma_v$  was from 5.0 to 0.7 kPa under the highest FWD stress level. Overall, the recorded  $\sigma_v$  at 1000-mm depth within SG showed 49 and 120 percent increase as the average FWD stress level increased by 47 and 98 percent, respectively. The ratios between the  $\sigma_v$  values recorded in April-2014 and December-2014 were 2.2 on top of the GBC, 3.1 on top of SG and 7.1 at 1000-mm within SG.



(a)



(b)

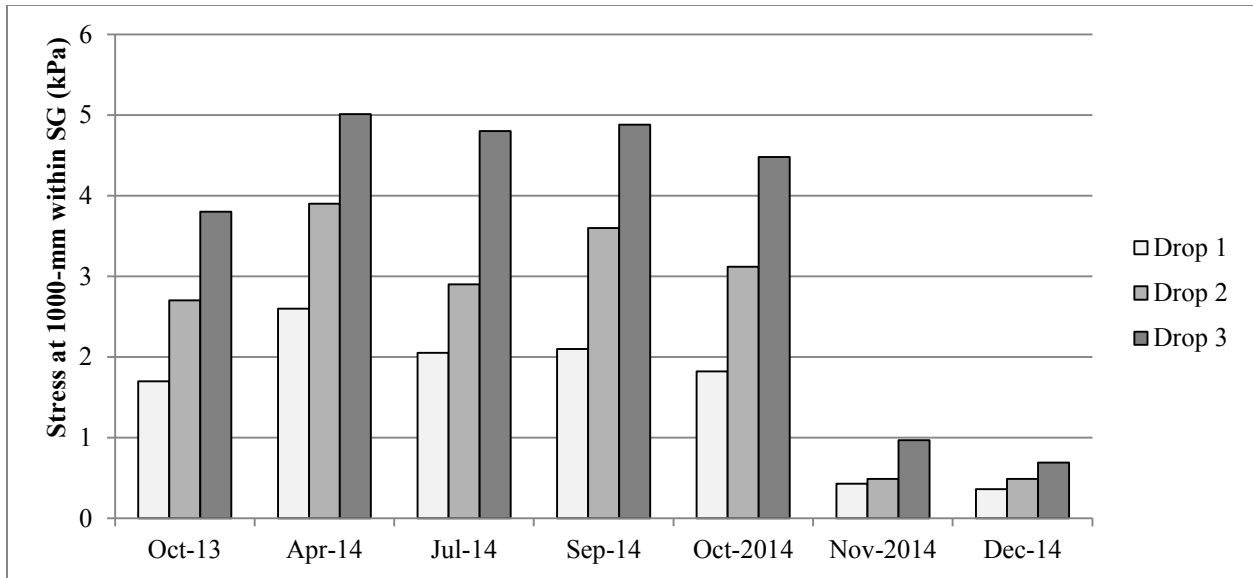
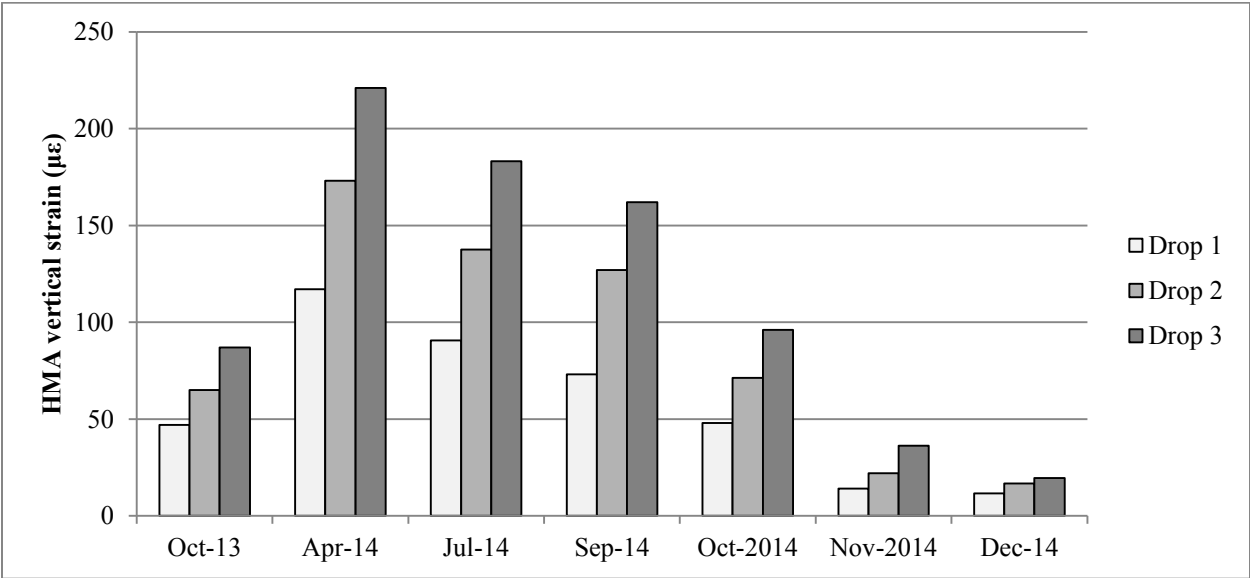


**Figure 6-3 Measured vertical stresses at (a) top of the GBC, (b) top of SG and (c) 1000-mm depth within SG.**

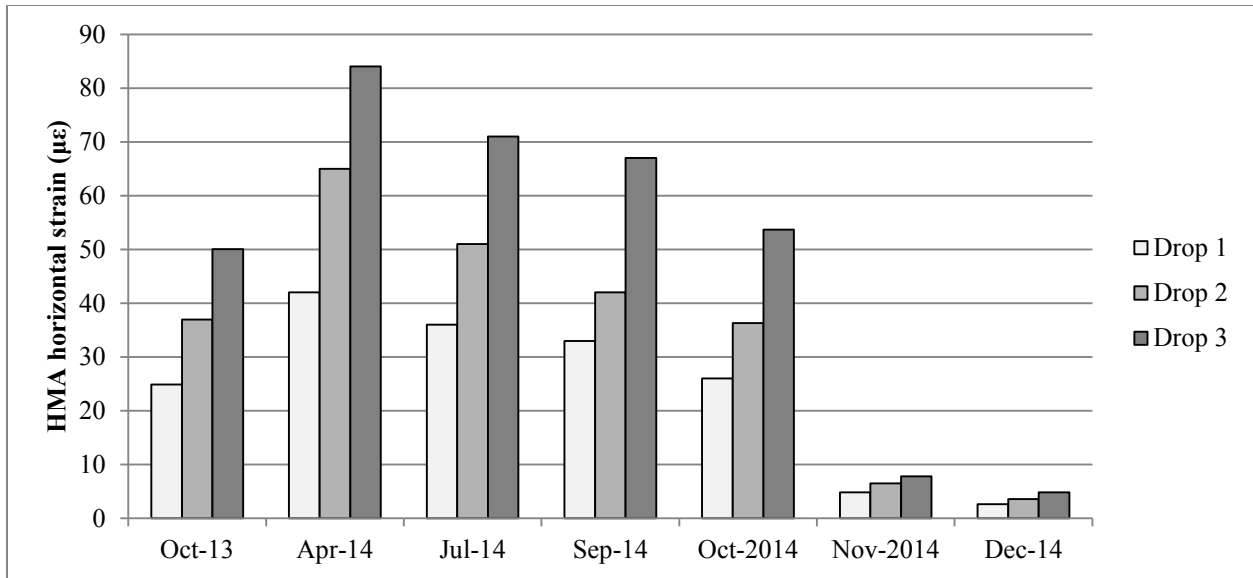
(c)

Strain measurements at the bottom of the HMA layer are provided in Figures 6-4 (a) and (b). Figure 6-4 (a) presents the  $\epsilon_v$  at the bottom of the HMA layer under the three FWD stress levels for the test conducted at ASG-V2 location. As expected, the maximum  $\epsilon_v$  of 221  $\mu\text{m}/\text{m}$  occurred in April-2014 when pavement experienced the thaw period, whereas the minimum value of 19  $\mu\text{m}/\text{m}$  was recorded in December-2014 as a result of freezing. The obtained difference between maximum and minimum observed  $\epsilon_v$  confers a pronounced dependency of such response to seasonal variation. Besides,  $\epsilon_v$  generally remained higher in April, July and September of 2014 signifying the importance of potential rutting in HMA at higher temperatures. In order to understand the stress-strain behavior of the HMA layer, the increments in  $\epsilon_v$  were calculated as 52 and 106 percent when the FWD stress increased by 47 and 98 percent on average. Figure 6-4 (b) depicts the  $\epsilon_t$  at the bottom of the HMA layer measured by ASG-T2 under three FWD load drops for the tests conducted directly over ASG-T2. Evaluation of  $\epsilon_t$  ranging from a low of 5

$\mu\text{m/m}$  to a high of  $84 \mu\text{m/m}$  revealed an identical behavior of response against seasonal change as explained for  $\sigma_v$  and  $\varepsilon_v$  previously. Although the magnitude of  $\varepsilon_v$  was approximately 2.3 times larger than those of  $\varepsilon_t$  for all the collected data, strong linear relationships were still evident for the FWD stress levels and  $\varepsilon_t$ . It means that  $\varepsilon_t$  exhibited 41 and 94 percent increase in parallel with 47 and 98 percent increase of stress exerted by FWD. According to Figure 6-4 (b), HMA layer was more prone to development of bottom-up fatigue cracking in April-2014 when it endured the maximum tensile strains. Based on Figure 6-4,  $\varepsilon_v$  and  $\varepsilon_t$  measured in April-2014 were 11.3 and 17.3 times larger than the corresponding values measured in December-2014, respectively.



(a)



(b)

**Figure 6-4 Measured (a) vertical strain and (b) horizontal strain at the bottom of HMA.**

To investigate the probable source of variation in the responses obtained in different seasons, deflection history data collected for each FWD test was also analyzed. Knowing that the variation of pavement behavior across different seasons can also be evaluated using deflection time history data (Deblois et al., 2010), the exerted FWD load attributed to the medium stress level was plotted against central geophone. As shown in Figure 6-5, the largest hysteresis curve was captured in April-2014 when pavement structure was weak due to thawed unbound layers and asphalt temperature was the highest. Hence, as the pavement temperature increased, the hysteresis curves tended to reflect more viscoelastic behavior of HMA. According to Figure 6-5, more plastic deflections were noticed in the warmer months which can be attributed to the viscous behavior of the HMA. This is in line with the higher magnitudes of  $\varepsilon_t$  and  $\varepsilon_v$  in the warmer months due to the lower stiffness of HMA. Hence, higher proportion of the applied FWD stress reaches to the unbound layer as previously shown in Figure 6-3.

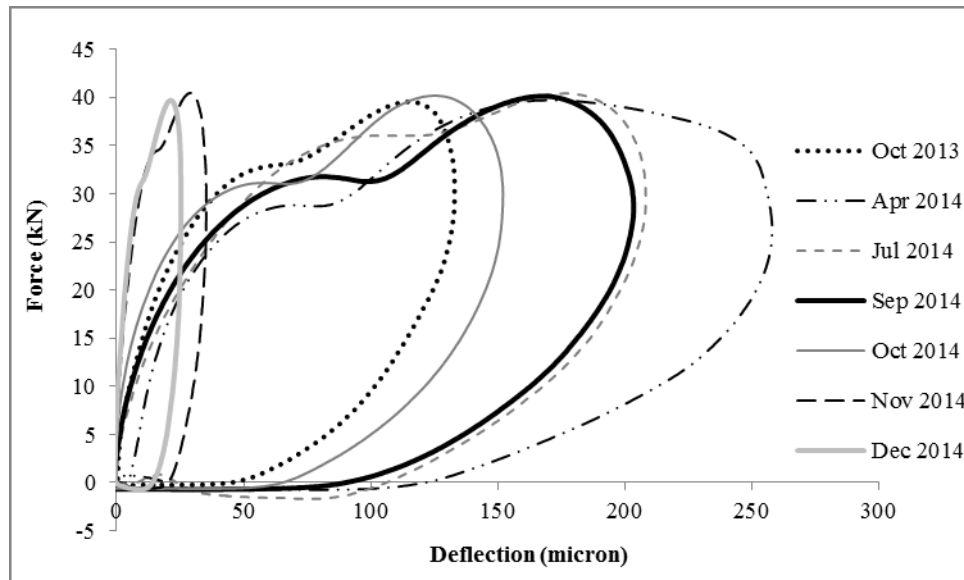


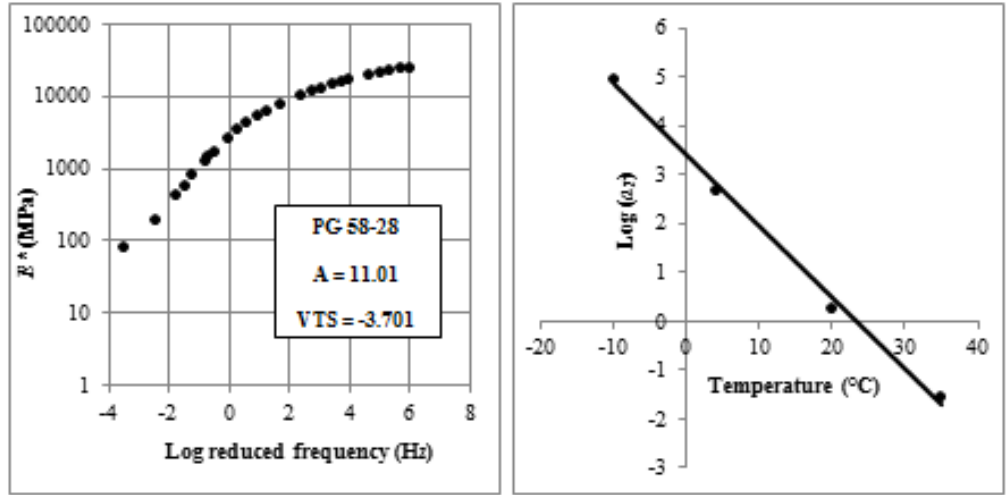
**Figure 6-5 Hysteresis curves for different FWD tests.**

### **Backcalculations of Layers Moduli**

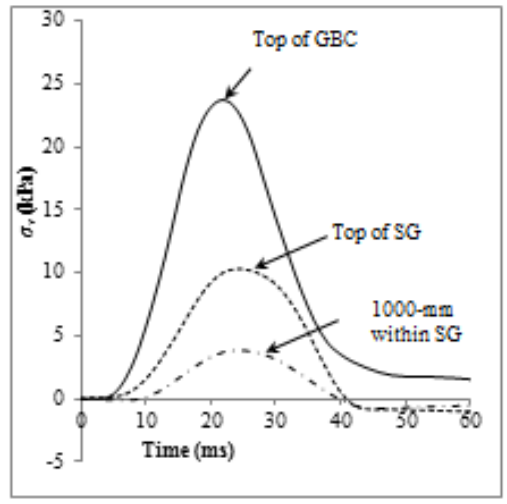
To interpret the FWD deflection data, the peak values from each geophone's deflection time history were used to determine pavement layers moduli through static backcalculation. The deflection basins recorded at the three test locations were used to determine the pavement layer's moduli. The deflection basins recorded at the three test locations had negligible differences, therefore the deflection basins obtained from the FWD tests conducted on top of EPC 1 were used for backcalculation. To investigate the agreement between the predictions and the measured pavement's structural responses, layers moduli needed to be established first. To do so, deflection data from the FWD tests were used to backcalculate the pavement layers moduli according to ASTM D5858 (ASTM, 2008). EVERCALC was used to backcalculate the elastic modulus of the HMA ( $E_{HMA}$ ), GBC layer ( $E_{GBC}$ ) and SG layer ( $E_{SG}$ ). EVERCALC includes the WESLEA forward calculation subroutine to predict the pavement's structural responses and uses

a modified Augmented Gauss-Newton algorithm for solution optimization. A stiff layer was considered in EVERCALC (the depth calculated internally), and the HMA modulus was set to be corrected internally based on the HMA temperature measured during testing.

In order to initialize the backcalculation process, each layer's seed modulus needs to be defined by the user. Due to its viscoelastic properties,  $E_{HMA}$  strongly depends on the loading frequency and temperature. In order to define a proper seed value for  $E_{HMA}$ , the laboratory-determined HMA mixture master curve was constructed based on AASHTO TP79 as shown in Figure 6-6(a) and (b). In order to find the appropriate loading frequency for the FWD tests, the average pulse duration measured by EPC 1, EPC 3 and EPC 5 was used according to Figure 6-6 (c). Results showed that the pulse duration did not vary amongst all FWD tests and also remained nearly constant at different depths below the surface. Thus, pulse duration determined by doubling the time elapsed from the beginning of the pulse to the peak in the first half of the pulse was calculated equal to 30 ms and selected as the representative pulse duration for further conversion to loading frequency. Therefore,  $E_{HMA}$  values associated with 33 Hz loading frequency, calculated based on the inversed pulse duration, were derived according to the developed master curve as summarized in Table 6-1.



(a) (b)



(c)

Figure 6-6 (a) Master curve and (b) shift factor for the HMA, (c) Typical stress pulses at different depths for April, 2014 test.

**Table 6-1 Summary of layers moduli from laboratory and FWD-backcalculation.**

Test	Temperature at 20-mm depth (°C)	Laboratory	Backcalculation			<i>RMSE</i> (percent)
		$E_{HMA}$ (MPa)	$E_{HMA}$ (MPa)	$E_{GBC}$ (MPa)	$E_{SG}$ (MPa)	
<b>Oct-13</b>	9	15640	10650	188	152	1.76
<b>Apr-14</b>	30	4100	2980	170	107	0.46
<b>Jul-14</b>	20	8500	3410	296	112	0.59
<b>Sep-14</b>	24	6300	4325	212	106	0.47
<b>Oct-14</b>	15	12340	9115	210	149	0.50

Typical values of 100 and 50 MPa recommended in ASTM D5858 were used to define the seed values for  $E_{GBC}$  and  $E_{SG}$ , respectively. Further, Poisson’s ratio was defined as 0.35, 0.4 and 0.4 for HMA, GBC and SG soil, respectively, as outlined in ASTM D5858. Table 6-1 also shows the backcalculated layers moduli in addition to the Root Mean Square Errors (*RMSE*) for individual FWD tests. It is worth noting that two percent limit recommended by ASTM D5858 was used as the criteria to select acceptable backcalculation results. It is noteworthy that backcalculation of layers moduli for FWD tests performed in November and December of 2014 did not return acceptable *RMSE* values probably due to the frozen condition of the unbound layers and high stiffness of the HMA layer at subzero temperature; thereby, the two FWD tests were excluded for further analysis of the responses.

## Analysis of Calculated Responses

To evaluate the validity of the backcalculated moduli, pavement responses were calculated using KENLAYER. To pursue this purpose, the EVERCALC-backcalculated moduli were used to define each layer's properties in each FWD test when using KENLAYER. The loading was defined as static, uniform circular load, resulting in FWD stress levels. Note that the analysis focuses only on the responses under the center of the FWD load plate, since the induced responses at adjacent gage locations were negligible. To do so, the validated models were used to extract the pavement structural responses to the three FWD stresses at each gage location. Table 6-2 presents the KENLAYER-predicted responses and the errors in prediction of in-situ measured values for all FWD tests. Percent of Prediction Errors (*PPE*) defines the accuracy of theoretical values according to Equation 6-1:

$$PPE = \left( \frac{M-P}{P} \right) \times 100 \quad (6-1)$$

where, M is the measured response and P is the predicted response.

According to Table 6-2, except for the  $\varepsilon_v$  at the bottom of HMA, other responses were overestimated when using backcalculated set of moduli in KENLAYER. It appears that the pattern of response variation with seasonal change in material properties was successfully captured through simulation of FWD tests. Taking the PPE of  $\varepsilon_t$  into account, the average *PPE* of the test in October, 2013 was -17 and it remained almost consistent in October, 2014 equal to -26. However, the average PPE decreased to -53, -45 and -46 in April, July and September of 2014, respectively. This shows higher discrepancies between measurement and prediction in thaw and summer periods. The absolute average PPE values of 32 for  $\sigma_v$  at top of GBC, 38 for  $\sigma_v$  at top of SG and 28 for  $\sigma_v$  at 1000-mm depth within SG are reasonably comparable with the

**Table 6-2 Summary of predicted responses and prediction errors.**

Test	FWD stress (kPa)	$\sigma_v$ at GBC		$\sigma_v$ at SG		$\sigma_v$ at 1000-mm within SG		$\varepsilon_v$ at the bottom of HMA		$\varepsilon_t$ at the bottom of HMA	
		$P^a$	PPE	$P$	PPE	$P$	PPE	$P$	PPE	$P$	PPE
		(kPa)	(percent)	(kPa)	(percent)	(kPa)	(percent)	( $\mu\varepsilon$ )	(percent)	( $\mu\varepsilon$ )	(percent)
Oct-13	391	12.0	-49	6.8	-39	2.8	-40	34	39	30	-18
	565	17.4	-41	10.0	-38	4.1	-35	50	30	45	-17
	732	23.3	-44	13.5	-39	5.6	-32	67	30	60	-17
Apr-14	380	21.6	-25	9.8	-29	3.3	-21	84	8	91	-54
	561	31.9	-29	14.4	-30	4.9	-20	125	8	134	-52
	744	42.7	-25	19.3	-33	6.5	-23	167	3	180	-53
Jul-14	379	21.3	-35	9.4	-47	3.2	-36	78	16	66	-45
	572	31.4	-32	13.9	-42	4.7	-39	116	19	97	-47
	758	42.1	-29	18.6	-41	6.3	-24	155	18	129	-45
Sep-14	382	18.0	-23	10.5	-44	3.2	-28	69	7	59	-44
	569	26.5	-11	15.4	-44	4.7	-20	101	26	87	-52
	764	35.5	-8	20.6	-47	6.3	-23	135	20	117	-43
Oct-14	381	13.4	-39	8.2	-29	2.8	-36	38	26	34	-23
	566	20.0	-49	12.2	-34	4.2	-26	56	26	50	-28
	761	26.8	-34	16.4	-32	5.7	-21	75	28	76	-29

average error of 30 percent reported by Yin (2012) [10] through 3D finite element modeling of flexible pavement response to FWD in Blair County, Pennsylvania. In addition, averaged *PPE* values of the  $\sigma_v$  at three depths were determined equal to -35 percent for drop 1, -32 percent for drop 2 and -30 percent for drop 3 suggesting the independence of *PPE* on FWD stress.

Figure 6-7 illustrates the variation of *PPE* against different response types. The *PPE* associated with  $\sigma_v$  at top of GBC varied in a larger range of values than other responses. For  $\sigma_v$  recorded at top of SG, the median of *PPE* values was the lowest, while the *PPE*s were more in agreement with each other in comparison to the cases of  $\sigma_v$  recorded at top of GBC and at 1000-mm within SG. Furthermore, *PPE* values for  $\epsilon_v$  had a better level of agreement with each other when compared to those of  $\epsilon_t$ . Using the linear elastic approach, average *PPE* for  $\epsilon_t$  was determined to be -37, while it was near 20 for  $\epsilon_v$ .

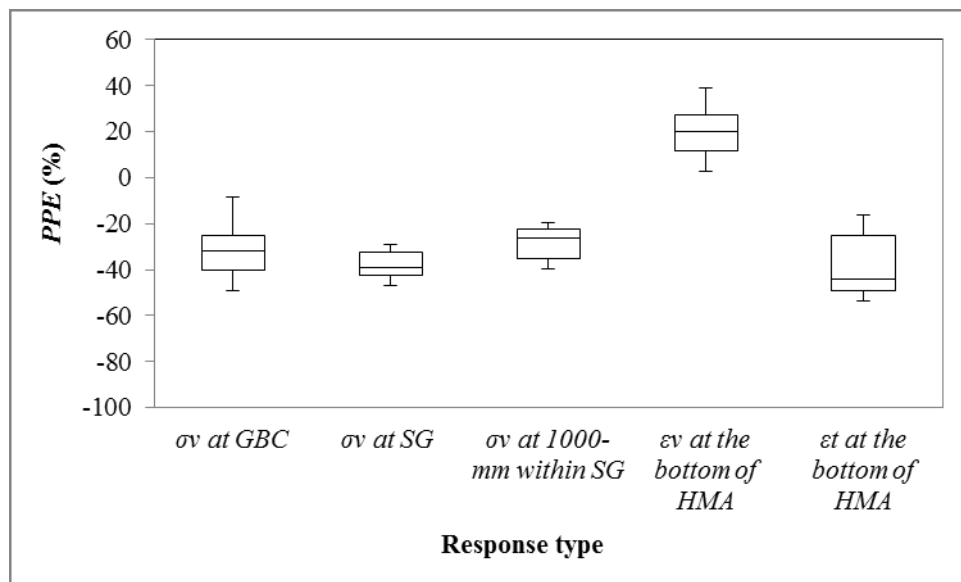


**Figure 6-7 Comparison of response prediction errors.**

This analysis shows that consideration of linear elastic isotropic and homogenous materials, and static circular loading of FWD can contribute to inaccurate backcalculation of layers moduli and consequently erroneous prediction of response. To summarize, direct validation of theoretically calculated responses in the field and their comparison to the in-situ measured responses revealed the potential error in application of commonly-used FWD analysis methods.

## **Conclusion**

FWD tests were performed directly on top of ASGs and EPCs embedded in the IRRF test road in Edmonton, AB, Canada, to monitor the seasonal variation in pavement responses. This research focused on the evaluation of horizontal ( $\varepsilon_t$ ) and vertical ( $\varepsilon_v$ ) strains at the bottom of the HMA layer, as well as the vertical pressure ( $\sigma_v$ ) at different depths within the unbound layers when subjected to FWD testing. The maximum values of recorded strains and stresses occurred in April, 2014 due to thawing in pavement layers. As a result,  $\sigma_v$  on top of the GBC recorded in the thaw season was 2.2 times larger than the corresponding values in the freeze season. Besides,  $\varepsilon_v$  and  $\varepsilon_t$  at the bottom of the HMA layer were also 11.3 and 17.3 times larger than those in Dec-2014, respectively. Using hysteresis curves for each test, it was found that higher measured responses in warmer months can be attributed to the more viscous behavior of the HMA. Comparisons were made between the in-situ measured and predicted responses using EVERCALC-backcalculated-layers moduli in KENLAYER. It was observed that using a computer simulation led to over-prediction of  $\sigma_v$  within unbound layers and  $\varepsilon_t$  at the bottom of the HMA, while  $\varepsilon_v$  values at the bottom of the HMA were generally underestimated. The average Percent of Prediction Error (*PPE*) values were found equal to -32 for  $\sigma_v$  on top of the GBC, -38

for  $\sigma_v$  on top of SG, -28 for  $\sigma_v$  at 1000-mm within SG, 20 for  $\varepsilon_v$  at the bottom of the HMA and -37 for  $\varepsilon_t$  at the bottom of the HMA. It was found that the magnitudes of *PPEs* associated with  $\sigma_v$  at GBC varied in a larger range when compared to other responses. However, a better level of agreement was observed between *PPEs* of  $\varepsilon_v$  rather than those of  $\varepsilon_t$  both at the bottom of the HMA. Finally, the average *PPEs* tended to be higher during warmer months due to the deviation of HMA behavior from linear elasticity.

## **Acknowledgements**

The authors would like to acknowledge Alberta Transportation, Alberta recycling, and The City of Edmonton for providing financial and in-kind support for the construction and instrumentation of the IRRF's test road. Alberta Transportation is also acknowledged for conducting the falling weight deflectometer (FWD) tests for this study. The close cooperation of Tetra Tech EBA FWD test crews during testing is also greatly appreciated.

# **Chapter 7 -Field Investigation of Thermal-Induced Strains in Flexible Pavement Structures**

A version of this chapter was submitted to International Journal of Pavement Engineering in December 2015.

## **Abstract**

Thermal-induced strains caused by daily temperature fluctuations are considered to be a direct impact of environmental factors on flexible pavements. Thermal fatigue cracking occurs when the daily temperature cycles lead to reoccurring tensile stress at the bottom of the Hot Mix Asphalt (HMA) layer. Individually, the stresses may not exceed the tensile strength of the asphalt, but when repeated over time, cyclic loading will cause the occurrence of cracks. Therefore, it is necessary to experimentally quantify the range of variation for thermal-induced strains in order to evaluate the impact of daily and seasonal temperature fluctuations on thermal fatigue cracking. This paper investigates the thermal-induced strains in longitudinal, transverse, and vertical directions at the bottom of the HMA over the course of a 16-month monitoring period that includes a freeze and thaw cycle. This study was conducted at the Integrated Road Research Facility (IRRF)'s test road, which is fully equipped with structural and environmental monitoring instruments in Edmonton, Alberta, Canada. Based on the results, noticeable variations for horizontal and vertical strains at the bottom of the HMA were observed as a function of ambient air temperature change. This study showed that the highest strains occurred in winter and spring, while the most pronounced strain fluctuations were captured during the spring-thaw period. Using strain and temperature data, coefficients of thermal contraction and expansion were determined during different seasons. It was found that thermal coefficients are different in three directions, illustrating the anisotropic properties of HMA. However, the average of coefficient of thermal contraction obtained from the field in winter time was well matched with the calculated values according to MEPGD.

**Key words:** *Thermal-induced strains; Hot mix asphalt, Temperature fluctuation; Thermal contraction and expansion; Pavement instrumentation*

## Introduction

Pavement responses such as stress, strain and deflection can be directly and/or indirectly affected by environmental factors. Temperature is one of the main environmental factors that can directly cause strains due to the contraction and expansion of the Hot Mix Asphalt (HMA). On the other hand, temperature can also influence the HMA stiffness and indirectly affect the induced strain under traffic loading (ARA 2004). Although several researchers (Epps *et al.* 1997, Al-Qadi and Bhutta 1999, Loulizi *et al.* 2002, Mateos and Snyder 2002) have studied the indirect impact of temperature change on pavement responses due to traffic loading, only few studies have focused on evaluating the responses caused solely by temperature variation in the absence of traffic. Quantifying the amplitude of asphalt strain associated with thermal loading on flexible pavements in these studies indicated that considering thermal strains could be critical for accurate pavement performance prediction.

Thermal-induced longitudinal strains at the bottom of the HMA layer have been studied by Al-Qadi *et al.* (2005) at the Virginia Smart Road test facility in Montgomery County, Virginia, United States. In this study, the impacts of air temperature and pavement temperature change on the strain were evaluated using longitudinal Asphalt Strain Gauges (ASGs) placed at the bottom of the HMA. Daily thermal-induced strain fluctuations were estimated by calculating the cyclic strain range, defined as the difference between the maximum and minimum daily observed strain values according to Equation 7-1.

$$\Delta\varepsilon = \varepsilon_{max} - \varepsilon_{min} \quad (7-1)$$

where  $\Delta\varepsilon$  is the daily thermal-induced strain range,  $\varepsilon_{max}$  is the maximum daily strain and  $\varepsilon_{min}$  is the minimum daily strain.

Results from the study by Al-Qadi *et al.* (2005) showed that the daily  $\Delta\varepsilon$  can be as high as 350  $\mu\text{m}/\text{m}$ , which occurred during the spring-thaw weakening of the asphalt pavement. In another study conducted at the Centre for Pavement and Transportation Technology (CPATT) test track in Waterloo, Ontario, Canada, Bayat (2009) reported a daily  $\Delta\varepsilon$  of 680  $\mu\text{m}/\text{m}$  at the bottom of the asphalt during spring and summer. In addition to this, two years of measuring longitudinal strain due to thermal loading demonstrated major irrecoverable strains of up to 2338  $\mu\text{m}/\text{m}$  at the end of each year. Recently, Islam and Tarefder (2013) evaluated the diurnal variation of horizontal strain at different depths within HMA in New Mexico, United States. The in-situ measured daily  $\Delta\varepsilon$  was recorded as high as 690  $\mu\text{m}/\text{m}$  at a depth of 90 mm and 342  $\mu\text{m}/\text{m}$  at a depth of 300 mm below the surface, showing that the magnitude of horizontal thermal strain can decrease at deeper elevations. Also, it was found that thermal strain is generally tensile in the morning when the temperature is lower and compressive in the afternoon when the temperature is higher. Islam and Tarefder (2014) also conducted a field study on the thermal-induced strain to calculate the Coefficient of Thermal Contraction (CTC) and Coefficient of Thermal Expansion (CTE). Using ASGs installed in longitudinal and transverse directions along the road and temperature probes installed at the bottom of the HMA, the CTC and CTE of the HMA were found according to Equation 7-2.

$$CTC \text{ (or, CTE)} = \frac{\varepsilon}{\Delta T} \quad (7-2)$$

where,  $\varepsilon$  is the measured strain obtained from ASG and  $\Delta T$  is the temperature change indicated by the temperature probe. Results from the field study by Islam and Tarefder (2014) showed that the CTC values calculated for fall and winter seasons were  $2.69 \times 10^{-5}$  ( $1/^\circ\text{C}$ ) and  $2.47 \times 10^{-5}$  ( $1/^\circ\text{C}$ ), respectively. Similarly, the CTE values were calculated equal to  $2.47 \times 10^{-5}$  ( $1/^\circ\text{C}$ ) in fall

and  $2.77 \times 10^{-5}$  ( $1/^\circ\text{C}$ ) in winter. Later, a laboratory study performed at a temperature range of  $-20^\circ\text{C}$  to  $55^\circ\text{C}$  by Islam and Tarefder (2015) showed that CTC and CTE can vary from  $0.33 \times 10^{-5}$  ( $1/^\circ\text{C}$ ) to  $2.57 \times 10^{-5}$  ( $1/^\circ\text{C}$ ) and from  $3.12 \times 10^{-5}$  ( $1/^\circ\text{C}$ ) to  $2.63 \times 10^{-5}$  ( $1/^\circ\text{C}$ ), respectively.

Despite the lower frequency of thermal loading in contrast to that of traffic loading, the magnitude of thermal-induced strains can be comparable to those caused by traffic loading. As a result, field measurements have been obtained to compare the thermal-induced strains with the ones caused by traffic loading and evaluate the associated damage inflicted by each type of loading. According to Bayat *et al.* (2012), the ratio of the thermal-induced strains to the load-induced strains under a 49-kN wheel travelling at 25 km/hr can be up to 1.6 in warm months and 1.3 in cold months. In another study, Tarefder and Islam (2014) investigated the HMA's fatigue damage generated by single-, tandem-, and tridem-axle vehicles over the course of one year and compared it to the monthly average of damage caused by thermal-induced strains. This study also confirmed that the damage caused by daily temperature fluctuations was 1.3 times greater than the corresponding value from traffic loading.

## **Objectives**

The above literature review shows that it is of considerable importance to monitor the magnitude of thermal-induced strains in the horizontal direction under the HMA layer, while more comprehensive studies are needed to investigate strain variation in three-dimensional directions for accurate and stable measurements of the thermal load impact on the responses of HMA.

This paper summarizes findings from the site data collected at the Integrated Road Research Facility (IRRF) which is a fully-instrumented test road in Edmonton, Alberta, Canada. In

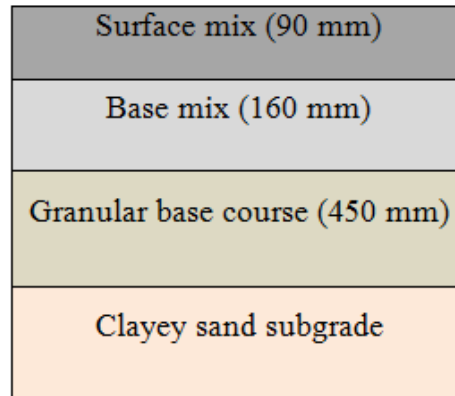
addition to ambient weather, the data used in this study includes HMA layer temperatures at different depths as well as the strain measurements from ASGs placed at the bottom of the HMA.

This paper focuses on the following objectives:

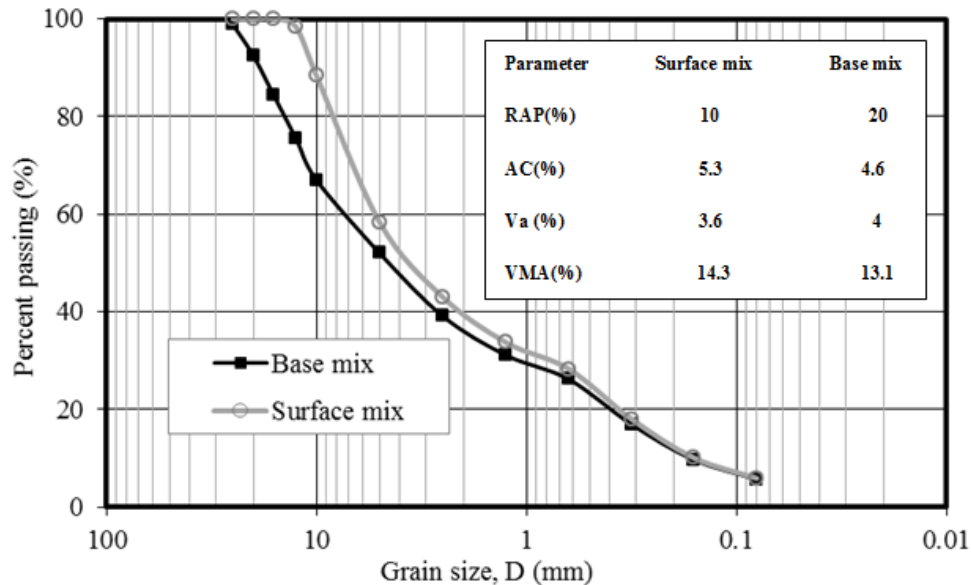
- (1) Investigating the daily thermal loading cycles and associated response cycles in horizontal (longitudinal and transverse) and vertical directions;
- (2) Examining the seasonal changes of thermal strains over a 16-month monitoring period;
- (3) Evaluating CTC and CTE in different seasons according to seasonal strain changes.

### **IRRF Test Road Facility**

The IRRF's test road facility is a newly constructed access road to the Edmonton Waste Management Centre (EWMC), located in northeast Edmonton, Alberta. The test road is comprised of two HMA layers, placed on top of a 450-mm Granular Base Course (GBC) on a Clayey Sand (SC) subgrade soil. At the time of this study, the road was not open to the traffic; however, the test road now carries more than 1,000 garbage trucks per day. Figure 7-1(a) shows the profile of the pavement control section and Figure 7-1(b) illustrates the grain-size distribution and volumetric properties of the HMA layers, including Voids in Mineral Aggregate (VMA) and Air Voids ( $V_a$ ). Reclaimed Asphalt Pavement (RAP) at different percentages was used in both HMA mixtures. The virgin bitumen and the bitumen extracted from the RAP materials were classified as PG 58-28 and PG 70-28, respectively. As well, the bitumen in the mix resulting from blending the RAP material met the PG 58-28 grade. The surface mix possessed a maximum aggregate size of 12.5 mm, while the maximum aggregate size was 25 mm for the base mix.



(a)



(b)

**Figure 7-1 (a) Pavement cross-section (b) Grain-size distribution of HMA at the IRRF.**

The subgrade soil was classified as Clayey Sand (SC) based on the Unified Soil Classification System (USCS) with a maximum particle size of 0.5 mm, liquid limit of 25 and Plastic Index (PI) of 9%. The GBC, composed of crushed aggregates with a maximum size of 19 mm, was

classified as Well-Graded Gravel (GW) according to the USCS. The IRRF's test road is composed of two pavement monitoring sections, each 20 m in length and approximately 100 m apart. These sections were identically instrumented during the road's construction in the summer of 2012. Using a remote monitoring system at the IRRF, data is retrieved from the test road to ensure functionality of the various gauges, thus reducing the number of unnecessary site visits (Figure 7-2).

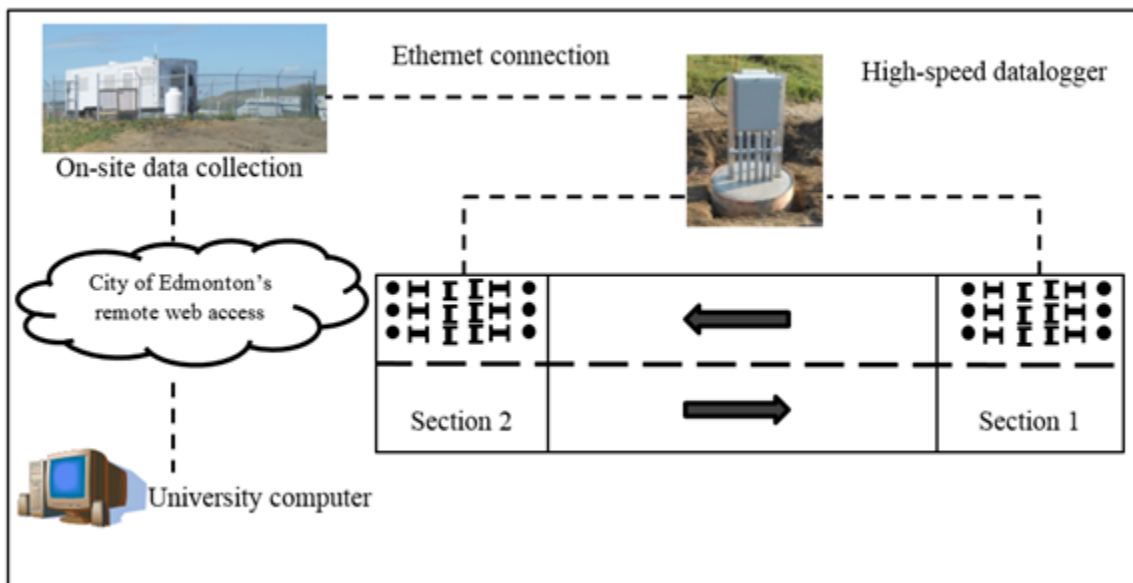


**Figure 7-2- Plan view of the pavement monitoring test sections at the IRRF.**

## Pavement Instrumentation

Figure 7-3 depicts the instrumentation layout at the pavement performance monitoring section. A total of eighteen H-Type ASGs manufactured by the CTL group were placed at the bottom of the HMA layer. Six ASGs in the longitudinal direction (ASG-L), six ASGs in the transverse direction (ASG-T), and six ASGs in the vertical direction (ASG-V) were installed at a 250-mm depth in the HMA layer. Static data from these sensors are collected at 15-minute intervals using a CR9000X datalogger from Campbell Scientific Corp. Canada. It is worth noting that a group of ASGs was laid along the Outer Wheel Path (OWP) to ensure repeatability of measurements and to capture the wheel wander of traffic. Arrangement of the ASGs along the OWP was replicated in two additional lines: 600 mm to the right and 600 mm to the left of the OWP.

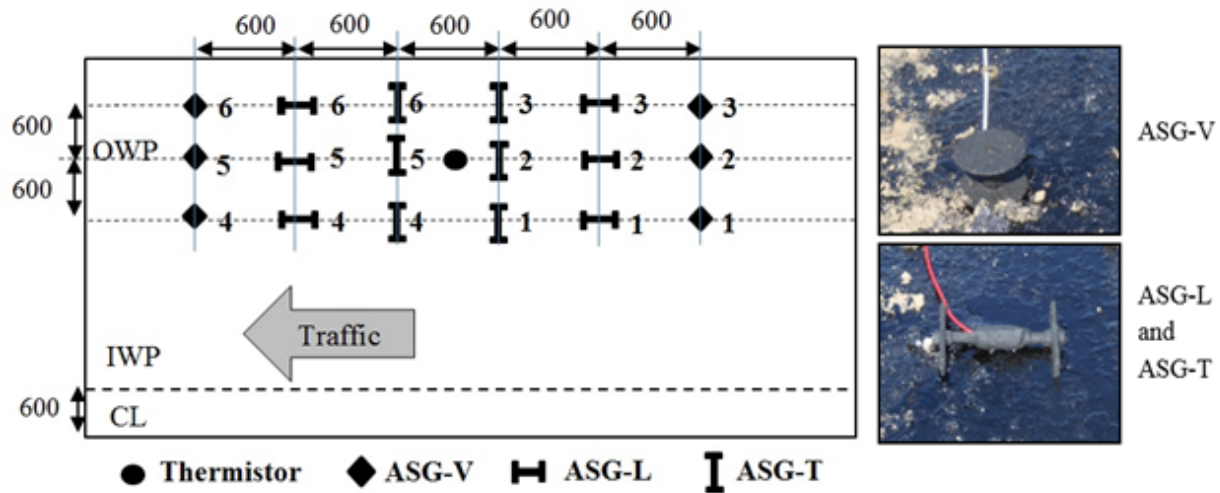


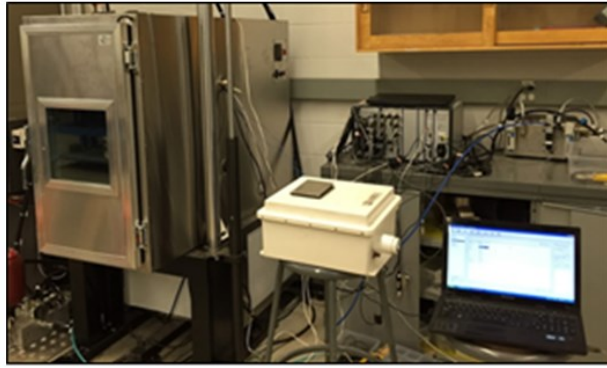
Figure 7-3 Schematic of instrumentation at the bottom of the HMA (all units in mm).

Ambient air temperature data was collected from the closest weather station at the EWMC, which was located about 700 m away from the test road. Maximum and minimum average hourly ambient air temperatures were 38.5°C and -30.0°C during the monitoring period (October 2013 to January 2015). Asphalt thermistors, model 44007 from OMEGA, were used to measure the temperature at different depths within the HMA layers. A thermistor tree composed of four gauges at depths of 20, 90, 170 and 250 mm from the surface was embedded in the HMA layer in August 2014. In addition to the weather station data, temperature data at the depth of the ASGs was collected from August 2014 to January 2015.

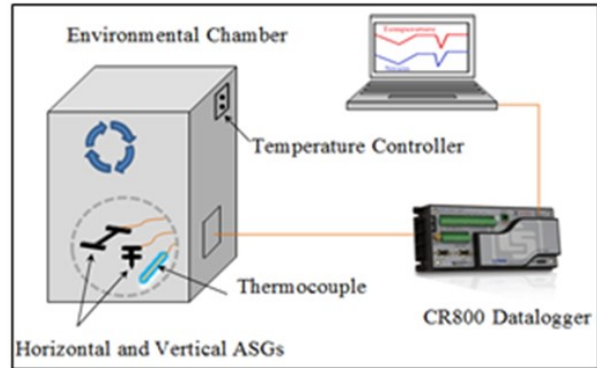
## **Data Collection and Analysis**

### **Laboratory Investigation of Thermal Behaviour of ASG**

In order to assess the temperature variation impact on the embedded ASGs, horizontal and vertical ASGs were placed in an environmental chamber and subjected to different temperatures in the laboratory. By exposing the ASGs to a range of temperatures varying from -30°C to +30°C, strain data was collected at 10-second intervals using a CR800 datalogger from Campbell Scientific Corp. Canada. Figures 7-4(a) and (b) show the experimental test setup and schematic of the data collection system, respectively. Using thermocouples to accurately monitor the temperature inside the environmental chamber, almost negligible thermal-induced strain fluctuations were observed. This showed insignificant temperature dependency of ASGs. Hence, application of the embedded ASGs in the IRRF can suitably reflect the inherent behaviour of the HMA under external thermal loading.



(a)



(b)

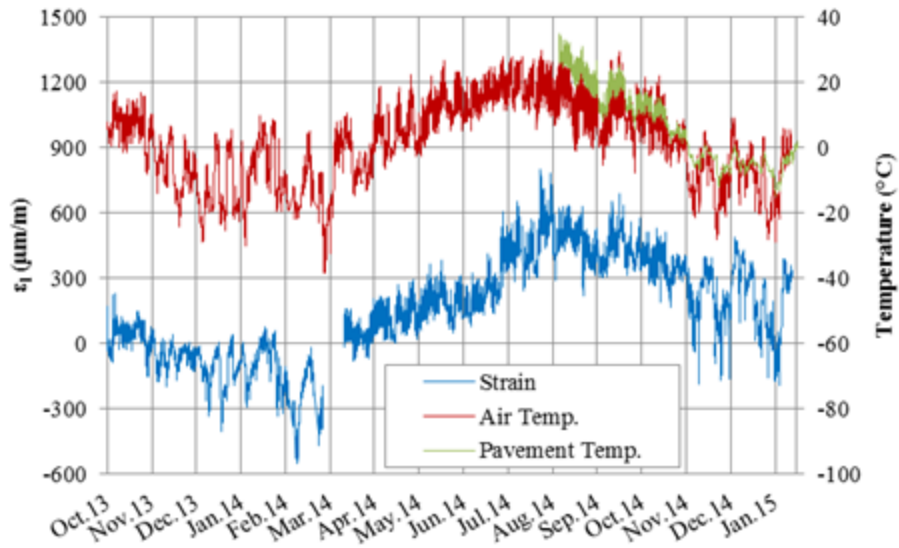
**Figure 7-4 (a) Laboratory test setup (b) Schematic of data collection system.**

### **Thermal-Induced Strain Magnitude**

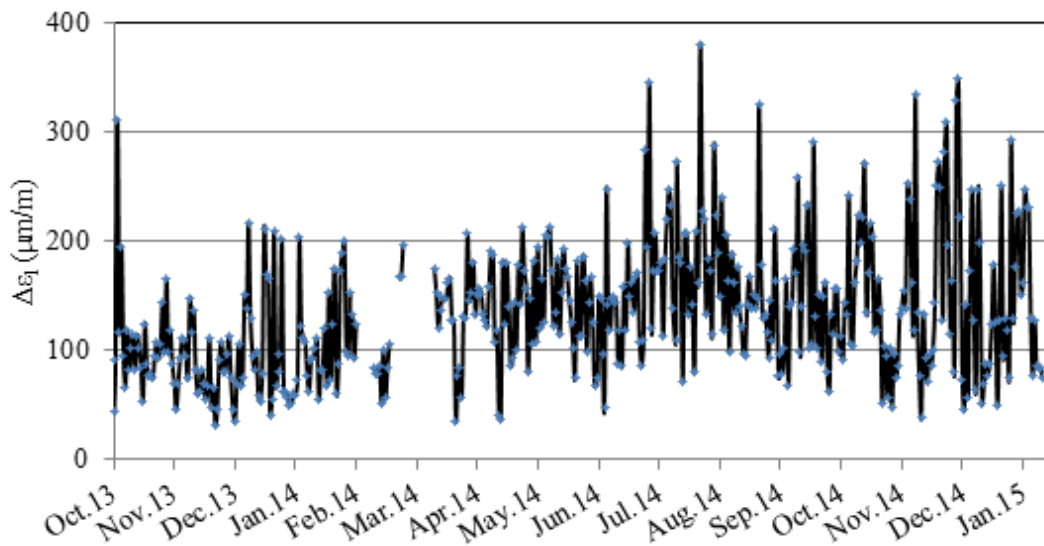
In order to obtain the most reliable and accurate strain data, the ASGs that were installed near each other were considered in an attempt to minimize the negative effect of the HMA's non-homogeneity on the responses. The 18 ASGs were initially divided in to six different groups, each containing one ASG-L, ASG-T and ASG-V based on their proximities. Later, five groups were excluded from the analysis cases due to technical issues including malfunctioning sensors and data collection problems. As a result, three sensors, namely ASG-L2, ASG-T2, and ASG-V2, located in Section 1 of the IRRF were selected to investigate the effect of temperature changes on the strain values. Moreover, to ensure the validity of strain data from the selected ASGs, comparisons were made between the strain values of similar ASGs, suggesting repeatability of strain behaviour in similar gauge types. To evaluate the seasonal variation of thermal-induced strains, HMA strains in three dimensions were monitored after placing the surface layer in October 2013 until January 2015. Figures 7-5, 7-6 and 7-7 depict the in-situ measured strains and strain variations during the monitoring period. It is worth noting that in

order to plot the figures, strain data measured on October 1, 2013, was considered to be zero. The positive strains represent the thermal expansion, while the negative values show the thermal contraction measured at the bottom of the HMA. The gaps in longitudinal strain ( $\epsilon_l$ ), transverse strain ( $\epsilon_t$ ) and vertical strain ( $\epsilon_v$ ) data from February 27, 2014 to March 14, 2014, in addition to the missed  $\epsilon_v$  data from April 28, 2014 to May 13, 2014, were due to a technical issue in the data collection system. The data acquisition system for the HMA's thermistors started working in August 2014, so the pavement temperature data has been available since then.

Figure 7-5(a) illustrates that the  $\epsilon_l$  followed the same trend as ambient and pavement temperature. Looking at the pavement temperature measured at the strain gauges' depths, it was observed that the fluctuations of the pavement temperature were certainly less than those of ambient temperature. Besides, the pavement temperature was generally higher than the ambient temperature in warmer months as opposed to colder months. Values of the strains measured in the longitudinal direction show that the average  $\epsilon_l$  during the first fall (October to December 2013) was around 50  $\mu\text{m}/\text{m}$ , while that value decreased to -92  $\mu\text{m}/\text{m}$  in the first winter (January to March 2014) and later increased to 170  $\mu\text{m}/\text{m}$  in the spring (April to June 2014). Consequently, the average  $\epsilon_l$  values were found equal to 459 and 285  $\mu\text{m}/\text{m}$  during the summer (July to September 2014) and the second fall (October to December 2014), respectively. The maximum  $\epsilon_l$  of 789  $\mu\text{m}/\text{m}$  occurred on July 29, 2014, when the average air temperature reached 23.5°C. According to Figure 7-5(b), the maximum daily  $\Delta\epsilon_l$  on the same day of July 29, 2014, was found equal to 381  $\mu\text{m}/\text{m}$ .



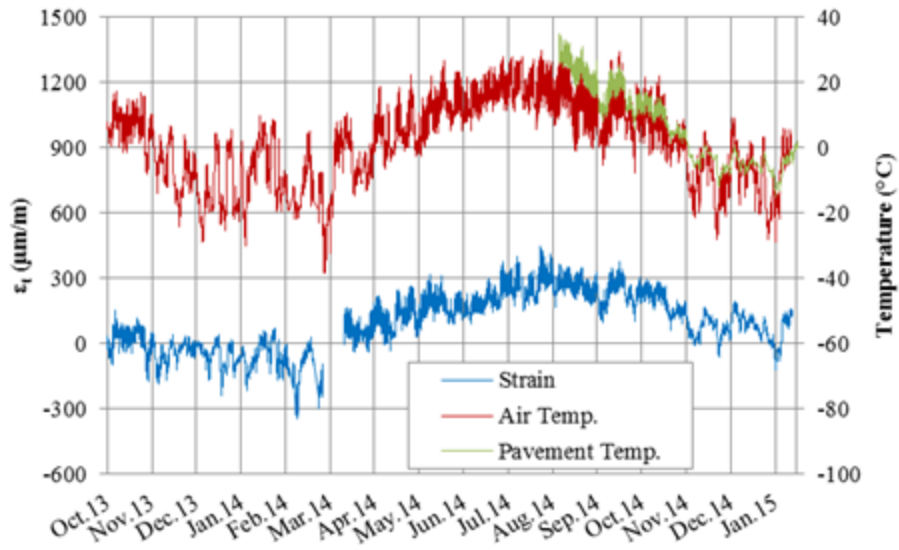
(a)



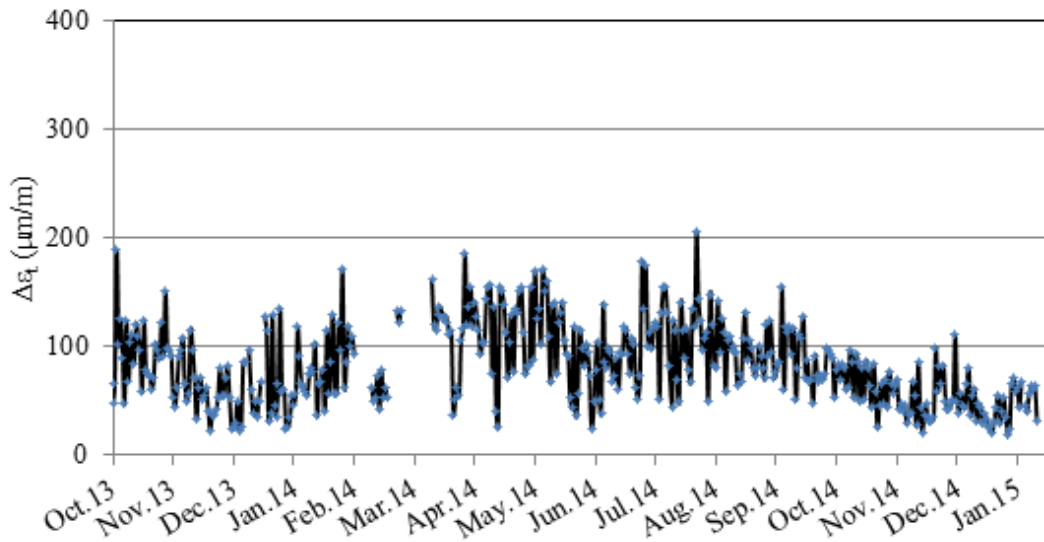
(b)

**Figure 7-5 Variation of (a)  $\epsilon_t$  and (b)  $\Delta\epsilon_t$  from October 2013 to January 2015.**

Figure 7-6(a) shows a similar trend for strains in the transverse direction. The average  $\epsilon_t$  in the first fall, winter, spring, summer and second fall was determined to be equal to -29, -33, 154, 260



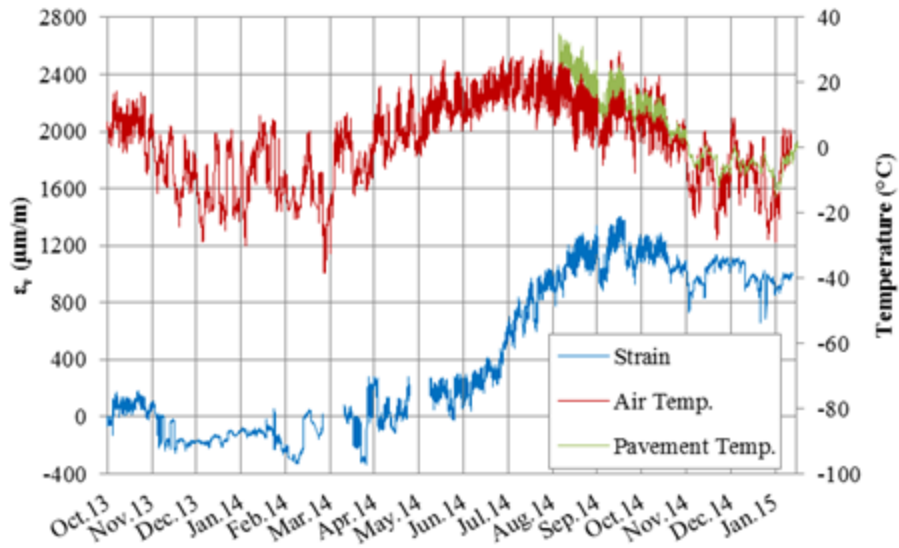
(a)



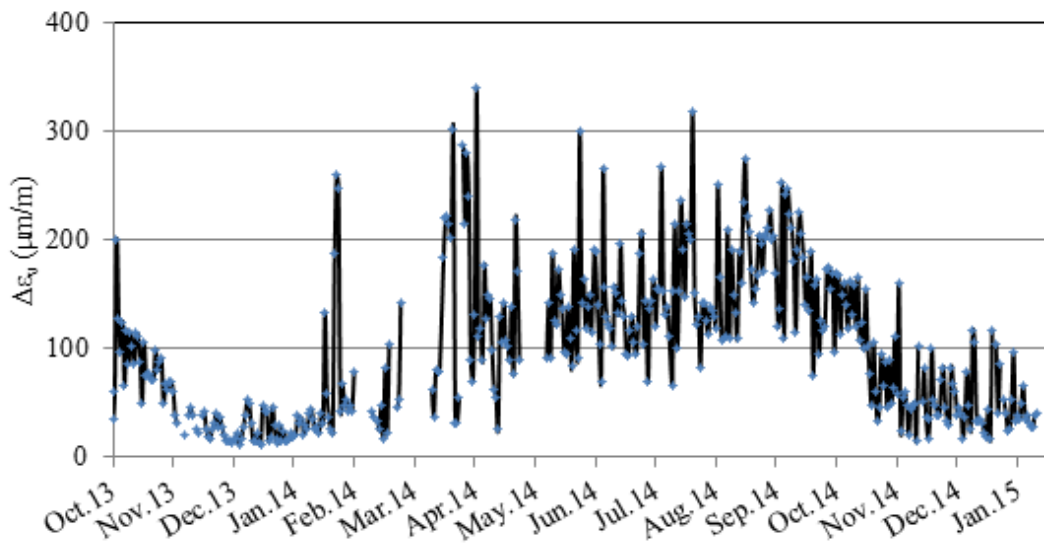
(b)

Figure 7-6 Variation of (a)  $\epsilon_t$  and (b)  $\Delta\epsilon_t$  from October 2013 to January 2015.

and 127  $\mu\text{m}/\text{m}$ , respectively. The maximum  $\varepsilon_t$  of 444  $\mu\text{m}/\text{m}$  occurred in the summer (July 29, 2014), and according to Figure 7-6(b), the maximum daily  $\Delta\varepsilon_t$  of 206  $\mu\text{m}/\text{m}$  occurred on the same day. A comparison of the absolute values and the daily fluctuations in both longitudinal and transverse directions indicated that the lower values corresponded to  $\varepsilon_t$ . Figure 7-7(a) illustrates variation of strain in the vertical direction over the course of the same monitoring period. The average  $\varepsilon_v$  in the first fall, winter, spring, summer and second fall was determined to be equal to -70, -116, 153, 965 and 1,051  $\mu\text{m}/\text{m}$ , respectively. The maximum  $\varepsilon_v$  as high as 1,403  $\mu\text{m}/\text{m}$  was recorded in September 2014, which was higher than the maximum of the horizontal strain. On the other hand, the minimum  $\varepsilon_v$  as low as -336  $\mu\text{m}/\text{m}$  was captured in March. Based on Figure 7-7(b), the maximum daily  $\Delta\varepsilon_v$  of 341  $\mu\text{m}/\text{m}$  was on April 7, 2014. Comparing the magnitude of all three types of strains revealed that  $\varepsilon_t$  experienced the highest strain fluctuation.



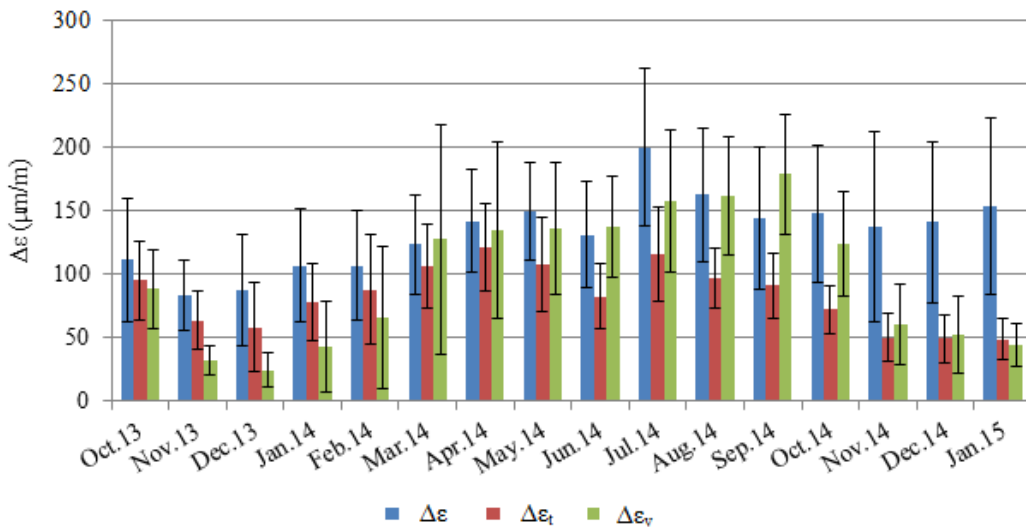
(a)



(b)

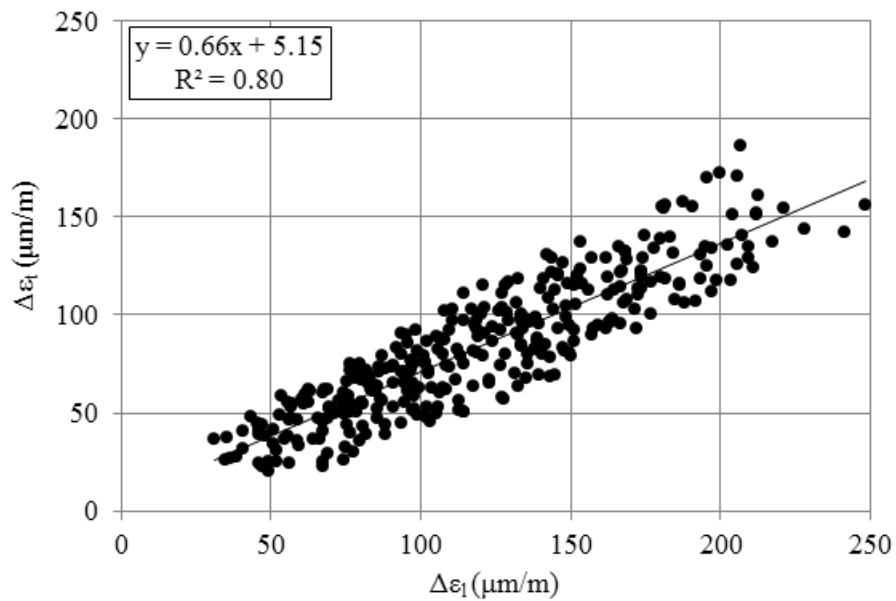
Figure 7-7 Variation of (a)  $\epsilon_v$  and (b)  $\Delta\epsilon_v$  from October 2013 to January 2015.

Figure 7-8 compares the average daily  $\Delta\varepsilon$  in each month for the three gauge types over the monitoring period. It was found that the monthly average  $\Delta\varepsilon$  at the bottom of the HMA was more pronounced in the longitudinal direction (190  $\mu\text{m/m}$ ) than compared to the transverse (120  $\mu\text{m/m}$ ) and vertical (180  $\mu\text{m/m}$ ) directions. According to Figure 7-8, it was also discovered that the highest values measured in the horizontal direction did not coincide with the ones in the vertical direction. In addition, the fluctuations typically tended to increase during the warmer months of the year. The monthly average  $\Delta\varepsilon$  in the longitudinal direction possessed larger values than the corresponding ones in the transverse and vertical directions. Also, the illustrated error bars of the three responses showed that the dispersion of strain values was more pronounced in the case of  $\varepsilon_l$  in comparison to other strain types.



**Figure 7-8 Monthly average fluctuation of thermal-induced strain**

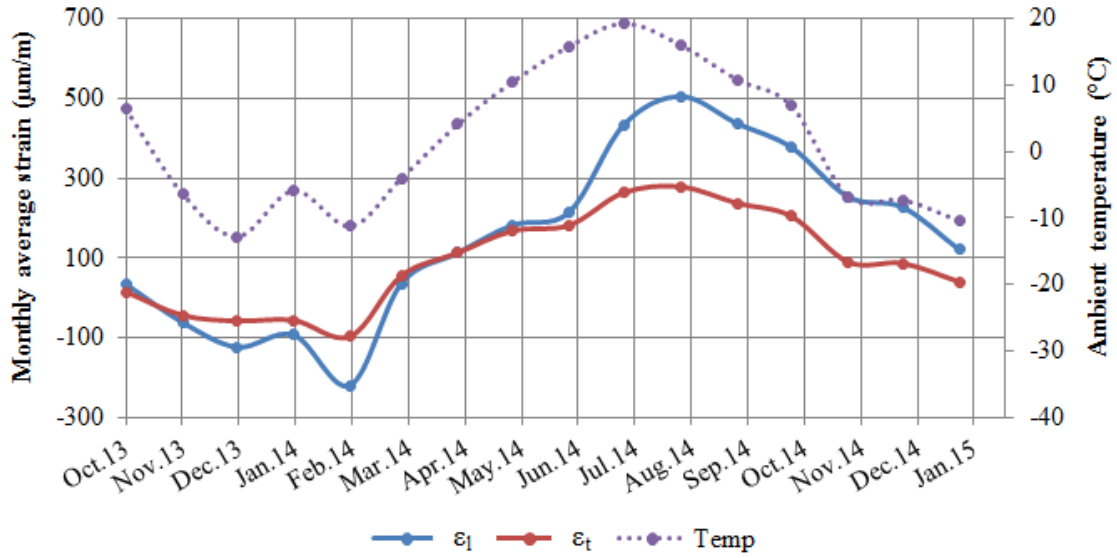
To establish the relationship between the daily fluctuation of horizontal strains at the bottom of the HMA,  $\Delta\varepsilon_l$  and  $\Delta\varepsilon_t$  were plotted against each other as depicted in Figure 7-9. The difference between the highest fluctuations in the horizontal direction was determined to be 175  $\mu\text{m}/\text{m}$ . Using the least squared regression method, a linear equation was established to relate the two parameters. The obtained equation suggests a strong relationship between the two parameters with a coefficient of determination ( $R^2$ ) equal to 0.80 and a standard error of regression equal to 40.6. The developed correlation shows that  $\Delta\varepsilon_t$  was generally 66% of the  $\Delta\varepsilon_l$  during the monitoring period.



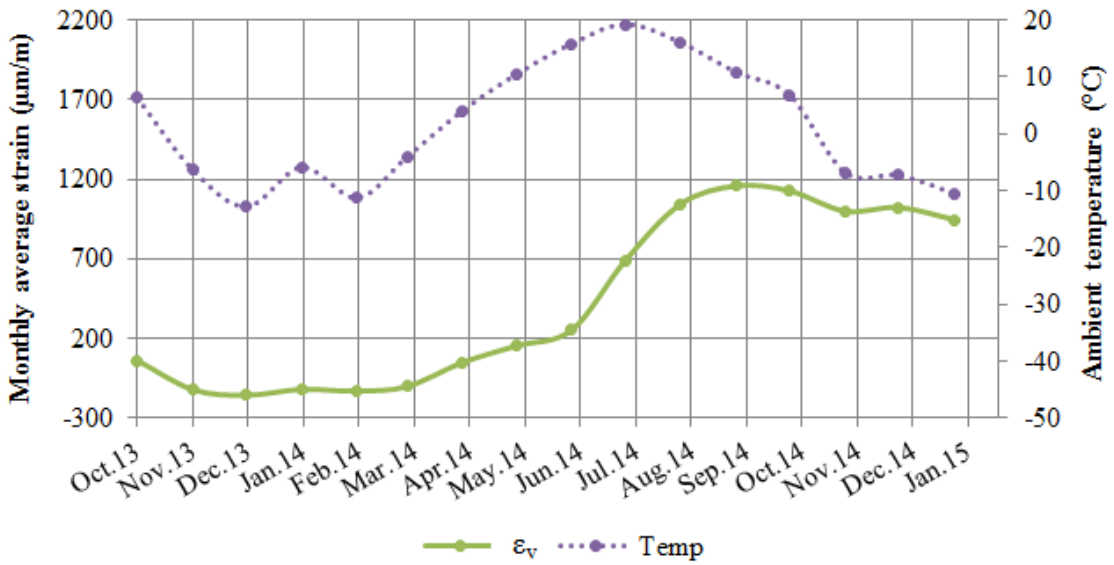
**Figure 7-9 Comparison of  $\Delta\varepsilon_t$  against  $\Delta\varepsilon_l$  at the bottom of the HMA.**

## Irrecoverable Strains

As suggested by Al-Qadi *et al.* (2005) and Bayat (2009), irrecoverable deformations caused by thermal-induced strain might result in thermal fatigue cracking in the pavement surface. To calculate the magnitude of irrecoverable strains in different gauges, the strains in horizontal and vertical directions were averaged for each month, as shown in Figures 7-10(a) and (b), respectively. The irrecoverable strains were calculated by subtracting the monthly average strains of two similar months in the monitoring period. As a result, the irrecoverable  $\varepsilon_l$  was found equal to 340  $\mu\text{m/m}$  in October, 310  $\mu\text{m/m}$  in November, 350  $\mu\text{m/m}$  in December and 210  $\mu\text{m/m}$  in January based on Figure 7-10(a). In a similar way, Figure 7-10(a) suggests that the irrecoverable  $\varepsilon_t$  was 190  $\mu\text{m/m}$  in October, 130  $\mu\text{m/m}$  in November, 140  $\mu\text{m/m}$  in December and 100  $\mu\text{m/m}$  in January, showing lower values in comparison to  $\varepsilon_l$ . However, the observed irrecoverable  $\varepsilon_v$  was found to be larger than those of the horizontal strain, as seen in Figure 7-10(b). Results showed that the irrecoverable  $\varepsilon_v$  was determined to be 1,060  $\mu\text{m/m}$  in October, 1,120  $\mu\text{m/m}$  in November, 1,180  $\mu\text{m/m}$  in December and 1,060  $\mu\text{m/m}$  in January. The change in  $\varepsilon_l$  and  $\varepsilon_t$  followed the ambient temperature trend; however, the rate of increase in  $\varepsilon_l$  was greater than that of  $\varepsilon_t$  from June to August, 2014. Although there was a fair agreement between  $\varepsilon_l$  and  $\varepsilon_t$  during October 2013 to June 2014, they deviated noticeably when the temperature dropped below zero from November 2013 to March 2014. Hence,  $\varepsilon_l$  remained higher than  $\varepsilon_t$  for the rest of the monitoring period in parallel with its decrease at lower temperatures. Even though  $\varepsilon_v$  behaved consistently with the ambient temperature, the measured strains did not fully recover during the colder months. Additionally, a delay was identified for the maximum monthly average  $\varepsilon_v$  against the maximum monthly average ambient temperature in contrast to the  $\varepsilon_l$  and  $\varepsilon_t$ .



(a)



(b)

Figure 7-10 Monthly average (a)  $\epsilon_l$  and  $\epsilon_t$ , (b)  $\epsilon_v$  from October 2013 to January 2015.

## Determination of CTC and CTE

According to the Mechanistic Empirical Pavement Design Guide (MEPDG) (ARA 2004), CTC is considered a main property of the HMA for predicting thermal cracking distress, which can be estimated based on empirical equation or by running a computer simulation. In the MEPDG, CTC for the lower temperature range is usually estimated based on the CTC of aggregate and bitumen, as well as volumetric properties of the mixture, as in Equation 7-3:

$$L_{mix} = \frac{VMA \times B_{ac} + V_{AGG} \times B_{AGG}}{3 \times V_{TOTAL}} \quad (7-3)$$

where  $L_{mix}$  is the linear CTC of the HMA in  $1/^\circ\text{C}$ ,  $B_{ac}$  and  $B_{AGG}$  represent the volumetric CTC of the aggregate and the asphalt cement in solid state both in  $1/^\circ\text{C}$ ,  $VMA$  is the percentage volume of voids in the mineral aggregate,  $V_{AGG}$  is the percentage volume of aggregate in the mix and  $V_{TOTAL}$  is 100 percent. Field data, including strain and temperature records, were utilized to obtain the thermal coefficients of the HMA. Figure 7-11 demonstrates the observed variation of the pavement temperature measured at the strain gauges' depths ( $T_p$ ) against the ambient temperature ( $T_a$ ). A non-linear regression equation with a coefficient of determination ( $R^2$ ) of 0.78 was fitted to the temperature data. Knowing that  $T_a$  and  $T_p$  can significantly vary from each other as shown in Figure 10, it is necessary to use the pavement temperature for the calculation of CTC and CTE.

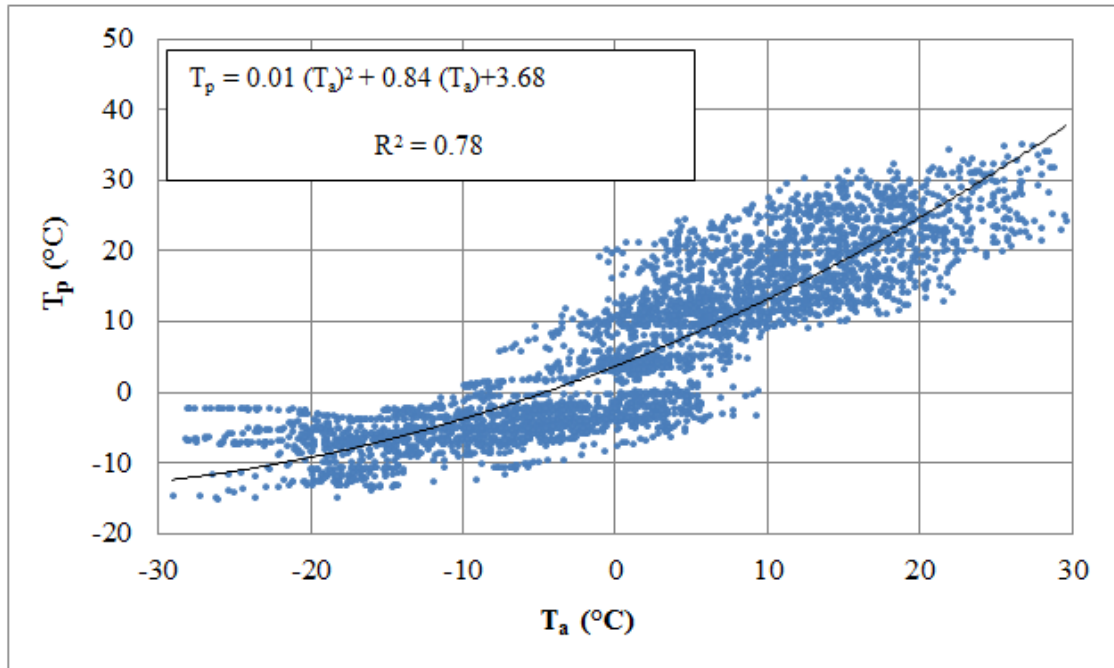
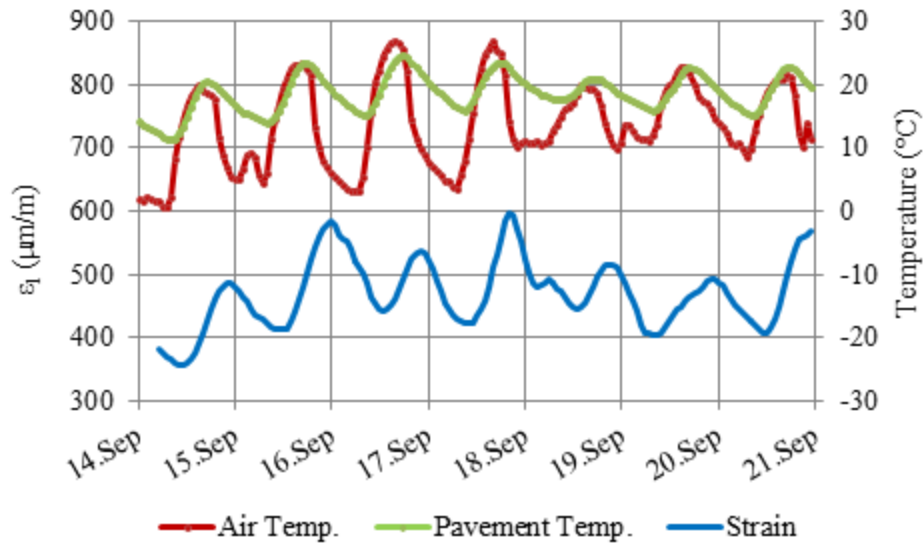
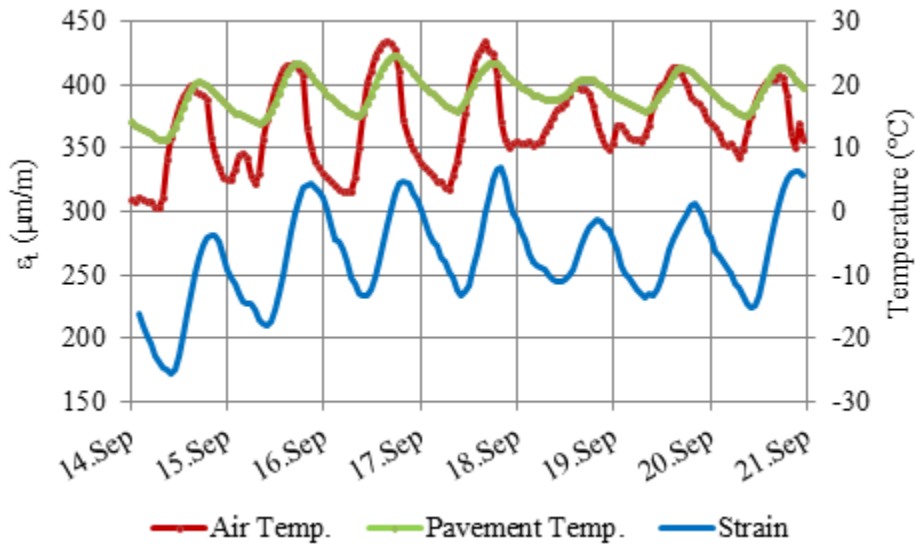


**Figure 7-11 Pavement and ambient temperature from August 2014 to January 2015.**

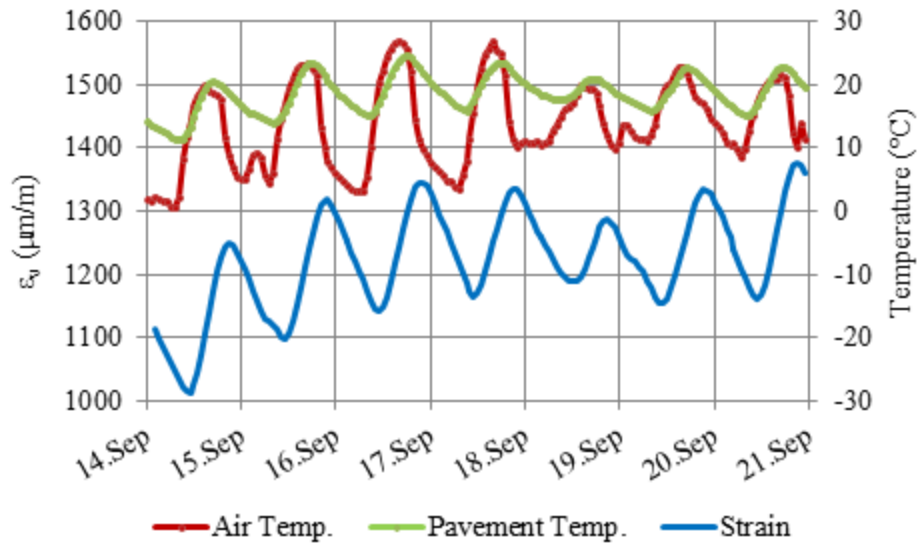
To facilitate the comparison and analysis, hourly averages of the strain and temperature data were plotted versus time. Figures 7-12(a), (b), and (c) typically show the induced  $\epsilon_l$  from ASG-L2,  $\epsilon_t$  from ASG-T2 and  $\epsilon_v$  from ASG-V2, respectively, at the bottom of the HMA layer from September 14 to September 21, 2014. It is worth noting that the pavement temperature was measured by a thermistor located at the same depth as the ASGs. HMA material expanding during rising temperatures and contracting during dropping temperatures was noticeable in all directions. Comparing the daily ambient and pavement temperature variation against measured strains indicated a cyclic behaviour of strain associated with cyclic temperature change.



(a)



(b)



(c)

**Figure 7-12 Thermal loading cycles and strain readings from (a)  $\epsilon_l$  (b)  $\epsilon_t$  and (c)  $\epsilon_v$ .**

The observed cyclic response of the HMA layer due to temperature variation revealed that the frequency of thermal loading was equal to one day. This agrees with findings in other studies, which reported one cycle of thermal loading per day for longitudinal strain gauges as also reported by Al-Qadi *et al.* (2005) and Bayat (2009). During the one-week monitoring period, the maximum strain and the maximum temperature did not occur at the same time. However, the temperature and the induced strains followed the same trend. The lag between ambient and pavement temperature of almost three hours may have occurred due to the relatively thick HMA layer and other influential parameters, including solar radiation and wind speed. As a result, the temperature measured by the thermistor located next to the ASGs is quite independent of the abovementioned impacts. This is confirmed by the trend shown in Figures 7-11(a), (b) and (c), where a better match between induced strain at the bottom of the HMA and pavement temperature was observed rather than the ambient temperature.

Using the available pavement temperature fluctuation data, average CTC and CTE as well as the standard deviations of the data, as shown in the bracket, were calculated for each season in Table 7-1. According to Table 7-1, the CTC values ranged between  $1.18 \times 10^{-5}$  ( $1/^\circ\text{C}$ ) to  $3.48 \times 10^{-5}$  ( $1/^\circ\text{C}$ ) and CTE values were in the range of  $1.32 \times 10^{-5}$  ( $1/^\circ\text{C}$ ) to  $3.41 \times 10^{-5}$  ( $1/^\circ\text{C}$ ) for the considered months. The computed values were compared against the CTC determined by the MEPDG method. Using the typical values recommended by the MEPDG for  $B_{ac}$  and  $B_{AGG}$  and volumetric properties of HMA mixes, the CTC was determined to be  $2.76 \times 10^{-5}$  ( $1/^\circ\text{C}$ ) for the surface mix and  $2.61 \times 10^{-5}$  ( $1/^\circ\text{C}$ ) for the base mix. Interestingly, based on Table 7-1, the CTC values determined based on the MEPDG method agreed reasonably with the average CTC determined from field data, specifically during winter. Hence, the MEPDG model, which is suited for lower temperatures, was able to produce approximately similar results as the field. Results showed that the calculated values associated with the  $\varepsilon_l$  were larger than those of the  $\varepsilon_t$ . In addition, CTC and CTE for  $\varepsilon_v$  were found almost consistent in different seasons. As expected, it was observed that the CTC values in colder seasons were generally larger in comparison to those measured in summer 2014.

**Table 7-1 Average and standard deviation (in parentheses) of seasonal thermal coefficients.**

Season	Longitudinal		Transverse		Vertical		Seasonal Average	
	CTC ( $\times 10^{-5}$ ) ( $1/^\circ\text{C}$ )	CTE ( $\times 10^{-5}$ ) ( $1/^\circ\text{C}$ )	CTC ( $\times 10^{-5}$ ) ( $1/^\circ\text{C}$ )	CTE ( $\times 10^{-5}$ ) ( $1/^\circ\text{C}$ )	CTC ( $\times 10^{-5}$ ) ( $1/^\circ\text{C}$ )	CTE ( $\times 10^{-5}$ ) ( $1/^\circ\text{C}$ )	CTC ( $\times 10^{-5}$ ) ( $1/^\circ\text{C}$ )	CTE ( $\times 10^{-5}$ ) ( $1/^\circ\text{C}$ )
Summer 2014	1.68 (0.05)	2.25 (0.09)	1.18 (0.14)	1.32 (0.11)	2.56 (0.06)	2.8 (0.08)	1.81	2.12
Fall 2014	3.48 (0.12)	2.34 (0.07)	2.56 (0.05)	1.76 (0.07)	2.68 (0.09)	2.79 (0.10)	2.91	2.30
Winter 2015	2.88 (0.08)	3.41 (0.06)	2.64 (0.15)	2.42 (0.16)	2.78 (0.13)	2.04 (0.12)	2.77	2.62

## Conclusion

Field measurements for  $\varepsilon_l$ ,  $\varepsilon_t$ , and  $\varepsilon_v$  were conducted at the IRRF's test road to monitor the impact of daily fluctuation and seasonal change in ambient temperature on the developed responses at the bottom of the HMA. The observations are summarized below:

- (1) A similar trend was observed between the ambient air temperature fluctuation and the induced strains fluctuation.
- (2) The most critical period in terms of highest absolute value for  $\varepsilon_l$  and  $\varepsilon_t$  was winter and spring, respectively, while maximum fluctuation for  $\varepsilon_v$  occurred during the spring-thaw season.
- (3)  $\varepsilon_v$  exhibited more fluctuation than  $\varepsilon_l$  and  $\varepsilon_t$  due to temperature changes.
- (4) The irrecoverable  $\varepsilon_l$ ,  $\varepsilon_t$ , and  $\varepsilon_v$  were as high as 86, 25 and 884  $\mu\text{m}/\text{m}$ , respectively, at the end of the 16-month monitoring period.
- (5) A consistent linear relationship was established between  $\Delta\varepsilon_l$  and  $\Delta\varepsilon_t$  daily fluctuations, implying that  $\Delta\varepsilon_t$  was approximately 66% of  $\Delta\varepsilon_l$ .
- (6) A nonlinear regression equation between ambient air temperature and pavement temperature emphasised the importance of using pavement temperature for CTC and CTE calculations.
- (7) The different CTC and CTE values in three directions demonstrated that the anisotropic properties of the HMA need to be considered when calculating these parameters.

- (8) Seasonal variation of the CTC and CTE of the HMA were determined using three types of strain gauges. The average range of variation was from  $1.81 \times 10^{-5}$  (1/°C) to  $2.91 \times 10^{-5}$  (1/°C) for CTC, and from  $2.12 \times 10^{-5}$  (1/°C) to  $2.62 \times 10^{-5}$  (1/°C) for CTE.
- (9) A reasonable agreement was found between the average field-determined CTC values during winter with the ones predicted by the MEPDG approach.

## **Acknowledgements**

The authors would like to acknowledge Alberta Transportation and The City of Edmonton for providing financial and in-kind support for the construction and instrumentation of the IRRF's test road.

# **Chapter 8 –Conclusions and Recommendations**

## Conclusions

Based on the established objectives in this research, the following conclusions were drawn:

- State-of-the art gauges along with an implemented high- and low-speed data acquisition system at IRRF provided a reliable and remarkable source of data for the structural analysis and environmental behaviour monitoring in this research. Secured remote connection, automatic and continuous data collection and the in-house data analysis tools worked exceptionally well during the conducted study.
- Controlled vehicle loading was designed and conducted on the instrumented section of the IRRF in order to measure and characterize the critical pavement responses, as described in **chapters 3 and 4**, and the following findings were noted:
  - Based on the loading tests at different speeds, the FFT-dominant loading frequency obtained for the longitudinal strain was higher than those of the transverse and vertical strains.
  - The depth from the surface notably affected the FFT-determined loading frequency of the vertical stress response within unbound layers.
  - Using the laboratory-established HMA master curves, it was concluded that the FFT method can result in a more accurate dynamic modulus in comparison to traditional time-domain analysis approaches, which are based on response pulse durations.

- This work investigated application of the Time-Frequency Domain analysis method, and results showed that the Continuous Wavelet Transform and Short-Time Fourier Transform can be effectively utilized for calculating loading frequency.
- The key advantage of the proposed Time-Frequency Domain method for pavement response pulse processing is its ability to reveal the frequency content of the recorded response at each time instant.
- Measuring and modeling the FWD-induced strains at the bottom of the HMA, as discussed in **chapter 5**, showed that:
  - Haversine function can reasonably approximate the shape of the horizontal and vertical strains. The measured pulse duration for vertical strain was found to be greater than that of the longitudinal strain.
  - Incorporating the viscoelastic behaviour of HMA characterized in the laboratory along with using field-determined backcalculated moduli of the unbound layers can improve the response prediction accuracy rather than the widely used MLET approach.
  - According to the MEPDG-recommended performance models, the discrepancy between predicted and measured longitudinal strain resulted in noticeable errors

in bottom-up fatigue cracking prediction; however, the impact of vertical strain prediction error on the HMA rut depth prediction error was less pronounced.

- Based on the detailed study of the seasonal variation in pavement response, as elaborated in **chapter 6**, it was found that:
  - The impact of freeze/thaw cycles on the recorded HMA strain, as well as the base and subgrade vertical stress, was clearly detectable using the installed instruments at pavement monitoring sections of the IRRF.
  - Hysteresis loops as recorded by FWD can clearly indicate the behaviour of the structure due to seasonal change, especially with regard to viscoelastic properties of HMA.
  - Utilizing the percent of prediction error to quantify the accuracy of MLET-predicted responses showed that, on average, the vertical strain at the bottom of the HMA was 20 percent underestimated while the horizontal strain was 37 percent overestimated.
- Monitoring thermal-induced strains at the IRRF over a period of more than a year, as illustrated in **chapter 7**, showed that:
  - The developed laboratory test set-up was able to examine the temperature-dependency of ASG readings.

- The observed daily and seasonal fluctuation of ambient air temperature in the field can vividly induce strains in longitudinal, transverse, and vertical directions at the bottom of the HMA; the irrecoverable strains had the highest vertical strain.
- Measured strain data can produce adequate data for field measurement of CTC/CTE of HMA; more realistic HMA thermal properties can be obtained using this approach compared to theoretical or laboratory methods.

## **Recommendations**

As traffic volume steadily increases and pavement structures are exposed to heavier loads, pavement networks across the world demand better design standards. Few facilities around the globe are featured with pavement instrumentation, but more experimental studies are required for long-term monitoring of pavement response to traffic loading, especially in regions with extreme weather conditions. Therefore, in the interest of future research, the following suggestions are proposed:

- Examine a wider range of pavement thicknesses, various pavement materials, heavier axle loads, and different axle types to measure responses and evaluate the recommended frequency calculation methods.
- Consider Frequency Domain and Time-Frequency Domain analysis methods within response prediction models to calculate critical strains and stresses.

- Investigate the aforementioned techniques for determining frequency of the FWD loading.
- Incorporate both surface deflection basin and in-situ measured responses to backcalculate the layers moduli.
- Develop numerical models to simulate pavement response to the combined impact of thermal and traffic loading.
- Evaluate the impact of temperature and moisture fluctuations on the unbound layers vertical stress.
- Conduct periodic surface distress survey to verify the predicted performance obtained based on the in-situ measured responses.

# Bibliography

AASHTO, 2009a. Determining the Dynamic Modulus and Flow Number for Hot Mix Asphalt (HMA) Using the Asphalt Mixture Performance Tester (AMPT), *AASHTO TP79-09*, American Association of State Highway and Transportation Official.

AASHTO, 2009b. Developing Dynamic Modulus Master Curves for Hot Mix Asphalt (HMA) Using the Asphalt Mixture Performance Tester (AMPT), *AASHTO PP61-09*, American Association of State Highway and Transportation Official.

Addison, P.S., 2002. *The Illustrated Wavelet Transform Handbook: Introductory Theory and Applications in Science, Engineering, Medicine and Finance*. CRC press.

Ahlborn, G., 1972. ELSYM5: Computer Program for Determining Stresses and Deformations in Five Layer Elastic System, *University of California, Berkeley*.

Akram, T., Scullion, T. and Smith, R.E., 1994. Comparing Laboratory and Backcalculated Layer Moduli on Instrumented Pavement Sections. In *Nondestructive Testing of Pavements and Backcalculation of Moduli*, Vol. (2). ASTM International.

Ali, H. and Lopez, A., 1996. Statistical Analyses of Temperature and Moisture Effects on Pavement Structural Properties based on Seasonal Monitoring Data. *Transportation Research Record: Journal of the Transportation Research Board*, Vol. 1540, pp.48-55.

Al-Qadi, I. and Bhutta, S., 1999. In situ Measurements of Secondary Road Flexible Pavement Response to Vehicular Loading. *Transportation Research Record: Journal of the Transportation Research Board*, Vol.1652, pp.206-216.

Al-Qadi, I., Elseifi, M., Yoo, P., Dessouky, S., Gibson, N., Harman, T., D'Angelo, J. and Petros, K., 2008. Accuracy of Current Complex Modulus Selection Procedure from Vehicular Load Pulse: NCHRP project 1-37a Mechanistic-Empirical Pavement Design Guide. *Transportation Research Record: Journal of the Transportation Research Board*, Vol. 2087, pp.81-90.

Al-Qadi, I., Hassan, M. and Elseifi, M., 2005. Field and Theoretical Evaluation of Thermal Fatigue Cracking in Flexible Pavements. *Transportation Research Record: Journal of the Transportation Research Board*, Vol. 1919, pp.87-95.

Al-Qadi, I., Loulizi, A., Janajreh, I. and Freeman, T., 2002. Pavement Response to Dual Tires and New Wide-Base Tires at Same Tire Pressure. *Transportation Research Record: Journal of the Transportation Research Board*, Vol. 1806, pp.38-47.

Al-Qadi, I.L., Xie, W. and Elseifi, M.A., 2008. Frequency Determination from Vehicular Loading Time Pulse to Predict Appropriate Complex Modulus in MEPDG. *Journal of the Association of Asphalt Paving Technologists*, Vol. 77.

Appea, A., Flintsch, G.W. and Al-Qadi, I.L., 2002. Backcalculation Validation through Field Instrumentation. In *Pavement Evaluation, A joint Conference of the FWD and Road Profiler's Groups, Roanoke, VA, USA*.

Appea, A.K., 2003. Validation of FWD Testing Results at The Virginia Smart Road: Theoretically and by Instrument Responses, *Ph.D. Thesis*, Virginia Polytechnic Institute and State University, Blacksburg, Virginia, USA.

ARA, Inc., 2004. ERES Consultant Division. *Guide for Mechanistic–Empirical Design of New and Rehabilitated Pavement Structures*. Final report, NCHRP Project 1-37A. Transportation

Research Board of the National Academies, Washington, D.C.  
<http://www.trb.org/mepdg/guide.htm>.

Asphalt Institute, 1982. *Research and Development of the Asphalt Institute's Thickness Design Manual (MS-1)*, 9th edition. Research Report 82-2.

ASTM, 2008. Standard Guide for Calculating In Situ Equivalent Elastic Moduli of Pavement Materials Using Layered Elastic Theory. *ASTM D 5858-96*, West Conshohocken, Pa.

Ayenu-Prah, A.Y. and Attoh-Okine, N.O., 2009. Comparative study of Hilbert-Huang transform, Fourier transform and wavelet transform in pavement profile analysis. *Vehicle System Dynamics*, Vol. 47, No.4, pp.437-456.

Bayat, A. and Knight, M., 2010. Investigation of Hot-Mix Asphalt Dynamic Modulus by Means of Field-Measured Pavement Response. *Transportation Research Record: Journal of the Transportation Research Board*, Vol. 2154, pp.138-145.

Bayat, A., 2009. Field and Numerical Investigation to Determine the Impact of Environmental and Wheel Loads on Flexible Pavement, *Ph.D. Thesis*, University of Waterloo, Ontario, Canada.

Bayat, A., Knight, M.A. and Soleymani, H.R., 2012. Field Monitoring and Comparison of Thermal-and Load-Induced Strains in Asphalt Pavement. *International Journal of Pavement Engineering*, Vol. 13, No. 6, pp.508-514.

Berg, R.L., Bigl S.R., Stark J.A. and Durell G.D., 1996. *Resilient Modulus Testing of Materials from Mn/ROAD, Phase 1*: U.S. Army Corps of Engineers Cold Regions Research & Engineering Laboratory, Special Report No. 96-19.

Brown, S. F., 1973. *Determination of Young's Modulus for Bituminous Materials in Pavement Design*. Highway Research Record, Vol. 431, pp. 38-49.

Burmister, D.M., 1945. The General Theory of Stresses and Displacements in Layered Systems. I. *Journal of Applied Physics*, Vol. 16, No. 2, pp.89-94.

Burmister, D.M., Palmer, L.A., Barber, E.S. and Middlebrooks, T.A., 1944. The Theory of Stress and Displacements in Layered Systems and Applications to the Design of Airport Runways. In *Highway Research Board Proceedings*, Vol. 23.

Carmichael III, R.F. and Stuart, E., 1985. Predicting Resilient Modulus: A Study to Determine the Mechanical Properties of Subgrade Soils (Abridgment). *Transportation Research Record: Journal of the Transportation Research Board*, Vol. 1043, pp.145-148.

Chamberlain, E.J., 1981. *A Statistical Evaluation of Soil and Climatic Parameters Affecting the Change in Pavement Deflection during Thawing of Subgrades* (No. CRREL-81-15). Cold Regions Research and Engineering Lab, Hanover.

Deblois, K., Bilodeau, J.P. and Dore, G., 2010. Use of Falling Weight Deflectometer Time History Data for the Analysis of Seasonal Variation in Pavement Response. *Canadian Journal of Civil Engineering*, Vol. 37, No. 9, pp.1224-1231.

Desai, C. S., 1979. *Elementary Finite Element Method*. Englewood Cliffs, New Jersey: Prentice-Hall.

Djakfar, L. and Roberts, F., 2000. Performance Prediction of Louisiana Accelerated Loading Facility Test Sections. *Transportation Research Record: Journal of the Transportation Research Board*, Vol. 1716, pp.108-115.

Dongre, R., Myers, L. and D'Angelo, J., 2006. Conversion of Testing Frequency to Loading Time: Impact on Performance Predictions Obtained from the ME Pavement Design Guide. In *85<sup>th</sup> Transportation Research Board Annual Meeting (Paper No. 06-2394)*, Washington, DC, USA.

Doré, G. and Imbs, C., 2002. Development of a New Mechanistic Index to Predict Pavement Performance during Spring Thaw. *Cold Regions Engineering*, pp.348-359.

Doré, G. and Zubeck, H.K., 2009. *Cold Regions Pavement Engineering*. ASCE Press, McGraw-Hill Construction.

Drumm, E., and Meier, R., 2003. *Daily and Seasonal Variations in In-Situ Material Properties*. : NCHRP Web Document 60 (Project 20-50[7/12]): Contractor's final Report, National Cooperative Highway Research Program, Transportation Research Board, Washington, D.C.

Drumm, E.C., Reeves, J.S., Madgett, M.R. and Trolinger, W.D., 1997. Subgrade Resilient Modulus Correction for Saturation Effects. *Journal of Geotechnical and Geoenvironmental Engineering*, Vol. 123, No. 7, pp.663-670.

Elseifi, M.A., Al-Qadi, I.L. and Yoo, P.J., 2006. Viscoelastic Modeling and Field Validation of Flexible Pavements. *Journal of Engineering Mechanics*, Vol. 132, No. 2, pp.172-178.

Elseifi, M., 2009. *Analysis of Seasonal Strain Measurements in Asphalt Materials under Accelerated Pavement Testing and Comparing Field Performance and Laboratory Measured Binder Tension Properties* (No. FHWA/LA. 09/444). Louisiana Transportation Research Center.

Epps, J., Monismith, C.L., Seeds, S.B., Alavi, S.H., Ashmore, S.C., Leahy, R. and Mitchell, T.M., 1998. WesTrack Performance: Interim Findings. In *Association of Asphalt Paving Technologists Technical Sessions, Boston, Massachusetts, USA*.

Epps, J., Seeds, S.B., Alavi, S.H., Monismith, C.L., Ashmore, S.C. and Mitchell, T.M., 1997. Westrack Full-Scale Test Track: Interim Findings. In *8<sup>th</sup> International Conference on Asphalt Pavements*, Seattle.

Fakhri, M., Ghanizadeh, A.R. and Dolatalizadeh, M., 2013. Characterizing Horizontal Response Pulse at the Bottom of Asphalt Layer based on Viscoelastic Analysis. *International Journal of Pavement Research and Technology*, Vol. 6, No. 4, pp.379-385.

Ferry, J. D., 1980. Viscoelastic Properties of Polymers. *John Wiley & Sons*.

Garcia, G. and Thompson, M., 2008. Strain and Pulse Duration Considerations for Extended-Life Hot-Mix Asphalt Pavement Design. *Transportation Research Record: Journal of the Transportation Research Board*, Vol. 2087, pp.3-11.

Garcia, G.S., 2007. *Concepts for Mechanistic-empirical Design Procedure for Extended Life Hot Mix Asphalt Pavements with a Multi-Layered Structure. Ph.D. Thesis*, University of Illinois at Urbana-Champaign, Illinois, USA.

Gramsammer, J.C., Kerzreho, J.P. and Odeon, H., 1999. The LCPC's APT Facility: Evaluation of Fifteen Years of Experimentations. In *Proceedings of 1<sup>st</sup> International Conference on Accelerated Pavement Testing, Reno, Nevada*.

Gröchenig, K., 2013. *Foundations of Time-Frequency Analysis*. Springer Science & Business Media.

Han, C., Lukanen, E. O. and Sambeek, R. V. 1994. *Seasonal Characterization and Fatigue Damage of Flexible Pavements in the North Central Region of FHWA-LTPP Study*. Transportation Research Board, 73<sup>rd</sup> Annual Meeting, Washington, D.C.

Haas, R. and Hudson, W.R. and Falls, L.C., 2015. *Pavement Asset Management*. John Wiley & Sons.

Hu, X., Zhou, F., Hu, S. and Walubita, L.F., 2009. Proposed Loading Waveforms and Loading Time Equations for Mechanistic-Empirical Pavement Design and Analysis. *Journal of Transportation Engineering*, Vol. 136, No. 6, pp.518-527.

Huang, B., Mohammad, L. and Rasoulian, M., 2001. Three-Dimensional Numerical Simulation of Asphalt Pavement at Louisiana Accelerated Loading Facility. *Transportation Research Record: Journal of the Transportation Research Board*, Vol. 1764, pp.44-58.

Huang, Y. H., 2004. *Pavement Analysis and Design*. Prentice Hall, Inc., Upper Saddle River, NJ.

Islam, M.R. and Tarefder, R.A., 2013. Measuring Thermal Effect in the Structural Response of Flexible Pavement based on Field Instrumentation. *International Journal of Pavement Research and Technology*, Vol. 6, No. 4, p.274.

Islam, M.R. and Tarefder, R.A., 2014. Determining Thermal Properties of Asphalt Concrete Using Field Data and Laboratory Testing. *Construction and Building Materials*, Vol. 67, pp.297-306.

Islam, M.R. and Tarefder, R.A., 2015. Coefficients of Thermal Contraction and Expansion of Asphalt Concrete In The Laboratory. *Journal of Materials in Civil Engineering*, Vol. 27, No. 11, p.04015020.

Janoo, V.C., 2002. Performance of Base/Subbase Materials under Frost Action. In *11<sup>th</sup> International Conference on Cold regions Engineering*, Anchorage, Alaska.

Jin, M.S., Lee, K.W. and Kovacs, W.D., 1994. Seasonal Variation of Resilient Modulus of Subgrade Soils. *Journal of Transportation Engineering*, Vol. 120, No. 4, pp.603-616.

Jones, M.P. and Witzcak, M.W., 1977. Subgrade Modulus on the San Diego Test Road. *Transportation Research Record: Journal of the Transportation Research Board*, Vol. 641, pp.1-6.

Kasianchuk, D. A., 1968. Fatigue Considerations in the Design of Asphalt Concrete Pavements, Ph.D. thesis, University of California, Berkeley, USA.

Kennedy Jr, J. and Everhart, R., 1998. Modeling Pavement Response to Vehicular Traffic on Ohio Test Road. *Transportation Research Record: Journal of the Transportation Research Board*, Vol. 1629, pp.24-31.

Leiva-Villacorta, F. and Timm, D., 2013. Falling Weight Deflectometer Loading Pulse Duration and Its Effect on Predicted Pavement Responses. In *Transportation Research Board 92<sup>nd</sup> Annual Meeting*, No. 13-2171.

Loulizi, A., Al-Qadi, I., Lahouar, S. and Freeman, T., 2002. Measurement of Vertical Compressive Stress Pulse in Flexible Pavements: Representation for Dynamic Loading Tests. *Transportation Research Record: Journal of the Transportation Research Board*, Vol. 1816, pp.125-136.

Loulizi, A., Al-Qadi, I.L. and Elseifi, M., 2006. Difference Between In Situ Flexible Pavement Measured and Calculated Stresses and Strains. *Journal of Transportation Engineering*, Vol. 132, No.7, pp.574-579.

Love, A.E.H., 1944. *A Treatise on the Mathematical Theory of Elasticity*, Vol. 1, Cambridge University Press.

Lukanen, E.O., 2005. Load Testing Of Instrumented Pavement Sections, *Minnesota Department of Transportation, Research Services Section*.

Mahoney, J.P., Winters, B.C., Chatti, K., Moran, T.J., Monismith, C.L. and Kramer, S.L., 1995. Vehicle/Pavement Interaction at the PACCAR Test Site.

Mateos, A. and Snyder, M., 2002. Validation of Flexible Pavement Structural Response Models with Data from the Minnesota Road Research Project. *Transportation Research Record: Journal of the Transportation Research Board*, Vol. 1806, pp.19-29.

Misiti, M., Misiti, Y., Oppenheim, G. and Poggi, J.M., 1996. Wavelet Toolbox User's Guide. *The Math Works Ins.*

Moore, W.M., Scrivner, F.H., Poehl, R. and Phillips, M.B., 1969. Detecting Seasonal Changes in Load-Carrying Capabilities of Flexible Pavements-Abridgment. *Highway Research Record*, Vol. 291.

Odemark, N., 1949. *Investigations as to the Elastic Properties of Soils and Design of Pavements According to the Theory of Elasticity*, Meddelande 77, Staten Vaeginstitut, Stockholm, Sweden.

Ovik, J., Birgisson, B. and Newcomb, D., 1999. Characterizing Seasonal Variations in Flexible Pavement Material Properties. *Transportation Research Record: Journal of the Transportation Research Board*, Vol. 1684, pp.1-7.

Papagiannakis, A.T. and Masad, E.A., 2008. *Pavement Design and Materials*. John Wiley & Sons.

Rada, G. and Witzak, M.W., 1981. *Comprehensive Evaluation of Laboratory Resilient Moduli Results for Granular Material*. *Transportation Research Record: Journal of the Transportation Research Board*, (810), pp.23-33.

Robbins, M. M. and Timm, D. H., 2009. *Temperature and Velocity Effects on a Flexible Perpetual Pavement*. 3<sup>rd</sup> International Conference on Accelerated Pavement Testing, Madrid, Spain.

Saleh, M., Steven, B. and Alabaster, D., 2003. Three-Dimensional Nonlinear Finite Element Model for Simulating Pavement Response: Study at Canterbury Accelerated Pavement Testing Indoor Facility, New Zealand. *Transportation Research Record: Journal of the Transportation Research Board*, Vol. 1823, pp.153-162.

Salem, H., Bayomy, F., Al-Taher, M. and Genc, I., 2004. Using Long-Term Pavement Performance Data to Predict Seasonal Variation in Asphalt Concrete Modulus. *Transportation Research Record: Journal of the Transportation Research Board*, Vol. 1896, pp.119-128.

Scullion, T., Michalak, C. H., 1991. *MODULUS 4.0, User's Manual*. Texas Transportation Institute, Research Report 1123-4, The Texas A&M University System, College Station.

Sebaaly, P.E. and Tabatabaee, N., 1992. Effect of Tire Parameters on Pavement Damage and Load-Equivalency Factors. *Journal of Transportation Engineering*, Vol. 118, No. 6, pp.805-819.

Shahin, M.Y., 2005. Pavement Management for Airports, Roads, and Parking lots, New York: Springer.

Siddharthan, R.V., Yao, J. and Sebaaly, P.E., 1998. Pavement Strain from Moving Dynamic 3D Load Distribution. *Journal of Transportation Engineering*, Vol. 124, No. 6, pp.557-566.

Siddharthan, R.V., Krishnamenon, N., El-Mously, M. and Sebaaly, P.E., 2002. Investigation of Tire Contact Stress Distributions on Pavement Response. *Journal of Transportation Engineering*, Vol. 128, No. 2, pp.136-144.

Simonsen, E., Janoo, V.C. and Isacsson, U., 1997. Prediction of Pavement Response during Freezing and Thawing Using Finite Element Approach. *Journal of Cold Regions Engineering*, Vol. 11, No. 4, pp.308-324.

Solanki, P., Zaman, M., Muraleetharan, K.K. and Timm, D., 2009. Evaluation of Resilient Moduli of Pavement Layers at an Instrumented Section on I-35 in Oklahoma. *Road Materials and Pavement Design*, Vol. 10, pp.167-188.

Stubstad, R.N. and Connor, B., 1982. Prediction of Damage Potential on Alaskan Highways During Spring Thaw Using the Falling Weight Deflectometer. *Alaska DOT&PF, Division of Planning and Programming, Research Section, Report No. AK-RD-83-11*.

Stubstad, R.N., Baltzer, S., Lukanen, E.O. and Ertman-Larsen, H.J., 1994. Prediction of AC Mat Temperatures for Routine Load/Deflection Measurements. In *4<sup>th</sup> International Conference, Bearing Capacity of Roads and Airfields*, Vol. 1, Minneapolis.

Systemes, D., 2013. ABAQUS User's and Theory Manual, Release 6:13-1. Providence, RI, USA.

Tarefder, R.A. and Islam, M.R., 2014. Measuring Fatigue Damages from an Instrumented Pavement Section due to Day-Night and Yearly Temperature Rise and Fall in Desert Land of the West. In *International Symposium of Climatic Effects on Pavement and Geotechnical Infrastructure*, Fairbanks, Alaska.

Tavafzadeh, N., Hashemian, L and Bayat, A., 2016. The Effect of Seasonal Variation on Load Bearing Capacity of Pavements Comprised of Insulation Layers. In *95<sup>th</sup> Transportation Research Board Annual Meeting*, January 10-14, Washington, D.C., USA.

Ullidtz, P., 1987. *Pavement Analysis*. Amsterdam, the Netherlands, Elsevier.

Ullidtz, P., Krarup, J. and Wahlman, T., 1994. Verification of Pavement Response Models. In *Nondestructive Testing of Pavements and Backcalculation of Moduli: Second Volume*. ASTM International.

Ullidtz, P., 2000. Will Nonlinear Backcalculation help?. In *Nondestructive Testing of Pavements and Backcalculation of Moduli*, Vol. 3, ASTM International.

Ulloa, A., Hajj, E.Y., Siddharthan, R.V. and Sebaaly, P.E., 2012. Equivalent Loading Frequencies for Dynamic Analysis of Asphalt Pavements. *Journal of Materials in Civil Engineering*, Vol. 25, No. 9, pp. 1162-1170.

Van Cauwelaert, F. J., Alexander, D. R., White, T. D. and Barker, W. R., 1989. Multilayer Elastic Program for Backcalculating Layer Moduli in Pavement Evaluation. *Nondestructive*

*Testing of Pavements and Backcalculation of Moduli*, ASTM STP 1026, A.J. Bush, G.Y. Baladi, Eds., pp. 171-188.

Van Cauwelaert, F.J., Alexander, D.R., White, T.D. and Barker, W.R., 1989. Multilayer Elastic Program for Backcalculating Layer Moduli in Pavement Evaluation. In *Nondestructive Testing of Pavements and Backcalculation of Moduli*. ASTM International.

van Gurp, C.A.P.M., 1995. *Characterization of Seasonal Influences on Asphalt Pavements with the Use of Falling Weight Deflectometers*. TU Delft, Delft University of Technology.

Von Quintus, H.L. and Simpson, A.L., 2002. *Back-Calculation of Layer Parameters for LTPP Test Sections, Volume II: Layered Elastic Analysis for Flexible and Rigid Pavements* (No. FHWA-RD-01-113).

Warren, H. and Dieckman, W.L., 1963. *Numerical Computational Stresses and Strains in Multi-Layer Asphalt Pavement System*, Internal Report, Chevron Res. Corporation, Richmond, Canada.

Wei, L. and Fwa, T., 2004. Characterizing Road Roughness by Wavelet Transform. *Transportation Research Record: Journal of the Transportation Research Board*, (1869), pp.152-158.

Willis, J. and Timm, D., 2009. Repeatability of Asphalt Strain Measurements under Falling Weight Deflectometer Loading. *Transportation Research Record: Journal of the Transportation Research Board*, Vol. 2094, pp.3-11.

Wong, M.W., 2011. *Discrete Fourier analysis*. Springer Science & Business Media.

Wu, Z., Hossain, M. and Gisi, A., 2000. Performance of Superpave Mixtures under Accelerated Load Testing. *Transportation Research Record: Journal of the Transportation Research Board*, Vol. 1716, pp.126-134.

Yin, H., 2012. Simulation of Flexible Pavement Response to FWD Loads: A Mechanistic Approach. *International Journal of Pavement Research and Technology*, Vol. 5, No. 4, pp.257-266.